

## Response and revisions for the manuscript

“A probabilistic assessment of calcium carbonate export and dissolution in the modern ocean ” Biogeosciences Discuss., doi:10.5194/bgd-12-20223-2015

by G. Battaglia, M. Steinacher, and F. Joos, March 2016

We thank the anonymous reviewer and W. Koeve for their constructive reviews and comments. We appreciate the effort and time committed by the reviewers.

We follow reviewer #1's advice and change the evaluation of the Monte Carlo ensemble by applying global skill scores instead of regional, basin-specific skill scores. This adjustment required to re-run the Monte Carlo ensemble and implied changes in illustrations, tables and text. While the results of the new global approach are numerically not identical to that of the regional approach, conclusions remain unchanged from the previously submitted manuscript and numerical results are similar for the two approaches. This agreement further illustrates the robustness of our Monte Carlo approach.

At this occasion, we also corrected a recently found error in the physical core of the model. The evaluation section and the illustrative runs are updated; the corrections are minor and negligible.

We also follow both reviewers' suggestion to improve the structure of the paper and the figure numbering. The figures are now in order of appearance in the text.

We add a revised manuscript with track changes in addition to the answers presented here. The intention is to thoroughly document our changes in response to the review comments. We are aware that the new editorial procedure of BG does not require the submission of a revised manuscript at this stage and that the editor's decision will apply to the previously submitted manuscript.

Please find below our response (normal font) to the comments by the reviewers (*in italic*) and suggested text additions to the manuscript (**in blue**).

---

*Anonymous Referee #1*

*General comment:*

*This is a very interesting article concerned with a probabilistic assessment of calcium carbonate export and dissolution. The probabilistic assessment chosen by the authors is very promising and approaches like this are urgently needed in order to arrive at a better model presentation of CaCO<sub>3</sub>. The article is therefore definitely worthy of publication.*

Many thanks.

*Specific comments:*

*\* The regional skill assessment seems to be problematic. Figure 8 shows clear inconsistencies for*

*the median CaCO<sub>3</sub> export, especially when considering the Southern Ocean. There is a visible mismatch between the Atlantic, Indian and Pacific part of the CaCO<sub>3</sub> export of the Southern Ocean, generated by the regional skill assessment. The credibility of the solution is therefore questionable. I advice to shift the focus of this paper from the regional skill assessment to the global skill assessment. This includes a significant re-write and different illustrations.*

Done – switched to global skill assessment.

We do not share the reviewer's opinion on the credibility of the regional skill assessment. However, the perception by the reviewer and the general reader is important. The application of global skill scores is easier to explain and offers the advantage of a fully self-consistent solution. We therefore followed the reviewer's advice and present results from a global skill assessment in the revised manuscript. We emphasize that the results from the new global skill assessment are similar to those of the regional approach and that our conclusions remain unchanged. The results appear therefore robust within the model context and only weakly dependent on details of the setup.

A new Monte Carlo ensemble was set up, run, and evaluated. The results from the ensemble simulations presented in the previous manuscript version imply that the application of a uniform rain ratio for the entire Southern Ocean appears overly simplistic. Therefore, the Southern Ocean sectors of the Pacific, Indian, and Atlantic are treated individually in the new setup. In addition, the previous results also imply that the prior ranges for the rain ratio values in the Atlantic regions were very broad. Thus, narrower prior ranges are applied in the Atlantic in the new setup.

The visible step-like changes in CaCO<sub>3</sub> export between the Atlantic and the Indian and Pacific sector of the Southern Ocean with lower export (per unit area) in the Atlantic sector than in the Indian and Pacific sectors also emerge in the new setup. This is attributable to the choice of the regional boundaries and the assumption that the spatial pattern of export within a region is identical to the pattern simulated by the standard version of the model. The standard model yields relatively little zonal variation in the CaCO<sub>3</sub> export fluxes in the Southern Ocean in contrast to the data assimilation with lower than zonally-averaged export in the Atlantic. While our Monte Carlo approach is suitable to estimate export fluxes over larger regions, the detailed spatial patterns in CaCO<sub>3</sub> export remain unconstrained.

The following text is added after the first paragraph of section 4.2:

**“Median CaCO<sub>3</sub> export production per unit area in the constrained ensemble is considerably lower in the Atlantic sector of the Southern Ocean (135 mmol-C m<sup>-2</sup> yr<sup>-1</sup>) as compared to the Pacific (301 mmol-C m<sup>-2</sup> yr<sup>-1</sup>) and Indian (326 mmol-C m<sup>-2</sup> yr<sup>-1</sup>) sectors (Fig. 7 top). This is attributable to the choice of the regional boundaries for the rain ratio regions and the assumption that the spatial pattern of export within a region is identical to the pattern simulated by the standard version of the model. The standard model yields relatively little zonal variation in the CaCO<sub>3</sub> export fluxes in the Southern Ocean in contrast to the data assimilation with lower than zonally-averaged export in the Atlantic. This reflects the much lower TA\* reconstructed in the deep Atlantic as compared to the deep Pacific and Indian (Fig. 1). A large export in the Atlantic sector of the Southern Ocean tends to yield high simulated TA\* concentrations in the Antarctic Bottom Water that fills the deep Atlantic. The Monte Carlo data assimilation therefore requires low CaCO<sub>3</sub> export in the Atlantic sector to minimize model-data mismatches in the deep Atlantic. It is difficult to correctly represent water mass formation and circulation in the Southern ocean and our model may be biased. A**

**known bias is that the Atlantic Bottom Water circulation is too sluggish, also evidenced by simulated low radiocarbon signatures (Figs A2. A4). The influence of a potential bias in South Atlantic export on global CaCO<sub>3</sub> export is estimated to be relatively small; assuming the same (median) CaCO<sub>3</sub> export per unit area in the Atlantic sector as estimated for the Indian sector would yield 0.06 Gt-C yr<sup>-1</sup> higher export than suggested by the ensemble median. While our Monte Carlo approach is suitable to estimate export fluxes over larger regions, the detailed spatial patterns in CaCO<sub>3</sub> export remain unconstrained.”**

*\* Throughout the whole paper, there are barely any time periods mentioned. Yet, the knowledge of the considered time periods is of importance, especially when mentioning mean concentrations and when comparing the model results to observations. Please add the considered time periods whenever necessary.*

Done – time periods mentioned.

All ensemble runs are spun up to equilibrium under preindustrial boundary conditions, with atmospheric CO<sub>2</sub> set to 278 ppm and with wind-stress forcing prescribed from a monthly wind-stress climatology (NCEP/NCAR) as mentioned already in the manuscript.

The text at the beginning of section 2 is modified to read:

**“Total alkalinity data are from the GLODAP carbon climatology (Key, 2004) and salinity (Antonov et al., 2010), temperature (Locarnini et al., 2010), oxygen and phosphate (Garcia et al., 2010a, 2010b) data from the World Ocean Atlas. These observational data serve to split the alkalinity signal into its different physical and biogeochemical components such as TA\*, our target variable in the data assimilation. The gridded data products from GLODAP and the World Ocean Atlas are derived from samples taken during the previous few decades. “**

New text was added at the end of the 1. paragraph of section 3.1:

**“We implicitly neglect potential changes in TA\* over the industrial period by comparing model results for preindustrial conditions with TA\* data reconstructed from recent measurements. Such changes are negligible in simulations with prescribed anthropogenic forcing in the Bern3D model.”**

*\* Further, Figure A2 & A3 and page 20244 refer to the year 1994. Here, it would be preferential to at least compare to a ten-year average in order to analyse a more robust model result.*

Done. The model results for CFC11 shown in Figure A3 are now given for the period 1990-1999. This did hardly affect the evaluation as inter-annual variability is low in our model. The radiocarbon results shown in Figure A2 are for the preindustrial period.

In addition the following clarification is added in the appendix:

**“The atmospheric history of CFC11 is prescribed according to Bullister 2011. Here we do not account for potential changes in ocean circulation and CFC11 solubility over the industrial period.”**

*Technical comments:*

*\* The figures and tables seem to appear in random order. Please fix this, so that Figure 1 is the first figure referred to in the text, Figure 2 the second one and so forth.*

Done. Figure and table numbering is adjusted as requested

\* page 20224, line 4: Correction: "... CaCO<sub>3</sub> export fluxes ..."

Corrected.

\* page 20224, lines 11-17: Please mention at least once that these are simulated results.

Done. Sentence modified to read:

**"The median (and 68% confidence interval) of the constrained model ensemble for global biogenic CaCO<sub>3</sub> export is 0.90 (0.72--1.049) Gt PIC/yr .."**

\* page 20224, line 11: Correction: "... that is within the lower half... "

\* page 20225, line 10: Correction: "... coccolithophorids, which ..."

\* page 20226, line 7: Correction: "... range over several orders ..."

\* page 20226, line 16: Correction: "... this method ..."

All sentences corrected.

\* page 20227, line 27 + page 20228, line 3 & line 25 + page 20229, line 11: Which time- periods and products are these mean concentrations from? Please denote.

Done. Please see answer to the second specific comment given above.

\* page 20229, line 19: Correction: "... in some places ..."

Inserted.

\* page 20230, lines 21-22: Is this resolution valid for all components of the Bern3D model?

Inserted extra information to clarify:

"Here an **ocean** version with a~horizontal resolution of 41 by 40 grid cells and 32 logarithmically-scaled vertical layers is used (see also Roth and Joos, 2014). **The horizontal resolution is the same for the components atmosphere, ocean, sea ice, and sediments of the Bern3D model.**"

\* page 20233, lines 9: Please explain the variable *keff* earlier in the text, i.e. directly after equation (4).

\* page 20235, line 18: Correction: "... (calculated from GLODAP (Key et al, 2004) and World Ocean Atlas 2009 (WOA09) (Locarnini et al., 2010; Antonov et al.,2010)) ..."

\* page 20237, line 19: Correction: "... to the part of ..."

\* page 20240, line 26: Is that the export flux at 75m depth? Please specify.

\* page 20241, line 27: Correction: "... are associated ..."

\* page 20242, line 7: Correction: "... are dissolving ..."

Text corrected and modified as suggested

\* page 20245, line 5: What about changes in the TA\*-profiles?

The figure below shows basin-average profiles in TA\* for low, standard and high diapycnal diffusivities and for the three idealized dissolution profiles (fast, slow, constant) discussed in the manuscript.

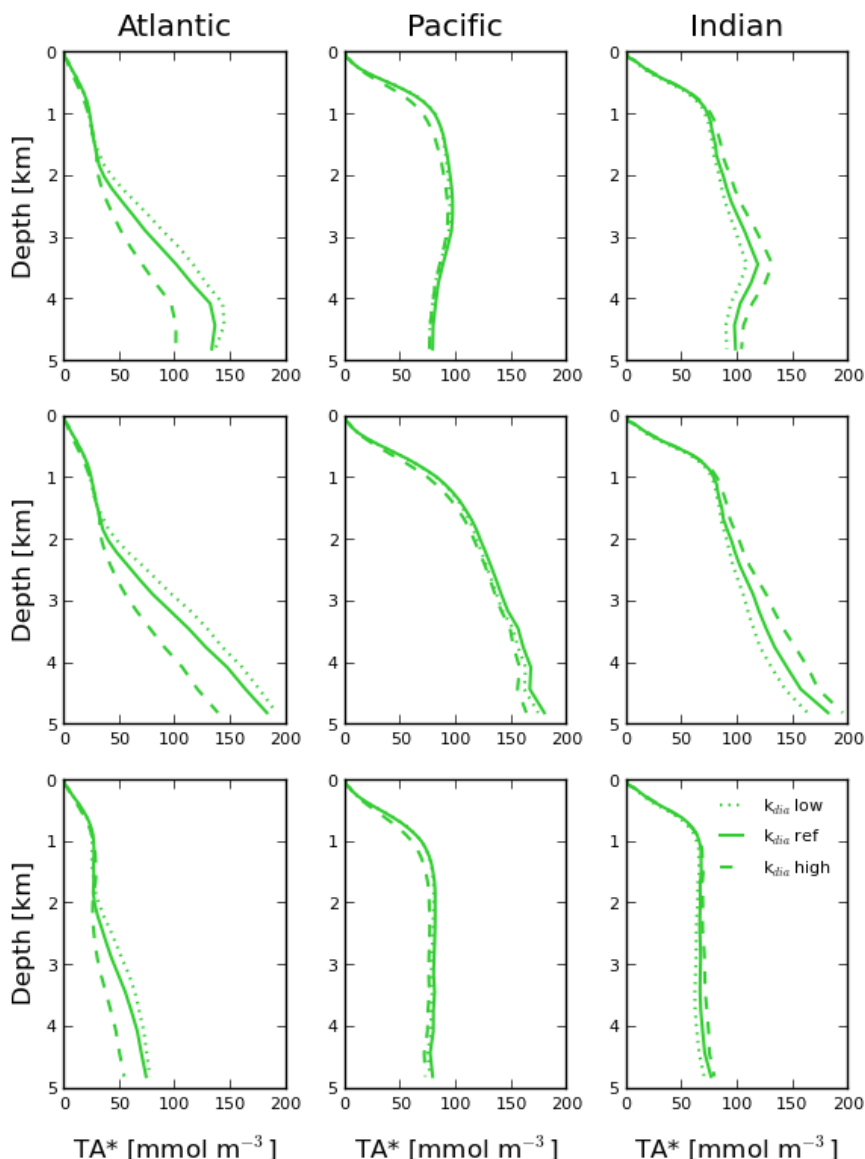


Figure: Simulated TA\* profiles for the Atlantic, Indian, and Pacific and for different diapycnal mixing coefficients and dissolution schemes. For these illustrative simulations, calcite and aragonite particles were assigned equal parameter values and 10% of export is assumed to be in the form of aragonite.  $k_{dia}$  is set to 0.1 (low), 0.2 (standard), and 0.5 (high)  $10^{-4} \text{ m}^2/\text{s}$ . Top row (“fast”):  $k_0=10/\text{day}$ ,  $n=1$ ,  $k_{bg}=0$ ; middle row (“slow”):  $k_0=0.16/\text{day}$ ,  $n=2$ ,  $k_{bg}=0$ ; bottom row (“constant”):  $k_0/v = 1/(2900 \text{ m})$ .

The following text is added in the revised manuscript to the second paragraph of section 4.3.2

**“Basin-average profiles in TA\* vary little in the upper ocean and the deep Pacific (< 14 mmol/m<sup>3</sup>) and modestly in the deep Atlantic (< 44) and deep Indian (< 18) when varying diapycnal diffusivity between 0.1 and 0.5 m<sup>2</sup> s<sup>-1</sup> ... In conclusion, simulated TA\* is only weakly affected by uncertainties in the diapycnal mixing coefficient. “**

\* page 20246, line 15: Correction: "... observation-based TA\* ..."

OK.

\* page 20246, lines 15-20: Correlation is just one measure which is not very informative in itself. What about standard deviation and the bias?

We do not agree with the reviewer. Correlation between TA\* fields simulated for different dissolution schemes is the metric of choice to illustrate that different dissolution schemes are difficult to distinguish or to constrain by the TA\* data. The highly correlated patterns in TA\* for the three dissolution profiles indeed imply that the spatial pattern in TA\* can hardly be used to discriminate between these schemes given existing uncertainties in the magnitude of CaCO<sub>3</sub> export. The absolute concentration of TA\*, and thus mean data-model bias and standard deviation, can be varied, completely independently from the dissolution scheme, by varying CaCO<sub>3</sub> export.

Nevertheless, we computed the standard deviation between normalized model and observational fields. The normalization for an individual TA\* field is achieved by dividing the TA\* data at each grid cell by the ocean average TA\* concentration:

$$TA^*_{norm} = TA^* / TA^*_{average}$$

The RMSE between normalized observed and modeled fields are 58%, 47%, and 42% for the three dissolution cases (fast, slow, constant).

To make this point clear, the text was changed to read:

**“Corresponding to the high correlation, the RMSE between normalized observed and normalized modelled fields vary within a limited range (42 to 58%) for the three dissolution cases. This high spatial correlation in simulated TA\* and uncertainties in CaCO<sub>3</sub> export make it difficult to distinguish different dissolution parameterizations. The magnitude of CaCO<sub>3</sub> exports modulates absolute TA\* concentrations and thus model-data bias and root mean square errors.** Given these uncertainties, we cannot objectively determine the preferred dissolution scheme from TA\* data.”

\* page 20247, line 23: Correction: "... a global CaCO<sub>3</sub> export ..."

Corrected.

\* page 20247, lines 7-11: What are the error-estimates of Sarmiento and Gruber (2006) and Lee (2001)?

Sarmiento and Gruber (2006) do not provide a quantitative error assessment. The uncertainty estimate by Lee 2000 of +/- 0.3 Gt-C yr<sup>-1</sup> is now given in the text.

\* Table 2: Please refer to the depth of the export flux.

\* Table 5: Correction: "... are estimated ...".

Done.

\* Figure 1: The bottom row should rather be displayed in a separate figure.

Agreed. The color bar of the lower panel is now adjusted to better visualize the influence of ocean-sediment fluxes on simulated TA\*.

\* Figure 2 & 4: Please enlarge the font - the labelling of the axes is not readable.

Done.

*\* Figure 3: What time period is depicted? Further, the western/eastern boundaries of the arctic part of North Pacific and North Atlantic are missing.*

Figure 3 is removed from the revised manuscript. It also showed results for a pre-industrial steady state.

*\* Figure 7, 8, A1, A2: What time period is depicted?*

Intro of Appendix now extended to:

„Results are for a **pre-industrial** steady state of the Bern3D ocean model configuration ..... **The atmospheric history of CFC11 is prescribed according to Bullister, 2011. Here we do not account for potential changes in ocean circulation and CFC11 solubility over the industrial period.**”

*\* Figure A1: The references for the World Ocean Atlas should be bracketed.*

Done.

*Review by W. Koeve (Referee)*

*The CaCO<sub>3</sub> cycle is an important component of the oceanic carbon cycle. Modelling and model evaluation of this component, however, appear to be less well developed, compared to that of the so called organic tissue pump. The manuscript of Battaglia and co-authors applies a probabilistic approach using the Bern3D ocean model to assess export and dissolution of calcium carbonate on global and basin scales and in the modern ocean. It is one of the most detailed studies on this subject, that the reviewer has seen. I regard it an important contribution to our quantitative understanding of the oceanic carbon cycle, its modelling and hence forecast.*

*The study provides new estimates of CaCO<sub>3</sub> export and the large scale distribution of its dissolution, both with respect to the three major oceans, as well as to the three principal domains where dissolution might occur (in/on top of the sediment, below the saturation horizon, and above it).*

*A major result of this study is that the kind of observations (alkalinity, CaCO<sub>3</sub> deep ocean flux data) and tracers constructed from them (TA\*) that are currently available do not allow to constrain at the same time CaCO<sub>3</sub> export and the functional form of its dissolution in the ocean. In particular, significant dissolution above the saturation horizon can not be ruled out based on the specific combination of data and the approach and model chosen. "Dissolution schemes, with and without dissolution above the saturation horizon, achieve realistic (i.e. observed) TA\* distributions". Ocean circulation, including mixing, affect concentration gradients such that different dissolution schemes can't be distinguished statistically.*

Thank you.

*I suggest publication of this work in BG, however, after moderate revisions of the ms. Important issues:*

*Structure: In particular, the organisation of the paper and of the arguments put forward lacks clarity. In fact, I got the strong impression that the authors have reorganised their paper very recently, but without making sure that the order of arguments supports reading and understanding of the presented material as good as it could. This reorganisation is very obvious from the order of references to several figures which are misplaced to a degree I have not seen before. For example, Fig 2 is referred to three text pages after Fig. 3, Fig. 4 is referred to 2 pages after first referral to Fig. 5. Finally Fig. 6 is referred to on p20245 for the first time, long after Figs 7, 8, and 9 have been discussed on the four pages before. This is clearly not a good practice and very confusing for the reader. Please improve this.*

Done. Figure numbering is adjusted to reflect first appearance of figures in the text.

*TA\*-CFC method: In the abstract, introduction and discussion you make reference to 'the TA\*-CFC-age' method, which has been used by others (e.g. Feely et al.) in support of shallow (above saturation horizon) dissolution of CaCO<sub>3</sub>. The way you present this material is not really appropriate. Since the paper of Friis et al. 2006 it is well acknowledged that TA\* as a tracer being produced in the interior of the ocean and being destroyed only at the very surface (either explicitly as in Friis et al. or Koeve et al. or implicitly when TA\* is diagnosed or 'constructed'). Such a tracer has to show gradients towards the surface, and significant concentrations far away from the site of TA\* generation. These gradients, if not properly corrected for the effect of mixing will give rise to artificial rate estimates when combined with age tracers. The Friis paper is well received by the*

*community, hence the TA\*-CFC-age based estimates are more a historical note, and not a state-of-the-art rate estimate. I would hence not consider the difference between rates estimates from this method and yours to be a surprising/important result worth to be mentioned in the abstract or the introduction. This avoids the problem of introducing this method in more detail there (you can't assume that everybody knows the TA\*-CFC-method!). I therefore suggest to discuss the older TA\*-CFC-age based estimates briefly in the discussion only. By the way, TA\* tracer mixing is only one of several issues with this approach.*

We followed the advice by the reviewer and de-emphasized the text on the TA\*-CFC method. Nevertheless, this method appears still to play some role in the general discussion. The widely cited Berelson et al, 2007 review relies on results obtained with the TA\*-CFC method and even more recently Carter et al., 2014 appear to argue for this method and Barrett et al., 2014, included estimates based on this method for comparison, though with a cautionary note.

We removed text referring to TA\*-CFC method from the abstract. In the introduction, the reference to this method is now extremely brief to establish the general context and current uncertainties. The following text was removed from the introduction: “In particular, this adds to the discussion initiated in Friis et al., 2006 on the difficulty to uniquely relate upper ocean TA\* concentrations to either dissolution or mixing processes.”

CO<sub>3</sub>-ions: *In the introduction you speak about carbonate ions in a sometimes strange, awk or wrong way. Eg. 20225, 11 you say that CaCO<sub>3</sub> is formed from Ca<sup>2+</sup> and CO<sub>3</sub><sup>2-</sup>. To the extend that the actual carbon species used in the formation of CaCO<sub>3</sub> is known it appears to be different for different CaCO<sub>3</sub> producers. Even if 1 mol of CO<sub>3</sub><sup>2-</sup> would be taken up per mol of CaCO<sub>3</sub> formed (and exported), the net effect would not be a decrease of 1mol of CO<sub>3</sub><sup>2-</sup> in the surface ocean. This is simply due to rapid re-adjustments within the carbonate system. The actual rate of change per mol of CaCO<sub>3</sub> depending on conditions. Also, 20225, 14-15, the 'uptake and release of CO<sub>3</sub><sup>2-</sup> introduces vertical gradients in alkalinity and DIC' is misleading, at least. 20226, 27: 'mixing of CO<sub>3</sub><sup>2-</sup>' is awk. CO<sub>3</sub><sup>2-</sup> is NOT a tracer, hence it is not mixed conservatively. Please consult e.g. Wolf-Gladrow et al., 2007, Mar. Chem., 106:287ff for details. Or use a tool like co2sys to take a look at the effect of mixing of e.g. two water masses with distinct TA and DIC for the effect on CO<sub>3</sub><sup>2-</sup> concentrations along the mixing line. Please carefully revise the text accordingly.*

Thank you for pointing out this misleading wording. Text adjusted to:

“The CaCO<sub>3</sub> cycle is driven by calcifying organisms such as coccolithophorids, foraminifera or pteropods, which remove calcium Ca<sup>2+</sup>, **alkalinity and dissolved inorganic carbon** from the pelagic surface ocean waters to form shells and structures of CaCO<sub>3</sub>.”

“The **formation and dissolution of** CaCO<sub>3</sub> introduces a~vertical gradient in alkalinity and dissolved inorganic carbon.”

“... physical transport and mixing of the **released alkalinity and dissolved inorganic carbon** and ocean--sediment fluxes.”

Methodology: *Latin-hypercube, the specific way in which skill scores are assigned and used when computing e.g. medians could at times be more specifically presented and/or supported by references. Having not done this myself (like most of the readers of BG), sometimes had to guess what you actually did. From the list of possible journals within the special issue you chose BG instead of GMD. Hence I think you should consider that the audience of BG consists of many non-modellers. Also your work should be understandable to people that address the CaCO<sub>3</sub> cycle from the*

*observational side in order to make your work most influential. Following to my argument about the organization of the paper, I sometimes had the impression that some details of your approach become clear late in the paper while the respective Fig. numbers indicate that that section may have been moved towards the back of the paper recently. In practice, section 3.3.2 could be extended providing more details on how eg. medians shown in Fig. 5 are computed. It is particularly in section 4.1 where I sometimes missed details of the approach, e.g. when you speak about 'the optimisation procedure with the application of regional skill scores' (20239, 19) or the 'median fields' (20240, 3) shown in Fig. 4. How are the latter actually computed. Potentially a reader (me) would better understand all this if s(he) reads Steinacher et al. carefully first, but then (s)he may not return to continue reading your paper. Which I would regard a pity.*

The revised text is hopefully easier to understand as we omit the regional skill score approach and present a global skill assessment following the request of reviewer 1. The text on skill scores in section 3.3.2 is expanded and the computation of median and similar measures is explained. The new text reads:

**“The skill scores  $S_m$  of the individual ensemble members are likelihood-type functions corresponding to a Gaussian distribution of the data-model discrepancy ( $TA^*_{\text{model}} - TA^*_{\text{obs}} - TA^*_{\text{sedcorr}}$ ) with zero mean and variance  $\sigma^2$ .  $S_m$  is an indication of the relative performance/credibility of each individual model configuration. Configurations which have relatively small deviations from the data are judged more probable than configurations which differ greatly from the observations.**

**$S_m$  are used as weight to compute probability density functions (PDFs) and related measures such as the median (50th percentile) and the 16th and 84th percentiles defining the one standard deviation confidence interval ( $1\sigma$ ) of the ensemble results. PDFs represent weighted and normalized histograms of the variables of interest. The normalization is such that the integral over a PDF equals 1. A cubic spline interpolation is used to arrive at a continuous PDF from the discrete, normalized histogram. For the computation of median and confidence ranges the histograms are converted to cumulative distribution functions (CDFs). We interpolate linearly within the discrete CDFs to arrive at the chosen percentiles (i.e. CDF=(0.16, 0.5, 0.68)).**

**The above explanations apply for any simulated quantity of interest. In the following we will present PDFs, median values, and  $1\sigma$  confidence ranges for aragonite and calcite export and dissolution as well as for tracer concentrations at individual grid cells or integrated over regions or the whole ocean. Spatial integrations are done for each ensemble member individually and before computing the PDFs and associated measures from the full ensemble.”**

Text on the Monte Carlo Ensemble in section 3.3.1 is also extended as explained under specific comments.

*Prescribing the saturation state from observations: This is potentially a (severe?) limitation of this study. The actual saturation state is due to the pressure effect, the pre-formed DIC and TA, the remineralised DIC and TA and the imprint of  $\text{CaCO}_3$  dissolution (in terms of DIC and TA). To the extent that  $\text{CaCO}_3$  dissolution is saturation dependent, the former feeds back on its conditions in the real ocean, but not in your modelling. I suggest to discuss, and potentially quantify in sensitivity runs, how significant that feed-back is for  $TA^*$  profiles and inventories in the non-constant cases.*

We do not agree with the reviewer that the application of observation-derived fields of the saturation of water with respect to  $\text{CaCO}_3$ ,  $\Omega$ , is a limitation of our study. To the contrary, the observation-derived  $\Omega$  -field provides the best possible boundary condition for the dissolution model in our approach. It is a strength rather than a weakness of the assessment.

As explained by the reviewer, the saturation of water with respect to  $\text{CaCO}_3$ ,  $\Omega$ , is affected both by the dissolution of organic matter and  $\text{CaCO}_3$ . The simulated saturation horizon and  $\Omega$ -field is thus not a direct and simple reflection of the  $\text{CaCO}_3$  feedback on these quantities. The magnitude of the mentioned  $\text{CaCO}_3$  dissolution feedback and its influence on  $\Omega$  and the saturation horizon is fully constrained by  $\text{TA}^*$ .  $\text{TA}^*$  is the quantity that reflects the dissolution of  $\text{CaCO}_3$  below the euphotic zone and defines its imprint on the fields of DIC and Alk, variables which in turn define (together with pressure, temperature, salinity and nutrient concentrations)  $\Omega$ . This is why we use  $\text{TA}^*$  as our target variable and not  $\Omega$  and the saturation horizon. If  $\text{TA}^*$  is modelled in agreement with observations, then the imprint of  $\text{CaCO}_3$  dissolution on DIC, Alk and thus on  $\Omega$  and on the saturation horizon is correctly modelled and the mentioned feedback is correctly represented.

Constraining the saturation horizon and the  $\Omega$ -field would require not only to constrain  $\text{CaCO}_3$  and dissolution, but also to constrain export and remineralization of organic matter in the form of particulate and dissolved organic matter. This would add another level of complexity and many free parameters in the assimilation. This is beyond the scope of this study.

In addition, the results imply that the probabilistic estimates of  $\text{CaCO}_3$  export and dissolution do not depend sensitively on the exact location of the saturation horizon. As discussed in the text, very similar patterns of the target variable  $\text{TA}^*$  emerge for dissolution parameterizations that do/do not depend on  $\Omega$  and on the saturation horizon. We note that the saturation horizon is reasonably well represented by the standard setup of the Bern3D model in the Atlantic, Indian, and South Pacific, and is too deep in the North Pacific.

The following text is added at the end of 3.3.1:

“... Mismatches in modelled and observed saturation states are particularly large in the **North Pacific**, where the modelled **calcite** saturation horizon is up to 1.5 km too deep. **The calcite saturation horizon is well represented in the South Pacific, Indian and Atlantic by the model. The results presented in section 4 suggest that estimated  $\text{CaCO}_3$  export production fields and dissolution rates are insensitive to the choice of the saturation field, because saturation-dependent and saturation independent parameterizations of dissolution yield similar  $\text{TA}^*$  fields.**”

*Units: In 20229, 22-25 you say that you will present  $\text{TA}^*$  in TA-units, but later you give  $\text{TA}^*$  inventories in Pmol C. I suggest that, for the purpose of your paper, it would be least confusing for the reader if you always use mol C based units (for local  $\text{TA}^*$ , its inventories, and ALSO the  $\text{CaCO}_3$  flux values, which are currently in Gt PIC; Gt PIC-C, or PIC- $\text{CaCO}_3$  is not specified). Currently you use three different sets of units, which is not helpful for the reader.*

Done. We specify that  $\text{TA}^*$  concentrations are always in alk-equivalents and add that  $\text{TA}^*$  inventories are in Pmol C, in line with Koeve et al. 2014.

For  $\text{CaCO}_3$  fluxes we used  $\text{Gt PIC yr}^{-1}$  for comparison with Berelson et al. 2007. We change the notation to  **$\text{Gt-C yr}^{-1}$** ,  **$\text{mmol-C m}^{-3} \text{yr}^{-1}$** ,  **$\text{mmol-C m}^{-2} \text{yr}^{-1}$**  to avoid any ambiguities.

Added: “**TA\* inventories are in P mol- C and CaCO<sub>3</sub> fluxes are given in carbon units (Gt-C yr<sup>-1</sup> , mmol-C m<sup>-3</sup> yr<sup>-1</sup> , mmol-C m<sup>-2</sup> yr<sup>-1</sup> ).**”

*Below I provide some more specific comments and suggestions, ordered largely by appearance in the ms;*

20225, 10: *name other CaCO<sub>3</sub> producers, please*

Added: “calcifying organisms such as coccolithophorids, **foraminifera or pteropods,**”

20225, 17: *'This redistribution' refers to mixing and transport in the sentence before, right? But isn't the CaCO<sub>3</sub> counter pump, which makes up the gradients (l 15) what in particular affects the ocean-atmosphere partitioning of CO<sub>2</sub>? The redistribution tends to reduce that effect. Rephrase please.*

Sentence modified to read:

“This redistribution of alkalinity and carbon **by biogenic and physical transport** affects the partitioning of carbon between the ocean and atmosphere ...”

20225, 20: *50ppm on century times scales appears to be a lot. I think, that that is not in agreement with e.g. Hofman and Schellnhuber, 2009 (PNAS, I think).*

Gangsto et al., BG, 2011 find a decrease of 30 ppm by year 2100 and of 50 ppm by year 2300 in response to a hypothetical stop of CaCO<sub>3</sub> export after 2000 CE (their Figure 15b). Text changed to read: “.. tend to decrease atmospheric CO<sub>2</sub> by **a few ppm, and in the extreme case by up to ~ 50 ppm,** on century time scales“

20226, 15: *'the TA\*-CFC age method'; you can't assume everybody to know what that is; either you introduce it here, or (better) leave it out; much of the issues raised by the TA\*-CFC-age approach disappears when understand the general nature of the TA\* tracer; however, that one (TA\*) has not even been introduced at this point to the reader; please do so at least in a generic sense (e.g. TA\* to reflect the imprint of CaCO<sub>3</sub> dissolution on TA) and rewrite the paragraph accordingly; perhaps point to section 2 for details)*

OK. Rephrased to:

“Friis et al. 2006 nevertheless, demonstrated that **the method** which is often employed to derive these upper ocean dissolution rates (**see Discussion section on TA\*-CFC age method**) (Berelson et al., 2007), might not be applicable, ..”

20226, 20-21: *perhaps add a reference here*

The following references are added at the end of line 21: **Archer et al.,1996**

20227, 27 & 20228, 3 & 20228, 25: *at this point it is not clear what the mean values are referring to, i.e. which dataset (GLODAP, WOA)?*

True. Added introductory sentence. See reviewer #1.

20228, 12: *'observations of TA', it is not clear whether you did this with observed TA (bottle data e.g. from WAVES) or gridded GLODAPv1 or regridded GLODAP to your Bern3D grid. Please*

*specify.*

Added to first paragraph:

**“... We first regridded all required, gridded datasets to the Bern3D model grid (40x41x32 grid boxes) using the area-weighted regridding method of Ferret before deriving the other properties.”**

20229, 12: *refer to Fig. 1a, not just Fig. 1*

Yes. Figure 1 a, b are now two separate figures (see request of reviewer 1).

20229, 20: *Is the fraction of TA\* above the saturation horizon similar to that reported in Koeve et al., 2014?, Compare, please.*

Slightly higher there, at 44.7%. Added:

**“..similar to Koeve et al., 2014 who found 44.7% above the calcite saturation horizon (Koeve et al., 2014.”**

20229, 22-25: *TA-units. Here, like in much of section 2 your description follows that of Koeve et al. 2014 to a certain extend. However, later in the text you don't follow your own advise. TA\* inventories are given in Pmol C, not Pmol TA. See my general comment above for consolidating the units.*

We follow the units used in Koeve et al. 2014.

20230, 6: *Latin-Hypercube. Since you don't introduce this method in too much detail, perhaps give at least some references pointing to papers that present more details, if possible from ocean studies, helpful to readers from that domain.*

Inserted:

“varied using **a Monte Carlo** sampling method (McKay, 1979, **Steinacher et al., 2013**)”

Added to section 3.3.1

**“Following Steinacher et al., 2013 and 2016, we run a 1000 member Latin Hypercube ensemble to constrain the export flux out of the surface ocean, and the dissolution of aragonite and calcite within the water column. Latin Hypercube sampling (McKay et al. 1979) is a statistical, Monte Carlo method to generate controlled random samples from a multidimensional distribution (15 dimensions in our case). The defined parameter ranges are divided into equally probable intervals (1000 in our case). Random samples are then generated in each interval. This method ensures that the sampled values are representative of the real variability while minimizing the number of required samples and thus the computational costs. We sample 15 parameters ...”**

Changed Latin-hypercube to **Monte Carlo** in many instances: Perhaps easier to associate with.

20231, 2 : *'scaling-factor', as used here is lab slang. Please be more specific.*

Changed to:

**“The global mean air-sea transfer rate is reduced by 19% compared to OCMIP-2 to match observation-based estimates of natural and bomb-produced radiocarbon (Müller et al., 2008).”**

20231, 3: 'describes'? 'represents'

Ok. Changed.

20231, 16: 'six regions (Fig. 3).,': *The regions are not really visible from that figure. This confusion is amplified by the fact that the text speaks about different values of the rain ratio while the caption of Fig. 3 talks about a constant value for the explicit experiment shown in the figure. I suggest to add a map in which the six regions are colour coded. This figure can be presented in the appendix. Fig. 3 should not be referred to here.*

The original Fig. 3 has become obsolete as we no longer discuss regional skill scores

20231, 23-29: *please give Friis et al. and Koeve et al. as references for the explicit TA\* tracer*

Added reference to **Koeve et al. 2014**. Friis et al. 2006 did not explicitly include TA\*, but TA0.

20232, 5-10: *perhaps mention explicitly that TA\* of the deepest wet box is affected/modified accordingly (from sediment fluxes)*

True. Added:

**“Simulated TA\* concentrations tend to be lower with the sediment module enabled than without sediment module, because a fraction of the CaCO<sub>3</sub> export flux is removed from the ocean and buried in the geosphere.”**

20232, 16, 'thereafter' ? *is there any thereafter? I though all your runs are spin-up runs. Delete the phrase 'and kept constant thereafter'.*

True. Deleted.

20233, 3: *(here and elsewhere) 'Gangstoet' al misses a blank before 'et'*

Thanks.

20234, 22: *Ref to Tab. 4. Looking at the table I don't understand k<sub>dia</sub> since that is introduced much later in the text. I suggest to improve the table caption accordingly.*

Inserted:

“CaCO<sub>3</sub> export and TA\* inventories for different physical mixing (**diapycnal mixing coefficient, k<sub>dia</sub>** and ...”

20234, 23 *(and elsewhere) a ratio is not to be given in % (but here in mol/mol) Also: I suggest to always be explicit 'molar CaCO<sub>3</sub>/POC export rain ratio' instead of just 'rain ratio'. Rain ratio may be easily mixed up with rain rate, which is POC flux to the sediment. It could also be the POC/PON rain ratio, or whatever. Avoid ambiguities.*

Inserted:

“We define eight such regions each assigned an independent value for the **export** rain ratio parameter (**mol inorganic carbon / mol organic carbon exported, later given in % inorganic to**

**organic carbon exported).** “

20234, 24-25: Units, see general remark above

We follow the units used in Koeve et al. 2014.

20235, 11: *f<sub>calc</sub>* is a fraction, but is given in %, correct please (see above)

Corrected.

20237, 15: change title to 'A first order correction to CaCO<sub>3</sub> burial' since that is the important aspect

Here, we intend to stress that it is about TA\* fluxes. Modified to read:

“A~first order correction for ocean-sediment **TA\*** fluxes ..”

20237, 20-21: isn't this in conflict with 20238, 12-13? '25%' is not equivalent to 'largely unchanged'; also the phrase on 20237 is presenting some results in the mid of the methods presentation. Improve please.

No. Largely unchanged on 20237, 20-21 refers to the fluxes of CaCO<sub>3</sub> export and of CaCO<sub>3</sub> dissolution within the water column. Text on 20238, 12-13 refers to the TA\* inventory. This is affected as CaCO<sub>3</sub> burial removes the corresponding alk-equivalents.

The results discussed in this section refer to the application of a sediment correction and do not represent a main result such as estimated export and dissolution fields and we prefer to keep the text as is.

20238, 8: 'sediment BURIAL correction'

Inserted.

20239, 8, 'by definition' this is explicitly true for your model TA\* tracer, but not 'by definition' for the reconstructed (or diagnosed) TA\*; you mentioned some non-zero (negative) values yourself, likely in waters close to outcrops or at the surface

Adjusted text to: “**close to zero**”

20239, 11, 'age of water' this is very implicitly known here only; you could refer to A2, though that is  $\delta^{14}C$  which is not age (see e.g. Koeve et al., 2015, GMD, and refs therein)

The sentence is intended to provide a qualitative explanation for the increase in TA\* from the deep Atlantic to the deep Pacific.

Added:

“... increasing with the age of water masses (see Fig. A2 showing the distribution of  $\Delta^{14}C$ , a **proxy for water mass age**).”

20241, 3: Fig. 7: I don't understand how the black line in Fig. 7 reflects the sums of the coloured lines ('the sums of regional PDFs', line 4).

In the previous regional skill assessment, the regional probability density functions (the coloured lines) are added to obtain the PDF for the global ocean (black line) by convolution

(<https://en.wikipedia.org/wiki/Convolution>). In the revised manuscript, we present a global skill-score approach and the convolution of regional results is not needed anymore. The computation of PDFs is now explained in section 3.3.2.

20141, Fig. 8: *SO export fluxes show strong discontinuities when moving from PAC to ATL and from ATL to IND. That points to some limitation of your realisation of a regional approach (e.g. not considering the SO as an explicit region). This should be discussed.*

This concerns the main issue raised by reviewer # 1. Please see our response to reviewer 1.

20241, 18-20: *treatment of deepest wet box in no-sediment runs needs to be presented earlier, i.e. section 3*

Done. Section 3.1 extended to read:

“In sensitivity simulations with the sediment module enabled, the flux of  $\text{CaCO}_3$ , and of other particles, reaching the sea floor is passed to the sediment module from where a  $\alpha$ -fraction potentially re-dissolves back into the water column. **In simulations without the sediment module, the entire flux reaching the ocean floor re-dissolves back into the water column.**”

20242, 6-14: *I wonder how sensitive that is to the aspect of having no feedback from  $\text{CaCO}_3$  dissolution on the imposed omega field*

Please see the response above.

20244, 3,  $k_{\text{dia}}$ . *This is one of the details I missed earlier in the paper.*

It is now explicitly mentioned in the Introduction that uncertainties in  $k_{\text{dia}}$  are discussed in Section 4.

20244: *are global mean  $\delta^{14}\text{C}$  values meaningful? Koeve et al., 2015 GMD showed that different ocean models which applied the same 'scaling factor' may have quite different preformed  $\delta^{14}\text{C}$ ; hence the global mean  $\delta^{14}\text{C}$  is not a good measure of the mean age; this is likely the case also for one model with different  $k_{\text{dia}}$  realisations, I suspect; please discuss*

The simulated global mean preindustrial  $\Delta^{14}\text{C}$  signature of DIC is a meaningful first-order measure to indicate model performance with respect to surface-to-deep transport and water mass age in our model. On basin average, simulated surface  $\Delta^{14}\text{C}$  signatures are close to observation-inferred signatures. In addition, surface values vary relatively little with the applied changes in diapycnal diffusivity. Thus,  $\Delta^{14}\text{C}$  difference in the thermocline and the deep ocean and mean ocean  $\Delta^{14}\text{C}$  reflect changes in the surface-to-deep exchange time scales. In other words, and as illustrated in Figure A4, surface-to-deep  $\Delta^{14}\text{C}$  and thus the surface-to-deep age difference is low for high diapycnal mixing (strong overturning) and low for low diapycnal mixing.

The following text is added in the first paragraph of section 4.3.3 (now section 4.3.2):

**“Simulated surface-to-deep  $\Delta^{14}\text{C}$  gradients are too low (high) relative to the observed gradients for the high (low) diapycnal diffusivity parameter, thereby indicating too fast (slow) surface-to-deep water exchange (Fig. A4).”**

20245, 26-28: *This is implicit only in the comparison of upper and lower panels of Fig. 6. Could you prepare a figure to make that explicit, please? Also, I think Fig. 6 should be shown much earlier in the paper. It could help to understand Figs. 7-9 which you discuss before Fig. 6.*

We prefer not to add additional figures as the number of figures is already large. Text added such that it is clear that this comparison is necessary.

20246, 5-9: *One of the CaCO<sub>3</sub> related papers by Andy Ridgwell should be discussed here. Didn't that show also that parameter values could not be constrained well/independently from TA data, if I recall correctly.*

The following text was added at the end of the second paragraph of section 5.1:

**“In addition, Ridgwell et al., 2007, used an Ensemble Kalman Filter approach to assimilate total alkalinity and phosphate data into their model and determined a global CaCO<sub>3</sub> export flux of 1.2 Gt-C y<sup>-1</sup>. “**

And at the end of section 5.4:

**“This approach is used in previous studies (Archer et al., 1994, Ridgwell et al., 2007).”**

20246, Section 4.5. *You use flux data instead of TA\* as a constraint. Is it possible to combine both? Would that be a better constraint?*

Ideally, multiple constraints would have a narrow and overlapping confidence interval, such that only a small interval fulfills both constraints and is therefore more probable. Here, the confidence interval arising from the TA\* data constraint is much smaller and well within the confidence interval obtained with the flux measurements. In this sense, flux measurements do not point to a more unique optimal solution.

20247: *You discuss the TA\*-CFC-age method before introducing it. I suggest to reorganise the text accordingly.*

A reference to the TA\*-CFC age method is needed here to explain the high export values reported by Berelson et al., 2007. The shortcomings of the method are, however, better explained in the context of upper ocean CaCO<sub>3</sub> dissolution.

The text has been modified to read:

**“This estimate is based on sediment trap data and other information constraining the flux to the deep ocean (> 2000 m to 0.6±0.4 Gt-C yr<sup>-1</sup>) and results obtained with the so-called TA\*-CFC age method suggesting an upper ocean dissolution of 1 Gt-C yr<sup>-1</sup>. The TA\*-CFC age method is heavily criticized by Friis et al., 2006 and tends to bias estimates systematically towards high values (Friis et al., 2006). This method and its shortcomings are further discussed in the next section on upper ocean dissolution.** While our estimated flux to the deep ocean of 0.52 (0.43-0.61) Gt-C yr<sup>-1</sup> is roughly consistent with the budget of Berelson et al., 2007, their export estimate, and upper ocean dissolution, is in clear conflict with our results and those of other studies (Lee, 2001, Sarmiento et al., 2006, Jin et al., 2006) that apply a range of different methodologies. We attribute this mismatch to deficiencies in the TA\*-CFC age method, **implying that the export estimate by Berelson et al., 2007 is biased high.”**

20249, *Fig. 10 very nicely reflects the current status of our quantitative understanding of CaCO<sub>3</sub> export. This is very helpful.*

Thank you.

20249, 26, *lab slang again: 'the TA\*-CFC age method' needs to be introduced before being*

*referred to that often; 20249-20250 (Section 5.2) Please rewrite this paragraph. First explain how the TA\*-CFC method is supposed to work, thereafter its by now well know caveats. Overall there is too much talking about estimates that have been disqualified 10 years ago by Friis et al.. But what about the work of Barrett, you cite that paper earlier, but do not refer much to the non-TA\* related details presented there. Do the same arguments apply?*

The caveat and the study by Friis et al. may not be known to all readers as suggested by the reviewer. As the method is still applied in a recent study (Barrett et al., 2014) and used to derive the widely cited estimates by Berelson et al., 2007 it seems appropriate to discuss this method in the context of our findings.

The references to the TA\*-CFC method are now deleted in the first paragraph of section 5.2, except in the last sentence where it is used to introduce the following paragraph on the method. The text of the first two paragraphs of section 5.2 is modified and the description of the TA\*-CFC age method is now extended to read:

“.. As mentioned above, we link **the differences between the estimates of Berelson et al. 2007 and this study** to methodological problems (**Friis et al., 2006**) associated with the TA\*-CFC age method **that very likely introduce a bias in the results of Berelson et al., 2007.**

The TA\*-CFC age method relies on deduced, observation-derived TA\* concentrations and estimates of water mass age, typically derived from measurements of chlorofluorocarbons (CFCs) and their known atmospheric history. **TA\* concentrations are plotted against their CFC-age and a line is fitted to this data.** The higher the TA\* concentration for a~given water mass, the more TA\* must have been added by dissolution to this particular water parcel **according to this method.** The slope of the relationship between TA\* and age **is in this sense** the CaCO<sub>3</sub> dissolution rate (**mol/(volume x time)**).”

Barrett et al. 2014 present estimates of CaCO<sub>3</sub> dissolution in the the top 1000 m of the North Atlantic along the A16N transect. These authors suggest upper ocean dissolution of CaCO<sub>3</sub> by biologically-mediated mechanisms based on the measured decrease of CaCO<sub>3</sub> particles with depth and an application of the TA\*-CFC age method. The following text is added in the first paragraph of section 5.2:

**“High dissolution rates in the range of ~ 0.1 to 0.4 mmol m<sup>-3</sup> yr<sup>-1</sup> are estimated by Barrett et al., 2014 for a transect in the upper tropical and northern North Atlantic. These values are much larger than our estimates of order 0.01 mmol m<sup>-3</sup> yr<sup>-1</sup> for the upper tropical and northern Atlantic. These high estimates are based on the measured decrease of suspended CaCO<sub>3</sub> particles with depth multiplied with a CaCO<sub>3</sub> particle settling velocity of 80 m day<sup>-1</sup>. These estimates may be affected by uncertainties in the assumed particle settling velocity. CaCO<sub>3</sub> particle settling velocities are reported by Jansen et al., 2002, to vary greatly (0.15 to 3440 m day<sup>-1</sup>) and to be typically order one m day<sup>-1</sup> for coccolitophorides and several 100 m day<sup>-1</sup> for foraminifera and pteropods. Our dissolution rates would be consistent with the measured depth gradient in suspended biogenic CaCO<sub>3</sub> particles for an average settling velocity of a few m day<sup>-1</sup>.”**

*Section 5.3: For the relative importance of shelf vs. open ocean CaCO<sub>3</sub> production, perhaps refer to Milliman or some other global CaCO<sub>3</sub> production review that considers non-open ocean realms.*

The following references are added at the end of section 5.3:

**Milliman, GBC, 1993, Vecsei and Berger, GBC, 2004**

*Section 5.4: I see the advantage applying the the 'constant' dissolution formulation to e.g. climate models, but are there potential downsides of your suggestion? Discuss please.*

Text added at the end of the paragraph:

**“A shortcoming of the application of an exponential particle flux profile for CaCO<sub>3</sub> is that it is not easy to account for the potential influence on dissolution of changes in environmental variables, including a decrease in saturation state as expected under ongoing ocean acidification, or in the the quality, form and size distribution of exported CaCO<sub>3</sub> particles.”**

*Section 6: Perhaps you should at least mention the limitation of your study, which I argued about above: i.e. that you prescribed the omega distribution from observations and CaCO<sub>3</sub> dissolution can not feed back on its conditions.*

Please see our response above. First paragraph extended with:

**“The saturation state of water with respect to calcite and aragonite is prescribed using observational estimates to provide realistic boundary conditions for the CaCO<sub>3</sub> dissolution parameterization.”**

*Overall, a very interesting work, which I was very happy to read and review - though it was not always easy. Looking forward to see an improved version being published.*

Many thanks for your helpful comments.

# A probabilistic assessment of calcium carbonate export and dissolution in the modern ocean

G. Battaglia<sup>1,2</sup>, M. Steinacher<sup>1,2</sup>, and F. Joos<sup>1,2</sup>

<sup>1</sup>Climate and Environmental Physics, Physics Institute, University of Bern, Bern, Switzerland

<sup>2</sup>Oeschger Centre for Climate Change Research, University of Bern, Bern, Switzerland

Correspondence to: G. Battaglia (battaglia@climate.unibe.ch)

**Abstract.** The marine cycle of calcium carbonate ( $\text{CaCO}_3$ ) is an important element of the carbon cycle and co-governs the distribution of carbon and alkalinity within the ocean. However,  $\text{CaCO}_3$  export fluxes and mechanisms governing  $\text{CaCO}_3$  dissolution are highly uncertain. We present an observationally-constrained, probabilistic assessment of the global and regional  $\text{CaCO}_3$  budgets. Parameters governing pelagic  $\text{CaCO}_3$  export fluxes and dissolution rates are sampled using a Monte Carlo Latin-Hypercube scheme to construct a 1000 member ensemble with the Bern3D ocean model. Ensemble results are constrained by comparing simulated and observation-based fields of excess dissolved calcium carbonate ( $\text{TA}^*$ ). The minerals calcite and aragonite are modelled explicitly and ocean–sediment fluxes are considered. For local dissolution rates either a strong or a weak dependency on  $\text{CaCO}_3$  saturation is assumed. In addition, there is the option to have saturation-independent dissolution above the saturation horizon. The median (and Median (68 % confidence interval) of global  $\text{CaCO}_3$  export in the constrained model ensemble for global biogenic  $\text{CaCO}_3$  export is 0.90 (0.72–1.05)  $\text{Gt-C GtPICyr}^{-1}$ , that is within the lower half of previously published estimates (0.4–1.8  $\text{Gt-C GtPICyr}^{-1}$ ). The spatial pattern of  $\text{CaCO}_3$  export is broadly consistent with earlier assessments. Export is large in the Southern Ocean, the tropical Indo–Pacific, the northern Pacific and relatively small in the Atlantic. The Dissolution within the 200 to 1500m depth range (0.33; 0.26–0.40  $\text{GtPICyr}^{-1}$ ) is substantially lower than inferred from the  $\text{TA}^*$ -CFC age method ( $1 \pm 0.5 \text{GtPICyr}^{-1}$ ). The latter estimate is likely biased high as the  $\text{TA}^*$ -CFC method neglects transport. The constrained results are robust across a range of diapycnal mixing coefficients and, thus, ocean circulation strengths. Modelled ocean circulation and transport time scales for the different setups were further evaluated with CFC11 and radiocarbon observations. Parameters and mechanisms governing dissolution are hardly constrained by either the  $\text{TA}^*$  data or the current compilation of  $\text{CaCO}_3$  flux measurements such that model realisations with and without saturation-dependent dissolution achieve skill. We suggest to apply saturation-independent dissolution rates in Earth System Models to minimise computational costs.

## 1 Introduction

The cycling of calcium carbonate ( $\text{CaCO}_3$ ) forms an important component of the marine carbon cycle. It co-governs the surface-to-deep gradients of alkalinity and dissolved inorganic carbon (DIC) in the ocean (Volk and Hoffert, 1985), dominates deep ocean alkalinity fluxes, and influences the surface fields of DIC dissolved inorganic carbon and alkalinity, thereby providing the background conditions for the uptake of excess anthropogenic carbon from the atmosphere. However, the export and dissolution fluxes of  $\text{CaCO}_3$  are highly uncertain. For example, current estimates of  $\text{CaCO}_3$  export diverge by a factor of  $\sim 4$  (0.4–1.8 Gt-C yr<sup>-1</sup>, summarised in Berelson et al., 2007).

The  $\text{CaCO}_3$  cycle is driven by calcifying organisms such as coccolithophorids, foraminifera or pteropods, which remove calcium ( $\text{Ca}^{2+}$ ), alkalinity, and DIC and carbonate ( $\text{CO}_3^{2-}$ ) ions from the pelagic surface ocean waters to form shells and structures of  $\text{CaCO}_3$ . These  $\text{CaCO}_3$  particles are eventually exported out of the surface, gravitationally sink through the water column and dissolve at depth or get buried in ocean sediments. The formation and dissolution of  $\text{CaCO}_3$  uptake and release of introduces a vertical gradient in alkalinity and DIC dissolved inorganic carbon. These gradients have been sustained against the counteracting forces of physical mixing and transport, which would otherwise have removed these gradients. This redistribution of alkalinity and carbon by biogenic and physical transport affects the partitioning of carbon between the ocean and atmosphere and a reduction, expected under ongoing ocean acidification, or even a complete stop of  $\text{CaCO}_3$  export tend to decrease atmospheric  $\text{CO}_2$  by a few ppm, and in the extreme case by up to  $\sim 50$  ppm, on century time scales (Heinze, 2004; Gangstø et al., 2011).

There are different mineral forms of  $\text{CaCO}_3$  and solubility is higher for high-magnesium calcite (typically present in fish) and aragonite (typically present in free-swimming pelagic sea snails and sea slugs (pteropods)) than for calcite (typically present in calcifying algae (coccolithophorids)). Thermodynamic considerations suggest that dissolution of  $\text{CaCO}_3$  particles occurs only when the product of the calcium and carbonate ion concentrations in the surrounding environment is below the saturation product. The saturation product of all minerals increases with increasing pressure (Mucci, 1983). At depth, respiration of organic matter additionally decreases the concentration of  $\text{CO}_3^{2-}$ . As a result, the bulk of the water in the deep ocean is undersaturated with respect to  $\text{CaCO}_3$  minerals, generally enabling their dissolution, and oversaturated in the upper ocean, thermodynamically hindering their dissolution (Steinacher et al., 2009). Overall, the quantitative understanding of dissolution kinetics is, however, low and published estimates of saturation-dependent dissolution kinetic parameters range over several orders of magnitude (summarised in Sarmiento and Gruber, 2006).  $\text{CaCO}_3$  dissolution may, nevertheless, still occur in the upper ocean in suitable, undersaturated microenvironments which would be present for instance in the guts of zooplankton, suspended organic aggregates, or fecal pellets (Bishop et al., 1980; Milliman et al., 1999; Jansen and Wolf-Gladrow, 2001). There are in fact several tracer-based studies reporting  $\text{CaCO}_3$  dissolution above the saturation horizon of bulk seawater (Barrett et al., 2014; Feely et al., 2002, 2004; Sabine et al., 2002b;

Chung et al., 2003). In a modelling study, Friis et al. (2006), nevertheless, demonstrated that the  
65 ~~method TA\*-CFC age method~~, which is often employed to derive these upper ocean dissolution  
rates (Berelson et al., 2007, see Discussion section on TA\*-CFC age method), might not be applica-  
ble, because this ~~method~~ methods neglects physical transport and mixing of alkalinity. It is therefore  
still debated where and how fast settling CaCO<sub>3</sub> particles are dissolved in the water column. Another  
70 complication, typically neglected in previous studies on open water CaCO<sub>3</sub> dissolution, is arising  
from ocean–sediment interactions and the influence of associated burial and redissolution fluxes on  
alkalinity and carbon concentrations in the open ocean (Archer, 1996).

Here we propose an alternative, probabilistic assessment of the global CaCO<sub>3</sub> budget. We con-  
sider explicitly the transport and mixing of alkalinity and account for ocean–sediment interactions  
to probabilistically constrain the CaCO<sub>3</sub> cycle with the observation-based distribution of the TA\*  
75 tracer. TA\* reflects the imprint of the CaCO<sub>3</sub> cycle on alkalinity (see Sect. 2) and is therefore im-  
pacted by CaCO<sub>3</sub> export, water column dissolution, physical transport and mixing of the released  
alkalinity and DIC and ~~and~~ ocean–sediment fluxes. For the probabilistic flux assessment, a large  
range of calcite and aragonite export and dissolution flux parameterisations are employed within  
our Earth System model of intermediate complexity (EMIC) – the Bern3D model – in a Monte  
80 Carlo Latin-Hypereube setup with 1000 members. The Bern3D model calculates the correspond-  
ing modelled steady-state tracer concentrations of TA\*. The most probable export and dissolution  
fluxes are then the ones resulting in modelled TA\* fields that match closely the observation-derived  
TA\* distribution. The aim is to assign uncertainty estimates that will be consistent with both the  
observations and model equations – a classical data assimilation problem (see Sect. 3.3). It is ex-  
85 pensive to perform simulations with interactive sediments (Heinze et al., 1999; Gehlen et al., 2006;  
Tschumi et al., 2011) due to long spin-up times required to bring ocean and sediments in equilibrium  
and we account a posteriori for the influence of sediment burial and dissolution fluxes on TA\* (see  
Sect. 3.3). This approach represents an alternative to the interpretation of concentrations without  
a physical model or the interpretation of flux/rate measurements within the water column, which are  
90 generally much sparser (~ 156 flux measurements in the water column (Wilson et al., 2012) and  
~ 56 benthic dissolution flux measurements (Berelson et al., 2007), globally) and more difficult to  
obtain. We apply the Wilson et al. (2012) data compilation of water column fluxes as an additional  
constraint for comparison. Additional sensitivity analyses with respect to vertical diffusion (k<sub>dia</sub>, see  
Sect. 4) are illustrated. The results are compared and contrasted to data-based estimates of export  
95 and dissolution (as summarised in Berelson et al., 2007). ~~In particular, this adds to the discussion  
initiated in on the difficulty to uniquely relate upper ocean TA\* concentrations to either dissolution  
or mixing processes.~~ Finally, implications for the parameterisation of CaCO<sub>3</sub> dissolution in Earth  
System Models are discussed.

## 2 Observation-derived TA\*

100 Total alkalinity data are from the GLODAP carbon climatology (Key et al., 2004) and salinity  
(Antonov et al., 2010), temperature (Locarnini et al., 2010), oxygen and phosphate (Garcia et al.,  
2010a, b) data are from the World Ocean Atlas. These observational data serve to split the alkalinity  
signal into its different physical and biogeochemical components such as TA\*, our target variable  
in the data assimilation. The gridded data products from GLODAP and the World Ocean Atlas are  
105 derived from samples taken during the previous few decades. We first regridded all required, gridded  
datasets to the Bern3D model grid (40x41x32 grid boxes) using the area-weighted regridding method  
of Ferret before deriving the other properties.

TA\*, our target variable in the data assimilation, is a constructed tracer (Feely et al., 2002; Sabine  
et al., 2002a; Chung et al., 2003; Koeve et al., 2014) to exclusively capture the imprint of CaCO<sub>3</sub>  
110 dissolution on alkalinity. TA\* is, in this sense, one of three components of measured total alkalinity  
(TA, Eq. 1, mean concentration 2.427 mol m<sup>-3</sup>). TA\* can be extracted from TA by accounting for  
preformed (TA<sup>0</sup>, Eq. 2) and remineralised alkalinity (TA<sup>r</sup>, Eq. 3):

$$TA = TA^0 + TA^r + TA^*. \quad (1)$$

TA<sup>0</sup> (mean concentration  $\sim 2.389$  mol m<sup>-3</sup>) is the background or preformed concentration, set at  
115 the ocean surface, and mixed conservatively in the ocean interior. Accordingly, TA<sup>r</sup> and TA\* are by  
definition zero in the surface ocean. To describe TA<sup>0</sup> in the ocean interior, one relies on a multi-linear  
regression relationship for surface ocean total alkalinity based on surface ocean salinity ( $S$ ) and  
PO ( $PO = O_2 + r_{-O_2:PO_4} \cdot PO_4$ ,  $r_{-O_2:PO_4} = 170$ , Broecker, 1974) and sometimes surface ocean  
temperature ( $T$ ) as explanatory variables (all conservative variables, see Eq. (2), Gruber et al., 1996;  
120 Sabine et al., 2002a; Feely et al., 2002).

$$TA^0 = a_0 + a_1 \cdot S + a_2 \cdot T + a_3 \cdot PO \quad (2)$$

The coefficients,  $a_i$ , are estimated from observations of TA (Key et al., 2004),  $S$  (Antonov et al.,  
2010),  $T$  (Locarnini et al., 2010), and PO (Garcia et al., 2010a, b) in the surface ocean. The linear  
regression fit is sometimes further subdivided to include only specific basins (Feely et al., 2002; Ko-  
125 eve et al., 2014). Table 1 summarises different regressions, including previously published regression  
estimates as well as new estimates by us calculated on the Bern3D model grid (B3D). ~~The We first  
regridded the explanatory variables on the Bern3D model grid (40x41x32 grid boxes) using the  
area-weighted regridding method of Ferret. The regression coefficients were then determined from  
these regridded fields.~~ The root mean squared deviations (RMSE) between these fits are smaller than  
130 0.00465 mol m<sup>-3</sup> (i.e. smaller than 0.2 %, excluding the Gruber et al. (1996) equation, which relies  
on an older database from 1996). From these different options, we accordingly chose the Global  
B3D linear regression as robust regression for TA<sup>0</sup>.

TA<sup>r</sup> (mean concentration  $-18 \text{ mmol m}^{-3}$ ) is linked stoichiometrically to the apparent oxygen utilisation (AOU, Garcia et al., 2010b, Eq. 3) and accounts for decreases in TA due to the oxidation  
135 of organic nitrogen, phosphorous, and sulfur (OM).

$$\text{TA}^r = r_{\text{Alk:OM}} \cdot r_{\text{NO}_3:-\text{O}_2} \cdot \text{AOU} = 1.26 \cdot 16/170 \cdot \text{AOU} \quad (3)$$

We set  $r_{\text{Alk:OM}}$  to 1.26 (Kanamori and Ikegami, 1982) and  $r_{\text{NO}_3:\text{O}_2}$  to 16/170 (Anderson and Sarmiento, 1994) to uniformly, and globally link AOU changes to changes in TA (as in Feely et al., 2004; Koeve et al., 2014). Wolf-Gladrow et al. (2007) propose an 8 % higher value for  $r_{\text{Alk:OM}}$  of  
140 1.36, based on a different sulphur to carbon ratio. In addition, we note that AOU has been suggested to overestimate true oxygen utilisation by 20–25 % (Ito et al., 2004; Duteil et al., 2013). Accordingly, TA<sup>r</sup> might be associated with an uncertainty of  $\sim 20$  %. ~~We used the area-weighted regridding method of Ferret to regrid the AOU observations to the Bern3D model grid.~~

The remaining signal, then, is TA\* (mean concentration  $\sim 57 \text{ mmol m}^{-3}$ ), the changes in alkalinity due only to the CaCO<sub>3</sub> cycle (Fig. 1). The ~~shown cross-sections always go through the Atlantic (25W), across the Southern Ocean (58S) into the Pacific, and through the Pacific (175W).~~ The global average RMSE of any of the described ways (16 in total) of accounting for TA<sup>r</sup> (25 % lower AOU or different  $r_{\text{Alk:OM}}$ ) and TA<sup>0</sup> (either 2 or 3 explanatory variables, and either global or regional) from our reference choices is  $\sim 4 \text{ mmol m}^{-3}$  (average RMSE 3.9, 3.8, 3.1  $\text{mmol m}^{-3}$  in  
145 the Atlantic, Pacific and Indian Ocean, respectively, i.e.  $\sim 7$  %). It is to note that this approach, inherent to its empirical nature, yields slightly negative TA\* values in some places. TA\* integrates to about 37.5 Pmol C or 75 Pmol Alk-equivalents of which  $\sim 41$  % come to lie above the calcite saturation horizon (similar to Koeve et al. (2014) who find 44.7 % of the TA\* inventory above the calcite saturation horizon). These estimates are robust across the different sources of uncertainty.  
155 TA\* concentrations are expressed in alkalinity equivalents throughout this paper and we do not divide TA\* concentrations by a factor of 2 as done in many observational studies which express TA\* in terms of carbon changes. TA\* inventories are in Pmol C and CaCO<sub>3</sub> fluxes are given in carbon units (Gt-C yr<sup>-1</sup>, mmol-C m<sup>-3</sup> yr<sup>-1</sup>, mmol-C m<sup>-2</sup> yr<sup>-1</sup>).

### 3 The modelling framework

160 To constrain the alkalinity fluxes associated with CaCO<sub>3</sub> cycling, we introduce different export and dissolution fluxes (with a total of 15 +3 degrees of freedom) within the biogeochemistry component of the Bern3D dynamic ocean model. The parameters of the new formulations describing the export and dissolution fluxes of CaCO<sub>3</sub> are varied using a Monte Carlo sampling method (McKay et al., 1979; Steinacher et al., 2013) ~~the Latin-Hypercube sampling method~~ and the resulting model  
165 ensemble, including 1000 members, is run to a pre-industrial steady state producing a broad range of solutions (see Sect. 3.2). The alkalinity fluxes associated with the CaCO<sub>3</sub> cycle are then constrained by comparing observation-based and simulated TA\* data using a Bayesian approach fol-

lowing Steinacher et al. (2013); a skill score is assigned to each ensemble member and used as a weight for the computation of median values and probability density functions from the ensemble results. The sediment module is not included in the ensemble due to extensive computational cost (~ 150 vs. ~ 8 CPU h for a single member run with and without the sediment, respectively). Instead, we re-run the model configurations which achieved the best skill scores with interactive sediments to account for CaCO<sub>3</sub> burial and sediment redissolution a posteriori ([see Sect. 3.3.3](#)). =

### 3.1 The Bern3D Model

175 The Bern3D model couples a dynamic ocean, sea ice, an energy-moisture balance atmosphere, a marine biogeochemical cycle, a dynamic global vegetation model, and an ocean sediment module (Müller et al., 2006; Tschumi et al., 2011; Ritz et al., 2011; Roth et al., 2014). Here [an ocean a-version](#) with a horizontal resolution of 41 by 40 grid cells and 32 logarithmically-scaled vertical layers is used (see also Roth et al., 2014). [The horizontal resolution is the same for the components atmosphere, ocean, sea ice, and sediments of the Bern3D model.](#) Transport and mixing of tracers in the ocean is based on Edwards et al. (1998) and Müller et al. (2006) as a three-dimensional frictional geostrophic model. The model has an isopycnal diffusion scheme and Gent–McWilliams parameterisation for eddy-induced transport (Griffies, 1998). The NCEP/NCAR monthly wind-stress climatology (Kalnay et al., 1996) is prescribed at the surface. Air–sea gas exchange for CO<sub>2</sub> is implemented according to OCMIP-2 protocols (Najjar et al., 1999; Orr and Najjar, 1999). [The global mean air-sea transfer rate is reduced by 19% compared to OCMIP-2 to match observation-based estimates of natural and bomb-produced radiocarbon](#) (Müller et al., 2008)~~with a reduced scaling factor following~~. A two-dimensional energy moisture balance model [represents the at the same horizontal resolution as the ocean describes the](#) atmosphere (Ritz et al., 2011). The model is spun up to equilibrium under preindustrial conditions, with atmospheric CO<sub>2</sub> set to 278 ppm. The spin-up period is 4000 years without the sediment module and 50 000 years with the sediment module. Remaining model drifts are negligible. [We implicitly neglect potential changes in TA\\* over the industrial period by comparing model results for preindustrial conditions with TA\\* data reconstructed from recent measurements. Such changes are negligible in simulations with prescribed anthropogenic forcing in the Bern3D model.](#)

195 The marine biogeochemical module computes the cycling of carbon(~~C~~), ~~alkalinity(Alk)~~, ~~phosphate()~~, ~~iron(Fe)~~, ~~oxygen()~~, ~~silica()~~, [alkalinity, phosphate, iron, oxygen, silica](#), and carbon isotopes. New production of organic material in the model is limited by temperature, light, phosphate, and iron following Doney et al. (2006) as described by Parekh et al. (2008) and Tschumi et al. (2011). [One third \(33%\)](#)~~Two thirds (68 %)~~ of the new production is exported out of the euphotic zone (defined at 75 m) as particulate organic matter (POM), with the reminder contributing to the dissolved organic matter pool. Within biogeochemically similar regions/provinces a parameter termed rain ratio linearly scales the pattern of POM export to CaCO<sub>3</sub> export ([silica-limitation is not considered here](#)).

We define ~~eight such regions~~~~six such regions~~(Fig. ??), each assigned an independent value for the  
205 ~~export rain ratio parameter (mol inorganic carbon / mol organic carbon exported, later given in %~~  
~~inorganic to organic carbon exported)~~~~rain-ratio parameter~~. These include the ~~Pacific, Atlantic and~~  
~~Indian sections of the~~ Southern Ocean (~~< 35<30° S, separated at 240° W, 63° W and 30° E~~), the  
tropical (~~3530° S to 30° N~~) Pacific, Atlantic, and Indian Ocean, and the northern (> 30° N) Atlantic  
(including the Arctic) and Pacific Ocean. A global parameter ( $f_{\text{calc}}$ ) determines how much of the  
210 total  $\text{CaCO}_3$  export flux represents calcite and how much represents aragonite ( $1 - f_{\text{calc}}$ ). Abiotic  
 $\text{CaCO}_3$  precipitation is virtually absent in today's ocean and not considered (reviewed in Sarmiento  
and Gruber, 2006).

In the model, we implemented  $\text{TA}^*$  as an explicit, idealised tracer (Koeve et al., 2014). It captures  
the alkalinity equivalents of  $\text{CaCO}_3$  dissolution whenever it occurs and mixes this signal, accord-  
215 ingly.  $\text{TA}^*$  values are set to zero throughout the surface ocean.

In sensitivity simulations with the sediment module enabled, the flux of  $\text{CaCO}_3$ , and of other  
particles, reaching the seafloor is passed to the sediment module from where a fraction potentially  
re-dissolves back into the water column. ~~In simulations without the sediment module, the entire flux~~  
~~reaching the ocean floor re-dissolves back into the water column. Simulated  $\text{TA}^*$  concentrations tend~~  
220 ~~to be lower with the sediment module enabled than without sediment module, because a fraction of~~  
~~the  $\text{CaCO}_3$  export flux is removed from the ocean and buried in the geosphere.~~ The sediment di-  
agenesis model (Heinze et al., 1999; Gehlen et al., 2006; Tschumi et al., 2011) features the same  
horizontal resolution as the ocean model and 10 layers resolving the top 10 cm of the seafloor. It dy-  
namically calculates the transport, remineralisation/redissolution and bioturbation of solid material  
225 within the top 10 cm of the seafloor as well as pore-water chemistry and diffusion as described in  
detail in Tschumi et al. (2011). Solutes diffuse over a boundary layer of 1 cm between the sediment  
column and the lowermost ocean grid cell. Four solid components ( $\text{CaCO}_3$ , opal, POM and clay)  
and pore water substances (carbon and carbon isotopes, total alkalinity, phosphate, nitrate, oxygen  
and silicic acid) are modelled. The pore water carbonate ion concentration determines whether, and  
230 at which rate,  $\text{CaCO}_3$  dissolves. Aragonite and calcite are not distinguished within the sediment  
module and  $\text{CaCO}_3$  is assumed to be in the form of calcite. Any solid material that is pushed out  
of the diagenetic zone disappears into the subjacent diagenetically consolidated zone. During the  
spin-up of the ocean–sediment model, the net loss of alkalinity, and other tracers such as carbon  
and nutrients, to the sediments is immediately replaced by corresponding riverine inputs which are  
235 distributed uniformly along the coastlines (and then taken to be part of  $\text{TA}^0$ ). The riverine input is  
diagnosed at the end of the spin-up~~and kept constant thereafter~~.

The model features the main water masses and mixing time scales of the ocean, an essential  
prerequisite to realistically simulate  $\text{TA}^*$  and other tracers. The simulated and observed distributions  
of the ventilation tracers  $\Delta^{14}\text{C}$  and CFC11 are provided in the supplementary information (~~Figs. A2~~  
240 ~~and A3~~) along with a Taylor Diagram (Taylor, 2001) of CFC11,  $\Delta^{14}\text{C}$ , temperature, salinity, DIC,

TA, PO<sub>4</sub>, oxygen, and TA\* (Fig. A1 to A3). Globally, the correlation coefficient and standard deviation of the median relative to the standard deviation of the observations ( $\sigma_{\text{rel.}}^{\text{obs.}}$ ) are 0.94 and ~~0.99~~ 0.97 for  $\Delta^{14}\text{C}$  and ~~0.91~~ 0.9 and 0.98 for CFC11.

### 3.2 CaCO<sub>3</sub> dissolution within the water column

245 The dissolution equations for calcite and aragonite are implemented using equations with identical functional forms, but with different parameters for each mineral. In the following, we do not explicitly distinguish the two minerals to ease notation. The dissolution of calcite and aragonite below the euphotic zone is assumed to ~~(possibly)~~ be a function of the saturation state of the bulk seawater,  $\Omega$ , and the particle concentration per unit of water volume,  $[\text{CaCO}_3]$  (see Gangstø et al. (2011) for  
250 a discussion):

$$\frac{d[\text{CaCO}_3]}{dt} = -k_{\text{eff}}(\Omega) \times [\text{CaCO}_3]. \quad (4)$$

~~The saturation state is defined by the ratio of the product of calcium ion concentration times carbonate ion concentrations to the saturation product,  $K_{\text{sp}}$ :~~

$$k_{\text{eff}}(\Omega) = k_0 \times (1 - \Omega)^n \times H(\Omega - 1) + k_{\text{bg}}.$$

255  $k_0$  and  $k_{\text{bg}}$  are rates in units of 1/time.  $H$  is the Heaviside function, which is zero for supersaturated and 1 for undersaturated water. The saturation state is defined by the ratio of the product of calcium ion concentration times carbonate ion concentrations to the saturation product,  $K_{\text{sp}}$  (Mucci, 1983):

$$\Omega = \frac{[\text{Ca}^{2+}][\text{CO}_3^{2-}]}{K_{\text{sp}}}. \quad (5)$$

260  $\Omega$  values larger than one correspond to oversaturated and  $\Omega$  values smaller than one to undersaturated conditions.  $\Omega$  and thus  $k_{\text{eff}}$  are grid cell specific. At super-saturation, the dissolution rate equals the constant background rate  $k_{\text{bg}}$  (which can be zero). With increasing under-saturation, the dissolution rate increases towards its maximum value ( $k_{\text{bg}} + k_0$ ).  $n$  is a unitless parameter and determines the deviation from linearity of this increase. For simplicity and to avoid the addition of further free  
265 parameters, a constant sinking velocity,  $v$ , is assumed and identical for both calcite and aragonite particles. The flux profile of CaCO<sub>3</sub> then takes the form

$$F_{i,j}(z_k) = F_{i,j}(z_{k-1}) \cdot \exp\left(\frac{-k_{\text{eff}}(\Omega_{i,j,k})}{v} \cdot \Delta z_k\right) \quad (6)$$

where  $F$  is the downward flux of either calcite or aragonite particles per unit area evaluated at the bottom of each tracer grid cell at depth  $z_k$ .  $i$ ,  $j$ , and  $k$  are grid cell indices indicating longitude,

270 latitude, and depth.  $\Delta z_k$  denotes grid cell height. The export flux is set equal to  $F$  ( $z = 75$  m) at the depth of the euphotic zone. Particles are dissolved instantaneously and sinking is not explicitly resolved in this formulation, reducing computational costs.  $v/k_{\text{eff}}$  is in units of m, and, if assumed constant, can be interpreted as the dissolution length scale, i.e. the depth at which the flux has decreased to  $1/e$  (~~i.e.~~ to  $\sim 37\%$ ) of the export flux at 75 m. Any particles reaching the sea floor  
275 are dissolved completely in the appropriate lowermost box, except when the sediment module is included.

In Fig. 2 we illustrate three dissolution cases to explore the sensitivity of  $\text{TA}^*$  to dissolution profiles which cover the sampled uncertainty in dissolution rate parameters. Table 2 ([middle column,  \$k\_{\text{dia,ref}}\$](#) ) summarises the resulting  $\text{TA}^*$  inventories and their relative distribution. The three dissolution rate profiles are selected to represent a case with constant, saturation-independent, dissolution  
280 (constant) and two cases where this background dissolution rate is set to zero and  $\text{CaCO}_3$  dissolves only below the saturation horizon. In the fast (slow) case, aragonite (chosen to represent 10 % of the total) and calcite (90 % of total export) dissolves quickly (slowly) below the saturation horizon. Aragonite and calcite dissolve within a few hundred meters below the saturation horizon in the fast  
285 case, while most  $\text{CaCO}_3$  dissolves on the ocean floor in the slow case.

The choice of the dissolution rate profile has a substantial influence on the simulated  $\text{TA}^*$  inventory ([Fig. 2, Table 2](#)). The global  $\text{TA}^*$  inventory is 38 Pmol C for the case with a constant, saturation-independent dissolution and a rain ratio of  $\sim 7\%$ , which is close to the observation-derived inventory of 37 Pmol C. The simulated inventory is [48 and 63](#)~~47 and 62~~ Pmol C for the fast and slow  
290 cases (where no dissolution occurs above the saturation horizon), respectively, and by that substantially higher.  $\text{TA}^*$  accumulates in the deep ocean when all  $\text{CaCO}_3$  is dissolved below the saturation horizon of aragonite and calcite and no dissolution is permitted above. The  $\text{TA}^*$  inventory and concentrations are sensitive to the choice of the dissolution rate profile, supporting our choice of  $\text{TA}^*$  as a target variable to constrain dissolution rates.

### 295 3.3 Ensemble simulations and metrics for skill assessment

#### 3.3.1 The [Monte Carlo Latin-Hypereube](#) Ensemble

Following Steinacher et al. (2013) [and](#) Steinacher and Joos (2016) ~~;~~ we run a ~~Latin-Hypereube ensemble with 1000 member Latin Hypercube ensemble members~~ to constrain the export flux out of the surface ocean, and the dissolution of aragonite and calcite within the water column. ~~To this end, 13 parameters are sampled using the~~ Latin Hypercube sampling ~~method~~ (McKay et al., 1979)  
300 [is a statistical, Monte Carlo method to generate controlled random samples from a multidimensional distribution \(15 dimensions in our case\). The defined parameter ranges are divided into equally probable intervals \(1000 in our case\). Random samples are then generated in each interval. This method ensures that the sampled values are representative of the real variability while minimising](#)

305 ~~the number of required samples and thus the computational costs. We sample 15 parameters and~~  
~~–~~We apply uniform priors based on literature information. The free parameters are the ~~eight~~ six  
rain-ratio parameters (prior range: 0 to 18 % ~~for the Pacific and South Indian regions, prior range:~~  
0 to 16 % for the tropical Indian, prior range: 0 to 7 % for the North and tropical Atlantic, and  
prior range: 0 to 10 % for the South Atlantic), defining the total amount of CaCO<sub>3</sub> export for each  
310 of the six regions. The prior ranges of the rain ratios for the three Atlantic regions are limited to  
maximal 10%. This selection is based on results from previous ensemble setups that revealed an  
overestimation of TA\* for high rain ratios in the Atlantic domain. Further we include the, ~~the~~-frac-  
tion  $f_{\text{calc}}$  (~~1–0.5~~100–50) defining the split between aragonite and calcite export, and  $3 \times 2$  param-  
eters governing the dissolution kinetics for calcite and aragonite, respectively. These are  $k_0$  (0.05–  
315  $10 \text{ day}^{-1}$ ) and  $n$  (1–4), describing fast and slow dissolution kinetics as a function of undersaturation,  
and  $k_{\text{bg}}/v$  ( $0–1/2500 \text{ m}^{-1}$ ), the length scale associated with a constant, background dissolution rate  
acting both above and below the saturation horizon.  $v$  is kept constant at  $100 \text{ m day}^{-1}$ .

The observation-based saturation-state of the bulk seawater with respect to aragonite and calcite is  
prescribed for each model grid cell. It was calculated with the carbonate chemistry package seacarb  
320 (Gattuso et al., 2010) from GLODAP (Key et al., 2004) and World Ocean Atlas 2009 (WOA09) (Lo-  
carmini et al., 2010; Antonov et al., 2010). Seacarb calculates carbonate chemistry based on pressure,  
temperature, salinity, alkalinity, DIC, silica and phosphate. ~~is prescribed for each model grid cell.~~  
This reduces computational costs as the carbonate chemistry package of the online model requires  
substantial computational time. Also, this avoids mismatches in the modelled and observation-based  
325 saturation states, which are also due to model deficiencies in the cycling of organic matter and phys-  
ical transport. Mismatches in modelled and observed saturation states are particularly large in the  
North Pacific, where the modelled calcite saturation horizon is up to 1.5 km too deep. The calcite  
saturation horizon is well represented in the South Pacific, Indian and Atlantic by the model. The  
results presented in Sect. 4 suggest that estimated CaCO<sub>3</sub> export production fields and dissolution  
330 rates are insensitive to the choice of the saturation field, because saturation-dependent and saturation  
independent parameterizations of dissolution yield similar TA\* fields.

### 3.3.2 Skill scores

Global ~~Regional~~-skill scores,  $S_m S_r$ , are assigned to each member,  $m$ , of the Latin-Hypercube en-  
semble. ~~The regions considered are the Atlantic, Pacific and Indian Oceans (each including their~~  
335 ~~section of the Southern Ocean):~~

$$S_{m,r} = \exp\left(-0.5 \cdot \text{MSE}_{r}^{\text{rel}}\right). \quad (7)$$

$MSE_r^{rel}$  is the relative mean squared error of the simulated  $TA^*$  concentrations from member  $m$  with respect to observation-derived  $TA^*$  within region  $r$ :

$$MSE_r^{rel} = \sum_j a_j \times \frac{(TA_j^{*model} - TA_j^{*obs} - TA_j^{*sedcorr})^2}{\sigma^2}. \quad (8)$$

The sum includes all grid cells (indexed  $j$ ) within the respective region.  $TA_j^{*model}$  denotes simulated  $TA^*$  concentrations for ensemble member  $m$  and  $TA_j^{*obs}$  observation-based  $TA^*$  concentrations estimated by using the Global B3D regression (Sect. 2).  $TA_j^{*sedcorr}$  is a correction term arising from  $CaCO_3$  burial in sediments, further explained below.  $a_j$  is the grid cell volume used as weight in the sum.  $\sigma^2$  represents the combined error of the observation-based  $TA^*$  estimates and of the model and sets the scale against which model deviations are evaluated. Model deviations from the observations are considered large or small relative to the magnitude of  $\sigma^2$  (Schmittner et al., 2009). The total uncertainty in observation-derived, gridded  $TA^*$  data is difficult to estimate and includes uncertainties due to extrapolation of limited number of measurements, uncertainties in individual tracer measurements, and in the computation of  $TA^*$  from tracer data. The error associated with the procedure to compute  $TA^*$  - in our case, the observational error (average RMSE 3.9, 3.8, 3.1  $mmol\ m^{-3}$  in the Atlantic, Pacific and Indian Ocean, respectively, see Sect. 2) is small compared to the model error (the best run achieves a RMSE of 11, 18, 16  $mmol\ m^{-3}$  in the Atlantic, Pacific and Indian Ocean, respectively). Following Steinacher et al. (2013) and Schmittner et al. (2009), we estimate  $\sigma^2$  as the (volume-weighted) variance of the model–data discrepancy for the ensemble member with the lowest MSE in each basin (this variance is 275, 120, 265, 240  $(mmol\ m^{-3})^2$  in the Atlantic, Pacific and Indian Ocean, respectively); this corresponds to  $MSE^{rel}$  close to unity for the best-fitting ensemble member.

The skill scores  $S_m$ ,  $S_r$  of the individual ensemble members are likelihood-type functions corresponding to a Gaussian distribution of the data-model discrepancy ( $TA^{*model} - TA^{*obs} - TA^{*sedcorr}$ ) with zero mean and variance  $\sigma^2$ .  $S_m$  is used as an indication of the relative performance/credibility of each individual model configuration. Configurations which have relatively small deviations from the data are judged more probable than configurations which differ greatly from the observations.

$S_m$  and  $S_r$  are used as weight to compute probability density functions (PDFs) and related measures such as the median (50<sup>th</sup> percentile) and PDF of the ensemble results for aragonite and calcite export and dissolution. Global values are the sums of the respective regional PDFs (by means of convolution) and global maps are composites of the respective regional skill scores. The application of individual skill scores for the Atlantic, Pacific, and Indian Ocean permits us to better account for potential differences in the dissolution parameters between individual basins, without increasing the numbers of free, tunable model parameters. This seems justified as the  $TA^*$  concentrations within each of these basins is predominantly influenced by export from within the basin as seen in Fig. ?? . Figure ?? shows the percentage contribution to the 16<sup>th</sup> and 84<sup>th</sup> percentiles defining the one

standard deviation confidence interval ( $1\sigma$ ) of the ensemble results. PDFs represent weighted and normalised histograms of the variables of interest. The normalisation is such that the integral over a PDF equals 1. A cubic spline interpolation is used to arrive at a continuous PDF from the discrete, normalised histogram. For the computation of median and confidence ranges the histograms are converted to cumulative distribution functions (CDFs). We interpolate linearly within the discrete CDFs to arrive at the chosen percentiles (i.e. CDF=(0.16, 0.5, 0.68)). ~~TA\* column inventory attributable to the export from one of the six selected rain-ratio regions and is further discussed in the result section. For comparison, we also computed and applied skill scores for the global ocean.~~

The above explanations apply for any simulated quantity of interest. In the following we will present PDFs, median values, and  $1\sigma$  confidence ranges for aragonite and calcite export and dissolution as well as for tracer concentrations at individual grid cells or integrated over regions or the whole ocean. Spatial integrations are done for each ensemble member individually and before computing the PDFs and associated measures from the full ensemble.

### 3.3.3 A first order correction for ocean-sediment TA\* fluxes

CaCO<sub>3</sub> burial removes alkalinity from the ocean water column and lowers concentrations and the overall TA\* inventory relative to a run without the sediment module. Riverine input compensates this loss. This input of alkalinity is added to the surface ocean and by that to the part of the preformed alkalinity component (TA<sup>0</sup>), leaving TA\* unchanged. CaCO<sub>3</sub> export and dissolution within the water column and the corresponding fluxes of alkalinity and TA\* remain largely unchanged between runs with and without sediments.

Ideally, the ensemble would be run fully interactively with the sediment module enabled to account for all important processes within the CaCO<sub>3</sub> cycle. However, this is computationally too expensive as the sediment module requires a long spin up to achieve equilibrium. A first order correction term TA\*<sup>sedcorr</sup> that accounts for the influence of CaCO<sub>3</sub> burial and dissolution fluxes on TA\* is estimated as follows. First, the ~~regional~~ skill scores are computed as described above with TA\*<sup>sedcorr</sup> set to zero. Then, the 14 ~~ten~~-best ensemble members are selected ~~for each of the three basins (regions)~~ and re-run with the sediment module enabled (~~3 × 10 simulations~~). The mean difference in the TA\* fields between the simulations with and without sediments yields the sediment correction, TA\*<sup>sedcorr</sup>, ~~for each region~~.

These simulations with sediments yield a mean global burial flux of 0.120.0737 Gt-C yr<sup>-1</sup> (see Table 3: 0.0110.0063 Gt-C yr<sup>-1</sup> in the Atlantic, 0.0620.043 Gt-C yr<sup>-1</sup> in the Pacific, and 0.0420.025 Gt-C yr<sup>-1</sup> in the Indian Ocean). This is within ~~smaller, but comparable to~~ the estimate by Feely et al. (2004) of 0.1–0.14 Gt-C yr<sup>-1</sup>.

The sediment burial correction on TA\* is largest ~~correction is substantial~~ in the Pacific and smallest ~~Indian Ocean and small~~ in the Atlantic (Figs. 3.4 and 4). The global TA\* inventory in runs with

the sediment is ~~6.98.55~~ Pmol C lower compared to the runs without the sediment (see Table 3:  
410 ~~0.90.39~~ Pmol C in the Atlantic, ~~4.66.9~~ Pmol C in the Pacific, and ~~1.41.24~~ Pmol C in the Indian  
Ocean). This reduction is equal to the inventory of the TA\*<sup>sedcorr</sup> correction and ~~~16 and ~20~25~~  
~~and ~17~~ % of the observation-derived TA\* inventory of the Pacific and Indian Ocean, respectively.  
TA\* concentrations are affected relatively uniformly below 1 km and differences in TA\* between  
simulations with and without sediment module tend to vanish toward the surface ocean (Figs. 3  
415 ~~and 4~~). Correspondingly, the spatial patterns of TA\* are very similar for simulations with and with-  
out sediments; correlation coefficients are ~~> 0.99 for the Atlantic, > 0.97 for the Indian and > 0.91~~  
~~for the Pacific Ocean~~. We expect that the correction will tend to increase the export flux of CaCO<sub>3</sub>  
in the optimisation to compensate for the loss by burial, but will not strongly affect dissolution  
parameters as the spatial patterns of TA\* remain similar with or without correction.

420 A few caveats apply to this first order estimate of TA\*<sup>sedcorr</sup>. First, our approach involves a few,  
likely minor, technical inconsistencies. Aragonite is not treated explicitly in the sediment module  
and all CaCO<sub>3</sub> is assumed to be in the form of calcite; this may tend to bias sediment burial high  
as calcite is less soluble. The saturation state within the sediments is computed interactively with  
modelled ocean boundary conditions; this may locally lead to inconsistencies as CaCO<sub>3</sub> dissolution  
425 within the ocean water column is computed using the prescribed, observation-based saturation state.  
The alkalinity flux associated with organic matter remineralisation within the sediment is not explic-  
itly distinguished and included in the flux of TA\* from sediments to the ocean; this results in a bias  
on order of 5 % in the redissolution flux and a negligible influence on the sediment correction. ~~More~~  
~~importantly, the simulated burial is at or below the lower range of observation-based estimates, and~~  
430 ~~our correction may be biased small.~~

## 4 Results

### 4.1 Observation-derived vs. simulated TA\*

Reconstructed TA\* (Fig. 1, TA\*<sup>obs</sup>) is – by definition – ~~close to~~ zero at the ocean surface and corre-  
spondingly low within the well-ventilated North Atlantic Deep Waters, Antarctic Intermediate and  
435 Mode Waters, and within North Pacific Intermediate Waters. TA\* concentrations in the deep ocean  
are increasing with the age of water masses (see Fig. A2 of  $\Delta^{14}\text{C}$  which is a proxy for water mass  
age) as the dissolution of CaCO<sub>3</sub> continues to add TA\* along the flow path. TA\* concentrations are  
around 40 to 50 mmol m<sup>-3</sup> in the deep Atlantic (Antarctic Bottom Water) and in the deep Southern  
Ocean and increase to 130 mmol m<sup>-3</sup> in the northern Pacific. The reconstructed basin-mean profiles  
440 in the Pacific and Indian basin (Fig. 4) show strong gradients in the upper 1500 m and relatively  
uniform values below that. ~~Concentrations Basin-mean concentrations~~ are generally much lower in  
the Atlantic than in the Pacific.

The unconstrained model ensemble yields a large range of TA\* concentrations (Fig. 4, grey shading). The optimisation procedure ~~with the application of regional skill scores~~ greatly reduces this range in simulated TA\* to a comparably narrow confidence interval (Fig. 4, green shading representing the 68 % confidence interval). For example, basin-averaged concentrations in the deep Pacific (4000 m) range between ~~11 to 287~~~~16 to 300~~ mmol m<sup>-3</sup> in the unconstrained ensemble, while the corresponding 68 % confidence interval in TA\* is ~~73 to 122~~~~97 to 130~~ mmol m<sup>-3</sup> in the constrained ensemble. The selected a priori parameter ranges are therefore wide enough to result in a very broad range of TA\* concentrations; the Bayesian optimisation framework confines this initial range around or close to the observation-based values.

The median field from the constrained model ensemble generally captures the ~~observation-based~~ observation-based TA\* pattern (Fig. 5). The correlation coefficient ( $r$ ) between the two fields are ~~0.83, 0.88, 0.77, 0.93~~, and 0.87 in the Atlantic, Pacific, and Indian Ocean, respectively, and the RMSE between the two fields are ~~17.7, 23.8, 19.8~~~~14.57, 20.33, 18.84~~ mmol m<sup>-3</sup> for the respective basins. These deviations correspond, respectively, to ~~57, 28~~ ~~60, 21~~ and 28 % of ~~their~~ the mean TA\* concentration in each basin. Large positive deviations are found in the intermediate waters of the Pacific. This is also evident in the observation-derived basin-mean profiles of TA\*, which generally fall within the 68 % confidence interval of the constrained model ensemble (Fig. 4). In the Atlantic, the ensemble median concentrations are, on basin-average, ~~somewhat~~ higher than the reconstructed ones. In the Pacific and Indian Oceans, the median clearly overestimates TA\* in the thermocline (the 68 % confidence range does not include the observations there) and somewhat underestimates TA\* in the deep ocean. This is likely linked to known deficiencies in the model's circulation. Intermediate and mode waters (with low TA\* concentrations) are not penetrating far enough towards the equator. As a consequence, mixing of TA\* depleted surface waters is too low and TA\* concentrations are too high in the thermocline. Alternatively, we cannot exclude that dissolution may be overestimated in the thermocline of the Pacific and Indian Ocean. This data-model mismatch could potentially be reduced by introducing more than one background dissolution rate constant ( $k_{bg}$ ) or a depth-dependent particle sinking velocity. However, this may simply mask deficiencies in the circulation and we do not attempt such a solution. Generally, the correlation between observed and modelled TA\* is remarkably high.

## 4.2 Probabilistic estimates of CaCO<sub>3</sub> and alkalinity fluxes

The estimated global median export flux of CaCO<sub>3</sub> ~~at 75 m~~ – with its 68 % confidence interval – is ~~0.90 (0.72–1.05)~~~~0.82 (0.67–0.98)~~ Gt-C yr<sup>-1</sup> (Table 4 and Fig. 6). Basin-wide, we find CaCO<sub>3</sub> median export fluxes (and 68 % confidence intervals) of ~~0.12 (0.078)~~~~0.14 (0.087–0.17)~~~~0.198~~ Gt-C yr<sup>-1</sup> from the Atlantic, ~~0.55 (0.39)~~~~0.47 (0.356–0.68)~~~~0.614~~ Gt-C yr<sup>-1</sup> from the Pacific, and ~~0.23 (0.21)~~~~(0.14–0.32)~~~~0.28~~ Gt-C yr<sup>-1</sup> from the Indian Ocean (Table 4 and Fig. 6). ~~Table 4). Recall that all results are based on regional, sediment-corrected skill scores based on TA\*; global values are the sums of the~~

~~regional PDFs.~~ Regionally, largest export fluxes are simulated in the Southern Ocean sector of the  
480 Pacific, in the Pacific equatorial upwelling regions, and in the northwestern Pacific (Fig. 7). In the  
Indian Ocean export fluxes are highest in its eastern tropical regions and in its section of the Southern  
Ocean. In the tropical and northern Atlantic export fluxes are generally low, consistent with the low  
TA\* values in the bulk of NADW and AABW.

Median CaCO<sub>3</sub> export production per unit area in the constrained ensemble is considerably  
485 lower in the Atlantic sector of the Southern Ocean (135 mmol-C m<sup>-2</sup> yr<sup>-1</sup>) as compared to the  
Pacific (301 mmol-C m<sup>-2</sup> yr<sup>-1</sup>) and Indian (326 mmol-C m<sup>-2</sup> yr<sup>-1</sup>) sectors (Fig. 7 top). This  
is attributable to the choice of the regional boundaries ~~The choice of regional skill scores yields~~  
~~different median estimates~~ for the rain ratio regions and the assumption that the spatial pattern of  
export within a region is identical to the pattern simulated by the standard version of the model. The  
490 standard model yields relatively little zonal variation in the CaCO<sub>3</sub> export fluxes in the Southern  
Ocean in contrast to the data assimilation with lower than zonally-averaged export in the Atlantic.  
This reflects the much lower TA\* reconstructed in the deep Atlantic as compared to the deep Pacific  
and Indian (Fig. 1). A large export in the Atlantic sector ~~ratios in the Atlantic, Indian, and Pacific~~  
~~sectors~~ of the Southern Ocean tends to yield high simulated TA\* concentrations in the Antarctic  
495 Bottom Water that fills the deep Atlantic. The Monte Carlo data assimilation therefore requires  
low CaCO<sub>3</sub> export. ~~The export flux~~ in the Atlantic sector to minimize model-data mismatches in  
the deep Atlantic. It is difficult to correctly represent water mass formation and circulation in the  
Southern ocean and our model may be biased. A known bias is that the Atlantic Bottom Water  
circulation is too sluggish, also evidenced by simulated low radiocarbon signatures (Figs A2, A4).  
500 The influence of a potential bias in South Atlantic export on global CaCO<sub>3</sub> export is estimated to  
be relatively small; assuming the same (median) CaCO<sub>3</sub> export per unit area in the Atlantic sector  
as estimated for the Indian sector would yield 0.06 Gt-C yr<sup>-1</sup> higher export than suggested by the  
ensemble median. While our Monte Carlo approach is suitable to estimate export fluxes over larger  
regions, the detailed spatial patterns in CaCO<sub>3</sub> export remain unconstrained. ~~is lower than in the~~  
505 ~~Pacific and Indian sectors. See Sect. 4.3 for further discussion of this feature.~~

Globally, the deposition flux on the respective deepest cells integrates to 0.16 (0.110.24(0.184–  
0.23.308) Gt-C yr<sup>-1</sup>, i.e., ~18~30% of the export flux (Fig. 7, Table 4). Local deposition de-  
pends on the local CaCO<sub>3</sub> export and on how much dissolution is occurring in the water column,  
which itself depends on the saturation state and on the depth of the water column. Particularly in the  
510 North Atlantic, along coastlines and in the Southern Ocean, high fluxes reach the ocean floor. These  
are dissolved into the water column in the ensemble setup without sediment module. Accordingly,  
~82~70% of the global median CaCO<sub>3</sub> export dissolves in the water column. More specifically,  
~37~35% of the CaCO<sub>3</sub> export dissolves in the upper water column above 1500 m, ~44~36%  
below 1500 m depth, with the remaining ~18~29% dissolving at the sea floor (Table 4).

515 Average dissolution profiles for aragonite (red) and calcite (olive) in different ocean regions are displayed in Fig. 8. A peak in aragonite and calcite dissolution is located at or below the depth of the aragonite and calcite saturation horizon, respectively. These dissolution peaks are ~~associated~~ ~~associate~~ with the saturation-dependent dissolution rate coefficients (Eq. 3.2). As is the saturation horizon, these peaks are located deep down in the water column of the north and tropical Atlantic region (at 3–4 km depth for aragonite), at intermediate depth of the South Atlantic, Indian, and Pacific (1.5 km for aragonite) and at relatively shallow depth of the tropical and north Pacific region (~ 700 m for aragonite). As the calcite saturation horizon is found deeper in the water column than the aragonite saturation horizon, so are these dissolution peaks located deeper down in the water column for calcite than for aragonite.

525 Our constrained ensemble includes non-zero values for the background dissolution rate. Consequently, calcite and aragonite ~~are~~ ~~is~~ dissolving throughout the water column, irrespective of the saturation state in the Atlantic, Pacific and Indian Ocean. The percentage of the export flux which dissolves in waters supersaturated with respect to calcite are ~~72~~ ~~79~~ % (~~60–80~~ ~~70–84~~ %), ~~43~~ ~~41~~ % (~~30–53~~ ~~28–53~~ %), ~~68~~ ~~70~~ % (~~55–78~~ ~~55–79~~ %) in the Atlantic, Pacific and Indian Ocean, respectively.

530 We will further investigate in Sect. 4.4 to which extent the finding that a fraction of the  $\text{CaCO}_3$  export dissolves above the calcite saturation horizon and our export and dissolution flux estimates are robust.

### 4.3 Sensitivity of results to ~~choice of metrics~~, ocean–sediment interactions, and circulation

#### 4.3.1 ~~Regional vs. global skill scores~~

535 ~~We assessed each ensemble member’s skill with respect to observation-derived  $\text{TA}^*$  for the three basins Atlantic, Pacific and Indian, separately. For comparison, we also evaluated the results by computing the skill of each member of the model ensemble for the global  $\text{TA}^*$  field.~~

~~The global and regional skill scores yield similar ensemble median  $\text{TA}^*$  fields in the Pacific. In the Indian Ocean and particularly in the Atlantic Ocean, agreement between ensemble median and reconstructed  $\text{TA}^*$  is worse for the global scores (not shown). The misfit in the Atlantic Ocean with global skill scores might arise due to the prescribed, uniform rain-ratio across the entire Southern Ocean. Alternatively, the ensemble size might be too small to fit  $\text{TA}^*$  in all basins using global skill scores. Also, the dissolution rate mechanisms might be different between the different basins. Lastly, deficiencies in the circulation might also cause some of the misfit. We recall that the  $\text{TA}^*$  signal in the Atlantic is dominated by export from Atlantic and Southern Ocean surface waters, whereas the imprint of  $\text{TA}^*$  signals from the Pacific or Indian Ocean ( $> 30\text{S}$ ) on  $\text{TA}^*$  patterns in the Atlantic is small (Fig. ??); export and dissolution from these regions are therefore not responsible for the misfit in the Atlantic.~~

545

The median estimates of global export and water column fluxes would be about  $\sim 20$  (or 0.2) higher and the spread  $\sim 30$  wider for the global skill score approach compared to the standard case; fluxes would be about 0.12 higher in the Atlantic, 0.04 higher in the Indian, and 0.046 higher in the Pacific Ocean with global rather than regional skill scores.

#### 4.3.1 Ocean-sediment interactions

As discussed in Sect. 3.3,  $\text{CaCO}_3$  deposition on, burial within, and redissolution from ocean sediments affects  $\text{TA}^*$  concentrations mainly in the Pacific and Indian Ocean in our model. To assess uncertainties in  $\text{CaCO}_3$  fluxes arising from uncertainties associated with the sediment correction, we set the sediment correction ( $\text{TA}^{*\text{sedcorr}}$ ) of the  $\text{TA}^*$  field to zero to calculate potential skill scores (Eq. 8). This alternative case also illustrates the potential error due to the neglect of ocean-sediment fluxes. Export fluxes of  $\text{CaCO}_3$  are 2, 12, 8, and 84, 14, 13, and 12 % smaller in the Atlantic, Pacific, Indian and global ocean, respectively while the variance is about the same. This is not surprising as we have already noted (Sect. 3.3) that a certain burial flux tends to decrease the  $\text{TA}^*$  pattern uniformly, i.e. the simulations with and without the sediment correlate highly in terms of  $\text{TA}^*$ . The PDF of fluxes is therefore shifted to higher export fluxes, while the preference for dissolution parameters remains the same. The ~~fraction of the total~~  $\text{CaCO}_3$  export that dissolves above 1500 m is ~~4, 6, 12, and 6.6 %~~ higher, 5 % lower, the same, and 4 % lower in the Atlantic, Pacific, Indian and global ocean, respectively, in the setup that neglects sediment fluxes compared to the standard setup.

#### 4.3.2 Implications of different diapycnal diffusivities illustrated for three dissolution rate profiles

The diapycnal diffusivity,  $k_{\text{dia}}$  of the model is varied to probe uncertainties related to the magnitude of the ocean overturning circulation.  $k_{\text{dia}}$  is either set to 0.1 (low), 0.2 (standard), or 0.5 (high)  $\times 10^{-4} \text{ m}^2 \text{ s}^{-1}$ . Increasing  $k_{\text{dia}}$  increases the strength of the overturning circulation, and deep ocean ventilation. Maximum Atlantic Meridional Overturning is 16, 18, and 23 ~~15.6, 17.6, and 22.8~~ Sv (Sverdrups), Southern Ocean overturning is ~~-16~~ 15.7, -14 ~~13.9, and -15~~ 14.6 Sv and maximal deep Pacific overturning is ~~-13, -14, and -20~~ 1.0, 1.4, and 4.1 Sv for the low, standard and high  $k_{\text{dia}}$  simulations, respectively. We compare the simulated (natural)  $\Delta^{14}\text{C}$  of DIC and CFC11 distributions (~~both conservative tracers~~) to their corresponding observations (Key et al., 2004) to evaluate the physical transport (see Appendix). Both are conservative tracers with a time information and indicative of the ventilation time scales of the thermocline and the deep ocean, respectively. The observation-based (Key et al., 2004) global mean (natural)  $\Delta^{14}\text{C}$  of DIC is ~~-151~~ 150.75 ‰. The reference simulation achieves a mean (natural)  $\Delta^{14}\text{C}$  of DIC of ~~-160~~ 159.0 ‰. Correspondingly, ocean radiocarbon signatures become too low (~~-176~~ 173.91 ‰) with the low diapycnal mixing rate and too high with the high (~~-126~~ 126.1 ‰) diapycnal mixing rate (see Fig. A4). Simulated surface-to-deep  $\Delta^{14}\text{C}$  gradients are too low (high) relative to the observed gradients for the high (low) diapycnal

diffusivity parameter, thereby indicating too fast (slow) surface-to-deep water exchange (Fig. A4).

585 The global observation-based CFC11 inventory is estimated to 575 Mmol. The reference simulation yields 513504.0 Mmol CFC11 as the mean inventory over the modelled period between 1990 and 2000. at model year 1994. In the low mixing simulation, this inventory is even lower (479472.3 Mmol) and in the high mixing simulation it is too high (631617.4 Mmol). On a global scale, our reference choice is therefore in better agreement with these physical tracers (see Fig. A4).

590 We vary  $k_{\text{dia}}$  for three illustrative dissolution rate profiles introduced in Sect. 3.2 (see Fig. 2 and Table 2). In the low diapycnal diffusivity case,  $\text{CaCO}_3$  export is 11 % lower and in the high diapycnal diffusivity case,  $\text{CaCO}_3$  export is 30 % higher compared to the standard case. Larger overturning and mixing yields more nutrient input into the euphotic zone and thus more organic matter export.  $\text{CaCO}_3$  export is independent of alkalinity in our model and does not depend on the choice of the dissolution rate. The simulated  $\text{TA}^*$  patterns remain similar and correlation between the patterns is at least 0.93. Basin-average profiles in  $\text{TA}^*$  vary little in the upper ocean and the deep Pacific ( $< 14 \text{ mmol m}^{-3}$ ) and modestly in the deep Atlantic ( $< 44 \text{ mmol m}^{-3}$ ) and deep Indian ( $< 18 \text{ mmol m}^{-3}$ ) when varying diapycnal diffusivity between  $0.1$  and  $0.5 \times 10^{-4} \text{ m}^2 \text{ s}^{-1}$ . Perhaps somewhat surprisingly, the simulated  $\text{TA}^*$  inventory is relatively weakly affected by the choice of  $k_{\text{dia}}$ ; the global  $\text{TA}^*$  inventory varies by less than 74% across the range of  $k_{\text{dia}}$  (Table 2). In other words, variations in the magnitude of ocean ventilation do hardly affect the  $\text{TA}^*$  inventory for a given dissolution rate profile. Higher (lower) export under higher (lower) mixing compensate each other. These changes in  $\text{TA}^*$  inventory are smaller than the influence of the sediment correction (see Table 3) or the choice of the dissolution profile. In conclusion, simulated  $\text{TA}^*$  is only weakly affected by uncertainties in the diapycnal mixing coefficient.

605 The choice of the dissolution rate profile has a substantial influence on the simulated  $\text{TA}^*$  inventory (Table 2). As mentioned previously,  $\text{TA}^*$  accumulates in the deep ocean when all  $\text{CaCO}_3$  is dissolved below the saturation horizon of aragonite and calcite and no dissolution is permitted above. This raises the question whether surface-to-deep transport is too slow in our model. As mentioned above, the radiocarbon signatures as well as CFC11 concentrations are on average close to observations (Figs. A3 and A2). Increasing ocean ventilation by increasing  $k_{\text{dia}}$  results in too young radiocarbon signatures and higher than observed CFC11 concentrations. However, it does not substantially reduce the overestimation of the  $\text{TA}^*$  inventory in those cases.

#### 4.4 How to parameterise $\text{CaCO}_3$ dissolution in an Earth System Model?

615 An important question is how to formulate the dissolution rate of calcite and aragonite particles in Earth System Models. Should the dissolution rate be a function of the simulated aragonite and calcite saturation state of the surrounding water? Should dissolution above the saturation horizon be permitted? In our ensemble, the degrees of freedom allow for either fast or slow dissolution kinetics as a function of saturation, and the option to also dissolve  $\text{CaCO}_3$  above the saturation horizon with

620 a constant dissolution rate. For a more systematic understanding of which parameterisations achieve high skill we return to the sensitivity simulations (Fig. 2).

Interestingly, the different dissolution schemes yield highly correlated patterns of TA\*; the correlation coefficient between the global fields from the fast and slow dissolution scheme is 0.85, and between the fields from the fast and constant scheme is 0.88 in simulations with the same CaCO<sub>3</sub> export (Fig. 2). The high correlation between fast and slow dissolution schemes is not surprising as only 35% of the modern ocean's volume is actually undersaturated with respect to calcite. Differences therefore cannot emerge over much of the ocean and skill is therefore distributed across the range of parameter values sampled.

Figure 9 displays the ~~We analyse the~~ relationship between model skill, background dissolution rate~~dissolution parameterisation~~, CaCO<sub>3</sub> export, and TA\* inventories in the model ensemble. ~~(see Fig. 9) to address these questions.~~ To achieve a high skill (green-to-red coloured dots in the upper panels of Fig. 9), an individual ensemble member needs to reproduce the observation-based TA\* inventory (dashed line) within a limited range. We identify an export range within which TA\* can be reproduced skillfully (vertical green range in the upper panels of Fig. 9). The background rate is responsible for this spread. ~~Surprisingly, a high skill is achieved across the range of different dissolution schemes applied and for a broad range of parameter values. In other words, neither the dissolution scheme nor its parameters are well constrained by the observation-based TA\* field.~~ This is illustrated by plotting the value of the background dissolution rate,  $k_{bg}$  (lower panels of Fig. 9) as a function of the TA\* inventory and export. Generally, the higher the global CaCO<sub>3</sub> export flux, the higher the background dissolution rate required to achieve a high skill. Likewise, lower export can be distributed skillfully without dissolution in supersaturated waters ( $k_{bg} = 0$ ). Apparently, there are trade-offs between the magnitude of export and the applied dissolution parameterisation in terms of TA\*, suggesting that export and dissolution parameters can only be constrained simultaneously within limits when using TA\* as the only constraint. In other words, neither the dissolution scheme nor its parameters are well constrained by the

~~These findings are in line with the results from our sensitivity simulations (Fig. 2, Table 2). The parameterisation with dissolution above the saturation horizon (constant) yields the lowest TA\* inventory, followed by the scheme with fast dissolution below the saturation horizon, and the scheme with dissolution near the ocean floor (slow). A high (low) export is thus required for parameterisations with high (low) dissolution above the saturation horizon to simulate the observation-based TA\* field. Corresponding to the high correlation, the RMSE between normalised observed and normalised modelled fields vary within a limited range (42 to 58%) for the three dissolution cases. The~~ Further, the different dissolution schemes yield highly correlated TA\* fields; the correlation coefficient between the global fields from the fast and slow dissolution scheme is 0.84, and between the fields from the fast and constant scheme is 0.88 in simulations with the same export (Fig. 2). This high spatial correlation in simulated TA\* and uncertainties in CaCO<sub>3</sub>

~~export make makes~~ it difficult to distinguish different dissolution parameterisations. ~~The magnitude of CaCO<sub>3</sub> exports modulates absolute TA\* concentrations and thus model-data bias and root mean square errors.~~ Given these uncertainties, we cannot objectively determine the preferred dissolution  
660 scheme.

#### 4.5 Flux measurements as additional constraint

Global sediment trap data represent another observational constraint of the CaCO<sub>3</sub> cycle. The database of Wilson et al. (2012, see Fig. A5) includes 156 measurements globally and is an update of the Honjo et al. (2008) compilation. For comparison, we constrained the model ensemble using  
665 these sediment trap data instead of the TA\* data as target (Figs. A5 and A6). Skill-scores are ~~again~~ calculated individually for the Pacific, Atlantic, and Indian Ocean. CaCO<sub>3</sub> export fluxes, dissolution profiles and parameters constrained with the sediment trap data are consistent within uncertainties with those constrained by the TA\* data. The sediment trap data, however, yield wider uncertainty ranges, as illustrated in Fig. A6, and do therefore not permit us to reduce uncertainty ranges any  
670 further.

### 5 Discussion

#### 5.1 Export of CaCO<sub>3</sub>

Berelson et al. (2007) summarised current estimates of CaCO<sub>3</sub> export out of the euphotic zone (based on models and data) to 0.4–1.8 Gt-C yr<sup>-1</sup> (spanning factor ~4). Our constrained median estimate of ~~~0.90 ~0.82~~ (ensemble range: ~~0.72–1.050.67–0.98~~) Gt-C yr<sup>-1</sup> therefore lies on the lower ~~part end~~ of these previously published estimates. ~~At the end~~~~In addition~~, these authors suggest that global CaCO<sub>3</sub> export must be higher than 1.6 Gt-C yr<sup>-1</sup>. This estimate is based on sediment trap data and other information constraining the flux to the deep ocean (> 2000 m) to 0.6 ± 0.4 Gt-C yr<sup>-1</sup> ~~and results obtained with the so-called and-on-the~~ TA\*-CFC age method  
680 ~~suggesting an which yields~~ upper ocean dissolution of 1 Gt-C yr<sup>-1</sup>. ~~The TA\*-CFC age method is heavily criticised by~~ Friis et al. (2006) ~~and tends to bias estimates systematically towards high values~~ (Friis et al., 2006). ~~This method and its shortcomings are further discussed in the next section on upper ocean dissolution.~~ While our estimated flux to the deep ocean of ~~0.52 (0.430.58 (0.44–0.61.74)~~ Gt-C yr<sup>-1</sup> is roughly consistent with the budget of Berelson et al. (2007), their export  
685 estimate, and upper ocean dissolution, is in clear conflict with our results and those of other studies (Lee, 2001; Sarmiento and Gruber, 2006; Jin et al., 2006) that apply a range of different methodologies. We attribute this mismatch to deficiencies in the TA\*-CFC age method, ~~implying that the export estimate applied~~ by Berelson et al. (2007) ~~is biased high~~ ~~that tends to bias estimates systematically towards high values (see later discussion).~~

690 Global scale  $\text{CaCO}_3$  export has been previously estimated ~~by the following three studies~~ (see Fig. 10). Jin et al. (2006) diagnosed a global  $\text{CaCO}_3$  export of  $1.1 \text{ Gt-C yr}^{-1}$  by restoring annual-mean potential alkalinity to observations (Key et al., 2004) in the euphotic zone and in the whole water column within the Modular Ocean Model. Sediment burial and sediment-ocean fluxes are included implicitly in this approach. They provide a relatively small uncertainty range of  $0.8$  to  $1.2 \text{ Gt-C yr}^{-1}$  which falls within our range. Most of the uncertainty is attributed to uncertainties in the alkalinity data by these authors. Sarmiento and Gruber (2006) estimated  $\text{CaCO}_3$  export ( $\sim 0.5 \text{ Gt-C yr}^{-1}$ ) by combining satellite NPP (as a mean of the three algorithms (Behrenfeld and Falkowski, 1997; Carr, 2002; Marra et al., 2003)) with the organic particle export model of Dunne et al. (2005) and the rain-ratio estimate of Sarmiento et al. (2002). Lee (2001) derived net  $\text{CaCO}_3$  production 700 ( $\sim 0.92 \pm 0.3 \sim 0.92 \text{ Gt-C yr}^{-1}$ ) from seasonal potential alkalinity decreases. Both approaches focus on information of the surface ocean without taking advantage of information displayed in the full biogeochemical depth profile. In addition, Ridgwell et al. (2007) used an Ensemble Kalman Filter approach to assimilate total alkalinity and phosphate data into their model and determined a global  $\text{CaCO}_3$  export flux of 1.2  $\text{Gt-C yr}^{-1}$ . On average, these ~~four~~ three studies yield a global mean  $\text{CaCO}_3$  export of  $0.930.83 \text{ Gt-C yr}^{-1}$ , close to our median estimate of  $0.900.82 \text{ Gt-C yr}^{-1}$ .

We find peaks in zonally-averaged export in the North Pacific, the tropical Pacific and Indian and in the Southern Ocean and low export fluxes in the subtropics and the tropical Atlantic (Fig. 11). This is in agreement with the results of Jin et al. (2006) and Lee (2001), with the exception that Lee (2001) suggest little  $\text{CaCO}_3$  export in all tropical regions. A significant  $\text{CaCO}_3$  export in the 710 tropics is consistent with deep ocean sediment trap data (Francois et al., 2002; Berelson et al., 2007). As noted by Jin et al. (2006), the low estimates of Lee (2001) for tropical regions is likely related to small signals in seasonal alkalinity in the tropics, hampering their calculations. Concerning the magnitude of the export, our zonally-averaged values are similar to these two studies in the Pacific sector of the Southern Ocean, and smaller in the Atlantic and Indian Southern Ocean sectors as well 715 as in the North Pacific.

Interestingly, Lee (2001) find significant  $\text{CaCO}_3$  export in the North Atlantic, in contrast to Jin et al. (2006), Sarmiento and Gruber (2006), and this study. The relatively low North Atlantic export suggested by these latter studies appears to be in conflict with the occurrence of coccolithophorid blooms in this region (Brown and Yoder, 1994). On the other hand, the low  $\text{TA}^*$  inventory in the 720 Atlantic (Fig. 1) argues for a limited export of  $\text{CaCO}_3$  in this basin.

Carter et al. (2014) defined another alkalinity tracer, termed  $\text{Alk}^*$ , that isolates the portion of the alkalinity signal that varies in response to calcium carbonate cycling and exchanges with terrestrial and sedimentary environments from the portion that varies in response to freshwater and organic matter cycling. These authors compiled a riverine input of alkalinity into the low-latitude Atlantic 725 ( $> 40^\circ \text{ S}$  and  $< 40^\circ \text{ N}$ ) equivalent to  $0.057 \text{ Gt-C yr}^{-1}$ , which is  $\sim 40\%$  of the global continentally derived alkalinity. Their  $\text{Alk}^*$  tracer in the Atlantic has the lowest open-ocean surface concentrations

despite this large riverine source. They conclude that these large riverine inputs must therefore be more than balanced by strong net  $\text{CaCO}_3$  formation. For comparison, our estimates of  $\text{CaCO}_3$  export between ~~35~~<sup>30</sup>° S and 30° N in the Atlantic are ~~0.06 (0.018-0.034 (0.001-0.1,074))~~  $\text{Gt-C yr}^{-1}$ .

730 We note, however, that a direct comparison between these two studies remains difficult. The river input does not strictly have to be compensated by the export flux but rather by the burial flux. Also, the river input gets mixed and is subducted and transported southward by North Atlantic Deep Water and interpretation of concentrations without explicit consideration of transport and mixing is always difficult.

735 Regional patterns of  $\text{CaCO}_3$  export (Fig. 10) vary among the different studies. In our approach  $\text{CaCO}_3$  export fluxes are scaled by a rain ratio to simulated export of particulate organic carbon within each of the ~~eight considered regions~~<sup>six considered regions</sup> and ~~median estimates of the rain ratio for the Atlantic, Indian and Pacific Sectors of the Southern Ocean are estimated individually~~. Thus, the total export for the three Southern Ocean sectors, the Indian Ocean, the tropical and northern Pacific and the tropical and northern Atlantic is constrained by the  $\text{TA}^*$  data, but not the pattern within each of these regions.

## 5.2 $\text{CaCO}_3$ dissolution in the upper ocean

The  $\text{CaCO}_3$  leaving the surface ocean dissolves within the water column, at the sea floor or gets buried. Berelson et al. (2007) get to global dissolution rates of  $\sim 1 \text{ Gt-C yr}^{-1}$  within upper level waters ~~based on the  $\text{TA}^*$ -CFC age method~~, clearly higher than our  $\text{TA}^*$ -based estimate of ~~0.35~~<sup>0.33</sup> ~~(0.26-0.46,40)~~  $\text{Gt-C yr}^{-1}$ . On a regional level, only two out of ten regional estimates ~~by Berelson et al. (2007) based on the  $\text{TA}^*$ -CFC age method~~ are within our Latin-Hypercube uncertainty ranges; these are the estimates for the tropical Pacific (taken as 5° N to 5° S) and the low- and mid-latitude Atlantic (40° S to 40° N) (Table 5). ~~High dissolution rates in the range of  $\sim 0.1$  to  $0.4 \text{ mmol-C m}^{-3} \text{ yr}^{-1}$  are estimated by Barrett et al. (2014) for a transect in the upper tropical and northern North Atlantic. These values are much larger than our estimates of order  $0.01 \text{ mmol-C m}^{-3} \text{ yr}^{-1}$  for the upper tropical and northern Atlantic. These high estimates are based on the measured decrease of suspended  $\text{CaCO}_3$  particles with depth multiplied with a  $\text{CaCO}_3$  particle settling velocity of  $80 \text{ m day}^{-1}$  and neglecting any temporal trend in the  $\text{CaCO}_3$  particle concentration. These estimates may be affected by uncertainties in the assumed particle settling velocity.  $\text{CaCO}_3$  particles settling velocities are reported by Jansen et al. (2002), to vary greatly ( $0.15$  to  $3440 \text{ m day}^{-1}$ ) and to be typically order one  $\text{m day}^{-1}$  for coccolitophorides and several  $100 \text{ m day}^{-1}$  for foraminifera and pteropods. Our dissolution rates would be consistent with the measured depth gradient in suspended biogenic  $\text{CaCO}_3$  particles for an average settling velocity of a few  $\text{m day}^{-1}$ .~~

760 As mentioned above, we link ~~the differences between the estimates of Berelson et al. (2007) and this study~~ <sup>this</sup> to methodological problems (Friis et al., 2006) associated with the  $\text{TA}^*$ -CFC age

method that very likely introduce a high bias in the results of Berelson et al. (2007)~~which were highlighted by~~.

765 The TA\*-CFC age method relies on deduced, observation-derived TA\* concentrations and estimates of water mass age, typically derived from measurements of chlorofluorocarbons (CFCs) and their known atmospheric history. TA\* concentrations are plotted against their CFC-age and a line is fitted to this data. The higher the TA\* concentration for a given water mass, the more TA\* must have been added by dissolution to this particular water parcel according to this method. The slope of  
770 the relationship between TA\* and age is in this sense ~~then yields~~ the CaCO<sub>3</sub> dissolution rate (mol volume<sup>-1</sup> time<sup>-1</sup>).

The method has been criticised for its neglect of explicit transport and mixing processes. In particular, Friis et al. (2006) noted that TA\* signals ended up above the saturation horizon in their model run, even though there was explicitly no dissolution allowed to occur there. This is confirmed by our  
775 sensitivity simulations with no dissolution above the saturation horizon (Fig. 2). This finding does not depend on the choice of the numerical model as mixing within the ocean must spread the TA\* signal within the ocean and establish a surface-to-deep gradient in TA\* in the upper ocean even when all CaCO<sub>3</sub> dissolves at great depth. The TA\*-CFC age method does not account for such processes and assigns dissolution rates in the waters above the saturation horizon irrespective of whether or not  
780 the signal stems from the deep ocean. Our approach to combine TA\* data within an ocean transport model and the approach by Jin et al. (2006) or Lee (2001) avoid this shortcoming.

In addition, we notice, that in most regions the upper ocean TA\* distribution remains remarkably similar within our ensemble, even for very different dissolution rate profiles (see Fig. 2). And in particular, that, for a given export,  $k_{\text{slow}}$  dissolution rate profiles, with most of the dissolution at or near  
785 the ocean bottom, tend to reach highest values of TA\* both in the deep ocean and the thermocline (see also inventories in Table 2). In these cases, most of the TA\* source is added to slowly ventilated waters in the deep where it accumulates over time along deep water flow paths. This high TA\* signal is being brought to the thermocline and eventually to the surface where TA\* is reset to its preformed value of zero. As a result, a larger TA\* gradient is established across the thermocline for deep compared to shallow dissolution. The TA\*-CFC age method would therefore have a tendency to assign  
790 higher dissolution rates in the wrong cases. This further illustrates the difficulty to uniquely relate upper ocean tracer concentrations to either dissolution or mixing processes.

### 5.3 CaCO<sub>3</sub> dissolution in the deep ocean

Turning to the deep ocean, Berelson et al. (2007) suggest based on sediment trap and benthic  
795 dissolution data that the particle flux below 2000 m is  $0.6 \pm 0.3 \text{ Gt-C yr}^{-1}$ , sea floor dissolution for sites > 2000 m averages  $0.4 \pm 0.3 \text{ Gt-C yr}^{-1}$ , and carbonate burial in deep marine sediments is  $0.1 \text{ Gt-C yr}^{-1}$ . Our estimate of the particle flux below 1500 m is 0.52 (0.430.58 (0.44–0.61.74)  $\text{Gt-C yr}^{-1}$ . Thus, the compilation of sediment trap data by Berelson et al. (2007) roughly

supports our particle flux at 1500 m. However, the split between sea floor dissolution and open water  
800 dissolution in the deep is different. We estimate that most of the deep ocean particle flux dissolves  
within the water column (0.40 (0.320.3(0.23–0.47.37) Gt-C GtPIC $\text{yr}^{-1}$  below 1500 m). The steady  
state burial flux for the runs with interactive sediments is 0.120.074 Gt-C $\text{yr}^{-1}$ , corresponding to the  
burial of 1.951.23  $\times 10^{13}$  mol Alk, $\text{yr}^{-1}$ , this is comparable in magnitude but smaller than the total  
alkalinity input by rivers estimated to be  $2.3 \times 10^{13}$  mol $\text{yr}^{-1}$  by Carter et al. (2014) or the burial flux  
805 estimated by Dunne et al. (2012) of 0.121 Gt-C $\text{yr}^{-1}$ . We note that  $\text{CaCO}_3$  formation by coral reefs  
and burial in shallow coastal waters (Milliman, 1993; Vecsei and Berger, 2004) is not considered in  
our coarse resolution model.

#### 5.4 Parameterisations of $\text{CaCO}_3$ within Earth System Models

Uncertainties appear too large to objectively determine well-defined parameter ranges for the disso-  
810 lution rates of calcite and aragonite (judging from both the  $\text{TA}^*$  and the flux data compilation).  
A good agreement between simulated and observed  $\text{TA}^*$  fields can be achieved irrespective of  
whether dissolution is assumed to depend on the calcite or aragonite saturation state or whether  
dissolution rates are assumed to be constant throughout the water column. We recall that the com-  
putation of the saturation state by carbonate chemistry routines across all grid cells and for each  
815 model time step poses a considerable computational burden. For simplicity and to minimise com-  
putational costs, we therefore recommend to describe  $\text{CaCO}_3$  dissolution by a constant dissolution  
rate in Earth System Models as long as these uncertainties exist. This yields an exponential particle  
flux profile when assuming constant settling velocities throughout the water column. This approach  
is used in previous studies (Archer and Maier-Reimer, 1994; Ridgwell et al., 2007). A shortcoming  
820 of the application of an exponential particle flux profile for  $\text{CaCO}_3$  is that it is not easy to account  
for the potential influence on dissolution of changes in environmental variables, including a decrease  
in saturation state as expected under ongoing ocean acidification, or in the quality, form, and size  
distribution of exported  $\text{CaCO}_3$  particles ~~has been in use, for example in the study by.~~

#### 6 Summary and conclusions

825 Constraining the  $\text{CaCO}_3$  cycle comes down to three fundamental questions: how much  $\text{CaCO}_3$   
is exported from the surface ocean, where is this  $\text{CaCO}_3$  dissolved in the water column and how  
much is buried in sediments. Here, we setup a probabilistic framework to constrain the  $\text{CaCO}_3$   
budget within the Bern3D EMIC with observationally-based ~~observationally-based~~  $\text{TA}^*$  as robust  
target variable. The saturation state of water with respect to calcite and aragonite is prescribed  
830 using observational estimates to provide realistic boundary conditions for the  $\text{CaCO}_3$  dissolution  
parameterization. In addition to the uncertainty estimates obtained by our Bayesian Latin-Hypercube  
framework, we also consider uncertainties related to the choice of metrics to define the assimilation

target, including ~~regional vs. global skill scores or~~ flux measurements as alternative target variable, uncertainties in ocean transport, and ocean sediment interactions.

835 We estimate that 0.72–1.05 Gt-C ~~0.67–0.98 Gt PIC~~ with a best estimate of 0.90 Gt-C ~~0.82 Gt PIC~~ are exported out of the surface ocean each year in the form of biogenic  $\text{CaCO}_3$ . Of this about 37.35 % (0.33 (0.20–0.44)  $\text{Gt-C yr}^{-1}$ ) are estimated to dissolve in the open water column above 1500 m, and 44.36 % (0.40 (0.32–0.47)  $\text{Gt-C yr}^{-1}$ ) in the open water column below, with the remainder (0.16 (0.11–0.24)  $\text{Gt-C yr}^{-1}$ ) deposited on open ocean sediments, 840 globally. Sensitivity simulations with interactive sediments suggest that about 30% ~~two-thirds~~ of the deposition flux dissolves back into the ocean and 70% ~~one-third~~ gets buried in consolidated sediments.

We find that the higher the export fluxes within the constrained, likely ranges, the more likely dissolution above the saturation horizon is needed to distribute  $\text{TA}^*$  skillfully in the model. Different kinds of dissolution schemes (with and without dissolution above saturation) achieve realistic 845  $\text{TA}^*$  distributions within the export ranges identified. Therefore, background dissolution above the saturation horizon cannot be ruled out from this Latin-Hypercube ensemble evaluated within the Bern3D EMIC. Future progress likely depends on a better observational characterisation of particle concentrations, size distribution, and settling ~~and size distribution~~ within the water column. Physical 850 transport and mixing reduces concentration gradients such that conceptually different dissolution schemes (e.g. dissolution permitted above saturation or not) cannot be distinguished statistically. This implies that concentrations cannot be used to infer dissolution rates directly. It also implies that dissolution parameterisations remain uncertain. For simplicity and to minimise computational costs, we suggest to use saturation-independent parameterisations of  $\text{CaCO}_3$  dissolution within Earth Sys- 855 tem Models.

## Appendix: Model evaluation and additional constraints

It is an essential prerequisite for the model to feature the main water masses and mixing time scales of the ocean to realistically simulate biogeochemical tracers such as  $\text{TA}^*$ . In this Appendix, we graphically document ocean model performance by comparing simulated and observation-based distribu- 860 tions for a range of tracers. Results are for a pre-industrial steady state of the Bern3D ocean model configuration with a horizontal resolution of 40 by 41 grid cells and 32 vertical layers as coupled to an energy balance and sea ice module without sediment module. The atmospheric history of CFC11 is prescribed according to Bullister (2011). Here we do not account for potential changes in ocean circulation and CFC11 solubility over the industrial period.

865 Figure A1 provides a Taylor Diagram (Taylor, 2001) of CFC11,  $\Delta^{14}\text{C}$ , temperature, salinity, DIC,  $\text{TA}$ ,  $\text{PO}_4$ , oxygen, and  $\text{TA}^*$  of the standard model configuration with a constant rain ratio of 7 % and of the median  $\text{TA}^*$  of the weighted model ensemble. Modelled and observed distributions of the

ventilation tracers  $\Delta^{14}\text{C}$  and CFC11 are compared along a section through the Atlantic, Southern Ocean and Pacific (Figs. A2 and A3). Simulated and observation-based basin-mean vertical gradients of CFC11 and natural  $\Delta^{14}\text{C}$  are compared in Fig. A4 for three simulations where diapycnal mixing is set to a low, the standard, and a high value ( $k_{\text{dia}} = (0.1, 0.2, 0.5) \times 10^{-4} \text{ m}^2 \text{ s}^{-1}$ ). Results bracket observation-based profiles with best agreement between model and observations for the standard setup.

*Acknowledgements.* Many thanks to [an anonymous reviewer and Wolfgang Koeve for their critical and constructive reviews. Also, thanks to](#) Kitack Lee, Xin Jin and Niki Gruber for sharing their data, and to Raphael Roth for his contributions to the modelling framework. This work was supported by the Swiss National Science Foundation and the European Project CARBOCHANGE (264879) which received funding from the European Commission's Seventh Framework Programme (FP7/20072013). [We acknowledge the support from the International Space Science Institute \(ISSI\). This publication is an outcome of the ISSI's Working Group on "Carbon Cycle Data Assimilation: How to consistently assimilate multiple data streams".](#)

## References

- Anderson, L. A. and Sarmiento, J. L.: Redfield ratios of remineralization determined by nutrient data analysis ,  
Global Biogeochemical Cycles, 8, 65–80, 1994.
- Antonov, J. I., Seidov, D., Boyer, T. P., Locarnini, R. A., Mishonov, A., Garcia, H. E., Baranova, O. K., Zweng,  
885 M. M., and Johnson, D. R.: World Ocean Atlas 2009, Volume 2: Salinity, NOAA Atlas NESDIS 69, U.S.  
Government Printing Office, Washington, D.C., 2010.
- Archer, D.: A data-driven model of the global calcite lysocline, Global Biogeochemical Cycles, 10, 511–526,  
doi:10.1029/96GB01521, <http://dx.doi.org/10.1029/96GB01521>, 1996.
- Archer, D. and Maier-Reimer, E.: Effect of deep-sea sedimentary calcite preservation on atmospheric CO<sub>2</sub>  
890 concentration, Nature, 367, 260–263, doi:10.1038/367260a0, 1994.
- Barrett, P. M., Resing, J. A., Buck, N. J., Feely, R. A., Bullister, J. L., Buck, C. S., and Landing, W. M.: Calcium  
carbonate dissolution in the upper 1000 m of the eastern North Atlantic, Global Biogeochemical Cycles, 28,  
386–397, doi:10.1002/2013GB004619, <http://dx.doi.org/10.1002/2013GB004619>, 2014.
- Behrenfeld, M. J. and Falkowski, P. G.: Photosynthetic rates derived from satellite-based chlorophyll concen-  
895 tration, Limnology and oceanography, 42, 1–20, 1997.
- Berelson, W. M., Balch, W. M., Najjar, R., Feely, R. a., Sabine, C., and Lee, K.: Relating estimates of CaCO<sub>3</sub>  
production, export, and dissolution in the water column to measurements of CaCO<sub>3</sub> rain into sediment traps  
and dissolution on the sea floor: A revised global carbonate budget, Global Biogeochemical Cycles, 21,  
doi:10.1029/2006GB002803, <http://doi.wiley.com/10.1029/2006GB002803>, 2007.
- 900 Bishop, J. K. B., Collier, R., Kettens, D., and Edmond, J.: The chemistry, biology, and vertical flux of particulate  
matter from the upper 1500 m of the Panama Basin, Deep Sea Res. A., pp. 615–616, 1980.
- Broecker, W. S.: “NO”, a conservative water-mass tracer , Earth Planet. Sc. Lett., 23, 100–107, 1974.
- Brown, C. W. and Yoder, J. a.: Cocolithophorid blooms in the global ocean, Journal of Geophysical Research,  
99, 7467–7482, 1994.
- 905 Bullister, J. L.: Atmospheric CFC-11, CFC-12, CFC-113, CCl<sub>4</sub> and SF<sub>6</sub> Histories.  
[http://cdiac.ornl.gov/ftp/oceans/CFC\\_ATM\\_Hist/](http://cdiac.ornl.gov/ftp/oceans/CFC_ATM_Hist/), Carbon Dioxide Information Analysis Center, Oak  
Ridge National Laboratory, US Department of Energy, Oak Ridge, Tennessee, 2011.
- Carr, M.-E.: Estimation of potential productivity in Eastern Boundary Currents using remote sensing, Deep-Sea  
Research Part II: Topical Studies in Oceanography, 49, 59–80, [http://www.scopus.com/inward/record.url?  
910 eid=2-s2.0-0036140387\(&partnerID=40\(&md5=580afff1a0622a900f0bd61548e6abbf](http://www.scopus.com/inward/record.url?eid=2-s2.0-0036140387(&partnerID=40(&md5=580afff1a0622a900f0bd61548e6abbf), 2002.
- Carter, B. R., Toggweiler, J. R., Key, R. M., and Sarmiento, J. L.: Processes determining the marine alkalinity  
and carbonate saturation distributions, Biogeosciences Discussions, 11, 11 139–11 178, doi:10.5194/bg-d-11-  
11139-2014, <http://www.biogeosciences-discuss.net/11/11139/2014/>, 2014.
- Chung, S.-N., Lee, K., Feely, R. A., Sabine, C. L., Millero, F. J., Wanninkhof, R., Bullister, J. L., Key, R. M.,  
915 and Peng, T.-H.: Calcium carbonate budget in the Atlantic Ocean based on water column inorganic car-  
bon chemistry, Global Biogeochemical Cycles, 17, doi:10.1029/2002GB002001, [http://dx.doi.org/10.1029/  
2002GB002001](http://dx.doi.org/10.1029/2002GB002001), 2003.
- Doney, S. C., Lindsay, K., Fung, I., and John, J.: Natural Variability in a Stable, 1000-yr Global Coupled  
Climate–Carbon Cycle Simulation, J. Climate, 19, 3033–3054, doi:10.1175/JCLI3783.1, 2006.

- 920 Dunne, J. P., Armstrong, R. a., Gnanadesikan, A., and Sarmiento, J. L.: Empirical and mechanistic models for the particle export ratio, *Global Biogeochemical Cycles*, 19, 1–16, doi:10.1029/2004GB002390, <http://www.agu.org/pubs/crossref/2005/2004GB002390.shtml>, 2005.
- Dunne, J. P., Hales, B., and Toggweiler, J. R.: Global calcite cycling constrained by sediment preservation controls, *Global Biogeochemical Cycles*, 26, doi:10.1029/2010GB003935, <http://dx.doi.org/10.1029/2010GB003935>, gB3023, 2012.
- 925 Duteil, O., Koeve, W., Oschlies, A., Bianchi, D., Kriest, I., Galbraith, E. D., and Matear, R.: A new estimate of ocean oxygen utilization points to a reduced rate of respiration in the ocean interior , *Biogeosciences*, 10, 7723–7738, 2013.
- Edwards, N. R., Willmott, A. J., and Killworth, P. D.: On the Role of Topography and Wind Stress on the Stability of the Thermohaline Circulation, *J. Phys. Oceanogr.*, 28, 756–778, 1998.
- 930 Feely, R. A., Sabine, C. L., Lee, K., Millero, F. J., Lamb, M. F., Greeley, D., Bullister, J. L., Key, R. M., Peng, T.-H., Kozyr, A., Ono, T., and Wong, C. S.: In situ calcium carbonate dissolution in the Pacific Ocean, *Global Biogeochemical Cycles*, 16, 12–91, doi:10.1029/2002GB001866, <http://dx.doi.org/10.1029/2002GB001866>, 2002.
- 935 Feely, R. a., Sabine, C. L., Lee, K., Berelson, W., Kleypas, J., Fabry, V. J., and Millero, F. J.: Impact of anthropogenic CO<sub>2</sub> on the CaCO<sub>3</sub> system in the oceans., *Science (New York, N.Y.)*, 305, 362–6, doi:10.1126/science.1097329, <http://www.ncbi.nlm.nih.gov/pubmed/15256664>, 2004.
- Francois, R., Honjo, S., Krishfield, R., and Manganini, S.: Factors controlling the flux of organic carbon to the bathypelagic zone of the ocean, *Global Biogeochemical Cycles*, 16, 34–1–34–20, doi:10.1029/2001GB001722, <http://doi.wiley.com/10.1029/2001GB001722>, 2002.
- 940 Friis, K., Najjar, R. G., Follows, M. J., and Dutkiewicz, S.: Possible overestimation of shallow-depth calcium carbonate dissolution in the ocean, *Global Biogeochemical Cycles*, 20, n/a–n/a, doi:10.1029/2006GB002727, <http://doi.wiley.com/10.1029/2006GB002727>, 2006.
- Gangstø, R., Joos, F., and Gehlen, M.: Sensitivity of pelagic calcification to ocean acidification, *Biogeosciences*, 8, 433–458, doi:10.5194/bg-8-433-2011, <http://www.biogeosciences.net/8/433/2011/>, 2011.
- 945 Garcia, H. E., Locarnini, R. A., Boyer, T. P., Antonov, J. I., Baranova, O. K., Zweng, M. M., and Johnson, D. R.: *World Ocean Atlas 2009, Volume 3: Dissolved Oxygen, Apparent Oxygen Utilization, and Oxygen Saturation*, NOAA Atlas NESDIS 70, U.S. Government Printing Office, Washington, D.C., 2010a.
- Garcia, H. E., Locarnini, R. A., Boyer, T. P., Antonov, J. I., K. Z. M., Zweng, M. M., Baranova, O., Johnson, D. R., Seidov, D., Mishonov, A., and D. R., J.: *World Ocean Atlas 2009, Volume 4: Nutrients (phosphate, nitrate, silicate) Utilization, and Oxygen Saturation*, NOAA Atlas NESDIS, U.S. Government Printing Office, Washington, D.C., 2010b.
- 950 Gattuso, J., Epitalon, J., Lavigne, H., Orr, J., Gentili, B., Hofmann, A., Proye, A., Soetaert, K., and Rae, J.: seacarb: Seawater Carbonate Chemistry, available online at <http://CRAN.R-project.org/package=seacarb>, 2010.
- 955 Gehlen, M., Bopp, L., Emprin, N., Aumont, O., Heinze, C., Ragueneau, O., Mer, D., and Copernic, P.: Reconciling surface ocean productivity, export fluxes and sediment composition in a global biogeochemical ocean model, *Biogeosciences*, 3, 521–537, doi:10.5194/bg-3-521-2006, 2006.

- Griffies, S. M.: The Gent–McWilliams Skew Flux, *J. Phys. Oceanogr.*, 28, 831–841, doi:10.1175/1520-0485(1998)028<0831:TGMSF>2.0.CO;2, 1998.
- 960
- Gruber, N., Sarmiento, J. L., and Stocker, T. F.: An improved method for detecting anthropogenic CO<sub>2</sub> in the oceans, *Global Biogeochemical Cycles*, 10, 809–837, doi:10.1029/96GB01608, <http://dx.doi.org/10.1029/96GB01608>, 1996.
- Heinze, C.: Simulating oceanic CaCO<sub>3</sub> export production in the greenhouse, *Geophysical Research Letters*, 31, L16 308, doi:10.1029/2004GL020613, <http://doi.wiley.com/10.1029/2004GL020613>, 2004.
- 965
- Heinze, C., Maier-Reimer, E., Winguth, A. M. E., and Archer, D.: A global oceanic sediment model for long-term climate studies, *Global Biogeochem. Cy.*, 13, 221–250, 1999.
- Honjo, S., Manganini, S. J., Krishfield, R. a., and Francois, R.: Particulate organic carbon fluxes to the ocean interior and factors controlling the biological pump: A synthesis of global sediment trap programs since 1983, *Progress in Oceanography*, 76, 217–285, doi:10.1016/j.pocean.2007.11.003, <http://linkinghub.elsevier.com/retrieve/pii/S0079661108000025>, 2008.
- 970
- Ito, T., Follows, M. J., and Boyle, E. A.: Is AOU a good measure of respiration in the ocean? , *Geophys. Res. Lett.*, 31, 2004.
- Jansen, H. and Wolf-Gladrow, D. A.: Carbonate dissolution in copepod guts: A numerical model, *Mar. Ecol. Prog. Ser.*, 221, 199–207, 2001.
- 975
- Jansen, H., Zeebe, R. E., and Wolf-Gladrow, D. A.: Modeling the dissolution of settling CaCO<sub>3</sub> in the ocean, *Global Biogeochemical Cycles*, 16, 11–1–11–16, doi:10.1029/2000GB001279, <http://dx.doi.org/10.1029/2000GB001279>, 2002.
- Jin, X., Gruber, N., Dunne, J. P., Sarmiento, J. L., and Armstrong, R. a.: Diagnosing the contribution of phytoplankton functional groups to the production and export of particulate organic carbon, CaCO<sub>3</sub>, and opal from global nutrient and alkalinity distributions, *Global Biogeochemical Cycles*, 20, 1–17, doi:10.1029/2005GB002532, <http://www.agu.org/pubs/crossref/2006/2005GB002532.shtml>, 2006.
- 980
- Kalnay, E., Kanamitsu, M., Kistler, R., Collins, W., Deaven, D., Gandin, L., Iredell, M., Saha, S., White, G., Woollen, J., Zhu, Y., Chelliah, M., Ebisuzaki, W., Higgins, W., Janowiak, J., Mo, K. C., Ropelewski, C., Wang, J., Leetmaa, A., Reynolds, R., Jenne, R., and Joseph, D.: The NCEP/NCAR 40-year reanalysis project, *B. Am. Meteorol. Soc.*, 77, 437–471, doi:10.1175/1520-0477(1996)077<0437:TNYRP>2.0.CO;2, 1996.
- 985
- Kanamori, S. and Ikegami, H.: Calcium–alkalinity relationship in the North Pacific , *J. Oceanogr. Soc. Jpn*, 38, 57–62, 1982.
- Key, R. M., Kozyr, a., Sabine, C. L., Lee, K., Wanninkhof, R., Bullister, J. L., Feely, R. a., Millero, F. J., Mordy, C., and Peng, T.-H.: A global ocean carbon climatology: Results from Global Data Analysis Project (GLODAP), *Global Biogeochem. Cy.*, 18, GB4031, doi:10.1029/2004GB002247, <http://doi.wiley.com/10.1029/2004GB002247>, 2004.
- 990
- Koeve, W., Duteil, O., Oschlies, a., Kähler, P., and Segschneider, J.: Methods to evaluate CaCO<sub>3</sub> cycle modules in coupled global biogeochemical ocean models, *Geoscientific Model Development*, 7, 2393–2408, doi:10.5194/gmd-7-2393-2014, <http://www.geosci-model-dev.net/7/2393/2014>, 2014.
- 995
- Lee, K.: Global net community production estimated from the annual cycle of surface water total dissolved inorganic carbon, *Limnology and oceanography*, 46, 1287–1297, 2001.

- Locarnini, R. A., Mishonov, A., Antonov, J. I., Boyer, T. P., Garcia, H. E., Baranova, O. K., Zweng, M. M., and Johnson, D. R.: World Ocean Atlas 2009, Volume 1: Temperature, Tech. rep., U.S. Government Printing Office, Washington, D.C, 2010.
- 1000 Marra, J., Ho, C., and Trees, C. C.: An algorithm for the calculation of primary production from remote sensing data , Lamont-Doherty Earth Obs., Palisades, N.Y, 2003.
- McKay, M. D., Beckman, R. J., and Conover, W. J.: A comparison of three methods for selecting values of input variables in the analysis of output from a computer code , *Technometrics*, 21, 239–245, 1979.
- 1005 Milliman, J. D.: Production and accumulation of calcium carbonate in the ocean: Budget of a nonsteady state, *Global Biogeochemical Cycles*, 7, 927–957, doi:10.1029/93GB02524, <http://dx.doi.org/10.1029/93GB02524>, 1993.
- Milliman, J. D., Troy, P. J., Balch, W. M., Adams, A. K., Li, Y. H., and Mackenzie, F. T.: Biologically mediated dissolution of calcium carbonate above the chemical lysocline?, *Deep-Sea Res. Pt. 1*, 46, 1653–1669, doi:10.1016/S0967-0637(99)00034-5, 1999.
- 1010 Mucci, A.: The solubility of calcite and aragonite in seawater at various salinities, temperatures, and one atmosphere total pressure, *American Journal of Science*, 1983.
- Müller, S. A., Joos, F., Edwards, N. R., and Stocker, T. F.: Water mass distribution and ventilation time scales in a cost-efficient, three-dimensional ocean model, *J. Climate*, 19, 5479–5499, doi:10.1175/JCLI3911.1, 2006.
- 1015 Müller, S. A., Joos, F., Edwards, N. R., and Stocker, T. F.: Modeled natural and excess radiocarbon: Sensitivities to the gas exchange formulation and ocean transport strength, *Global Biogeochem. Cy.*, 22, 14 pp, doi:10.1029/2007GB003065, 2008.
- Najjar, R. G., Orr, J., Sabine, C. L., and Joos, F.: Biotic-HOWTO. Internal OCMIP Report, Tech. rep., LSCE/CEA Saclay, Gif-sur-Yvette, France, 1999.
- 1020 Orr, J. and Najjar, R. G.: Abiotic-HOWTO. Internal OCMIP Report, Tech. rep., LSCE/CEA Saclay, Gif-sur-Yvette, France, 1999.
- Parekh, P., Joos, F., and Müller, S. A.: A modeling assessment of the interplay between aeolian iron fluxes and iron-binding ligands in controlling carbon dioxide fluctuations during Antarctic warm events, *Paleoceanography*, 23, PA4202, doi:10.1029/2007PA001531, 2008.
- 1025 Ridgwell, A., Hargreaves, J. C., Edwards, N. R., Annan, J. D., Lenton, T. M., Marsh, R., Yool, A., and Watson, A.: Marine geochemical data assimilation in an efficient Earth System Model of global biogeochemical cycling, pp. 87–104, 2007.
- Ritz, S. P., Stocker, T. F., and Severinghaus, J. P.: Noble gases as proxies of mean ocean temperature: sensitivity studies using a climate model of reduced complexity, *Quaternary Sci. Rev.*, 30, 3728–3741, doi:10.1016/j.quascirev.2011.09.021, 2011.
- 1030 Roth, R., Ritz, S. P., and Joos, F.: Burial-nutrient feedbacks amplify the sensitivity of atmospheric carbon dioxide to changes in organic matter remineralisation, *Earth System Dynamics*, 5, 321–343, doi:10.5194/esd-5-321-2014, <http://www.earth-syst-dynam.net/5/321/2014>, 2014.
- Sabine, C. L., Feely, R. A., Key, R. M., Bullister, J. L., Millero, F. J., Lee, K., Peng, T.-H., Tilbrook, B., Ono, T., and Wong, C. S.: Distribution of anthropogenic CO<sub>2</sub> in the Pacific Ocean, *Global Biogeochemical Cycles*, 16, 17–30, doi:10.1029/2001GB001639, <http://dx.doi.org/10.1029/2001GB001639>, 2002a.
- 1035

- Sabine, C. L., Key, R. M., Feely, R. A., and Greeley, D.: Inorganic carbon in the Indian Ocean: distribution and dissolution processes, *Global Biogeochemical Cycles*, 16, 2002b.
- Sarmiento, J. L. and Gruber, N.: *Ocean biogeochemical dynamics*, Princeton University Press, 2006.
- 1040 Sarmiento, J. L., Dunne, J., Gnanadesikan, a., Key, R. M., Matsumoto, K., and Slater, R.: A new estimate of the CaCO<sub>3</sub> to organic carbon export ratio, *Global Biogeochemical Cycles*, 16, 54–1–54–12, doi:10.1029/2002GB001919, <http://doi.wiley.com/10.1029/2002GB001919>, 2002.
- Schmittner, A., Urban, N. M., Keller, K., and Matthews, D.: Using tracer observations to reduce the uncertainty of ocean diapycnal mixing and climate-carbon cycle projections, *Global Biogeochemical Cycles*, 23, 1–16, doi:10.1029/2008GB003421, 2009.
- 1045 Steinacher, M. and Joos, F.: Transient Earth system responses to cumulative carbon dioxide emissions: linearities, uncertainties, and probabilities in an observation-constrained model ensemble, *Biogeosciences*, 13, 1071–1103, <http://www.biogeosciences.net/13/1071/2016>, 2016.
- Steinacher, M., Joos, F., Bopp, L., Cadule, P., Doney, S. C., Gehlen, M., Schneider, B., and Segsneider, J.: 1050 Projected 21st century decrease in marine productivity : a multi-model analysis, pp. 7933–7981, 2009.
- Steinacher, M., Joos, F., and Stocker, T. F.: Allowable carbon emissions lowered by multiple climate targets., *Nature*, 499, 197–201, doi:10.1038/nature12269, <http://www.ncbi.nlm.nih.gov/pubmed/23823728>, 2013.
- Taylor, K. E.: Summarizing multiple aspects of model performance in a single diagram, *Journal of Geophysical Research*, 106, 7183, doi:10.1029/2000JD900719, 2001.
- 1055 Tschumi, T., Joos, F., Gehlen, M., and Heinze, C.: Deep ocean ventilation, carbon isotopes, marine sedimentation and the deglacial CO<sub>2</sub> rise, *Clim. Past*, 7, 771–800, doi:10.5194/cp-7-771-2011, 2011.
- Vecsei, A. and Berger, W. H.: Increase of atmospheric CO<sub>2</sub> during deglaciation: Constraints on the coral reef hypothesis from patterns of deposition, *Global Biogeochem. Cy.*, 18, GB1035, doi:10.1029/2003GB002147, 2004.
- 1060 Volk, T. and Hoffert, M. I.: Ocean carbon pumps: Analysis of relative strengths and efficiencies in ocean-driven atmospheric CO<sub>2</sub> changes, *The Carbon Cycle and Atmospheric CO: Natural Variations Archean to Present*, pp. 99–110, 1985.
- Wilson, J. D., Barker, S., and Ridgwell, A.: Assessment of the spatial variability in particulate organic matter and mineral sinking fluxes in the ocean interior: Implications for the ballast hypothesis, *Global Biogeochemical* 1065 *Cycles*, 26, doi:10.1029/2012GB004398, <http://dx.doi.org/10.1029/2012GB004398>, 2012.
- Wolf-Gladrow, D. A., Zeebe, R. E., Klaas, C., Körtzinger, A., and Dickson, A. G.: Total alkalinity: The explicit conservative expression and its application to biogeochemical processes, *Marine Chemistry*, 106, 287–300, doi:10.1016/j.marchem.2007.01.006, <http://www.sciencedirect.com/science/article/pii/S0304420307000047>, 2007.

**Table 1.** Overview on suggested ways of regression for  $\text{TA}^0$  either including two ( $S$ ,  $\text{PO}$ ) or three ( $S$ ,  $\text{PO}$ ,  $T$ ) explanatory variables and either as a global or basin-wide fit. The last column shows the root mean square deviation relative to the Global B3D estimate.

	Equation [ueq kg <sup>-1</sup> ]	Mean [mol m <sup>-3</sup> ]	RMSE from Global B3D [mol m <sup>-3</sup> ]
Gruber et al. (1996):	$\text{TA}^0 = (367.5 + 59.9 \text{ psu}^{-1} \cdot S + 0.074 \text{ kg umol}^{-1} \cdot \text{PO}) \text{ ueq kg}^{-1}$	2.377	0.012
Feely et al. (2002):	$\text{TA}^0 = 148.7 + 61.36 \cdot S + 0.0941 \cdot \text{PO} - 0.582 \cdot T_{\text{pot}}$	2.39	0.0015
Friis et al. (2006):	as Feely et al. (2002)		
Global B3D 2V:	$\text{TA}^0 = (297.51 + 56.399 \text{ psu}^{-1} \cdot S + 0.1259 \text{ kg umol}^{-1} \cdot \text{PO}) \text{ ueq kg}^{-1}$	2.387	0.0022
Global B3D:	$\text{TA}^0 = (345.64 + 56.03 \text{ psu}^{-1} \cdot S + 0.069 \text{ kg umol}^{-1} \cdot \text{PO} - 0.9^\circ \text{C}^{-1} \cdot T) \text{ ueq kg}^{-1}$	2.389	0
Regional B3D:		2.385	0.0047
Atlantic	$\text{TA}^0 = (688.15 + 44.97 \text{ psu}^{-1} \cdot S + 0.129 \text{ kg umol}^{-1} \cdot \text{PO} + 1.34^\circ \text{C}^{-1} \cdot T) \text{ ueq kg}^{-1}$		
Pacific	$\text{TA}^0 = (381.05 + 55.26 \text{ psu}^{-1} \cdot S + 0.049 \text{ kg umol}^{-1} \cdot \text{PO} - 1.20^\circ \text{C}^{-1} \cdot T) \text{ ueq kg}^{-1}$		
Indian	$\text{TA}^0 = (637.70 + 47.38 \text{ psu}^{-1} \cdot S + 0.078 \text{ kg umol}^{-1} \cdot \text{PO} - 0.54^\circ \text{C}^{-1} \cdot T) \text{ ueq kg}^{-1}$		

Gruber et al. (1996) is the original, global regression based on two explanatory variables (based on their 1996 database), Feely et al. (2002) and Friis et al. (2006) are both taken from Sabine et al. (2002b) also including temperature as an additional explanatory variable and fitted to a Pacific subset. Global B3D 2V is a global regression with two explanatory variables (based on WOA09 Locarnini et al., 2010; Antonov et al., 2010; Garcia et al., 2010a, b) on the Bern3D grid (32 × 40 × 41 grid cells), Global B3D includes three explanatory variables and Regional B3D further distinguishes each basin, separately.

**Table 2.** Results from sensitivity simulations.  $\text{CaCO}_3$  export and  $\text{TA}^*$  inventories for different physical mixing (diapycnal mixing coefficient,  $k_{\text{dia}}$ ) and  $\text{CaCO}_3$  dissolution schemes. For these illustrative simulations, calcite and aragonite particles were assigned equal parameter values and 10% of export is assumed to be in the form of aragonite. Fast:  $k_0 = 10 \text{ day}^{-1}$ ,  $n = 1$ ,  $f_{\text{calc}} = 0.9$ ,  $k_{\text{bg}} = 0$ ; slow:  $k_0 = 0.16 \text{ day}^{-1}$ ,  $n = 2$ ,  $f_{\text{calc}} = 0.9$ ,  $k_{\text{bg}} = 0$ ; constant:  $k_{\text{bg}}/v = 1/2900 \text{ m}^{-1}$ .

	$k_{\text{dia, low}}$	$k_{\text{dia, ref}}$	$k_{\text{dia, high}}$
	$0.1 \times 10^{-4} \text{ m}^2 \text{ s}^{-1}$	$0.2 \times 10^{-4} \text{ m}^2 \text{ s}^{-1}$	$0.5 \times 10^{-4} \text{ m}^2 \text{ s}^{-1}$
<b>Export [Gt-C yr<sup>-1</sup>]</b>	0.727	0.818	1.071
<b>TA* Inventory [Pmol C]</b>			
(fraction of which lies above $\Omega_{\text{calc}} = 1$ )			
Fast	47.81 (54 %)	47.87 (52 %)	44.5 (51 %)
Slow	62.49 (45 %)	63.01 (44 %)	58.93 (43 %)
Constant	38.12 (52 %)	38.35 (51 %)	35.44 (50 %)

**Table 3.** Mean sediment burial fluxes [Gt-C yr<sup>-1</sup>] and observation-based vs. simulated TA\* inventories [Pmol C]. TA\*<sup>sedcorr</sup> are estimated by comparing output from the 14 Bern3D simulations that agree best with observation-based TA\* concentrations and with and without sediment module. The median estimate is from the constrained 1000 member ensemble (without sediment module).

	Atlantic	Pacific	Indian	Global
<b>Burial flux [Gt-C yr<sup>-1</sup>]</b>	0.011	0.062	0.042	0.117
<b>TA* Inventory [Pmol C]</b>				
TA* <sup>obs</sup>	2.5	27.9	7.0	37.4
TA* <sup>sedcorr</sup>	0.9	4.6	1.4	6.9
TA* <sup>obs+sedcorr</sup>	3.4	32.4	8.4	44.1
TA* <sup>median</sup>	5.4	31.1	8.7	45.5

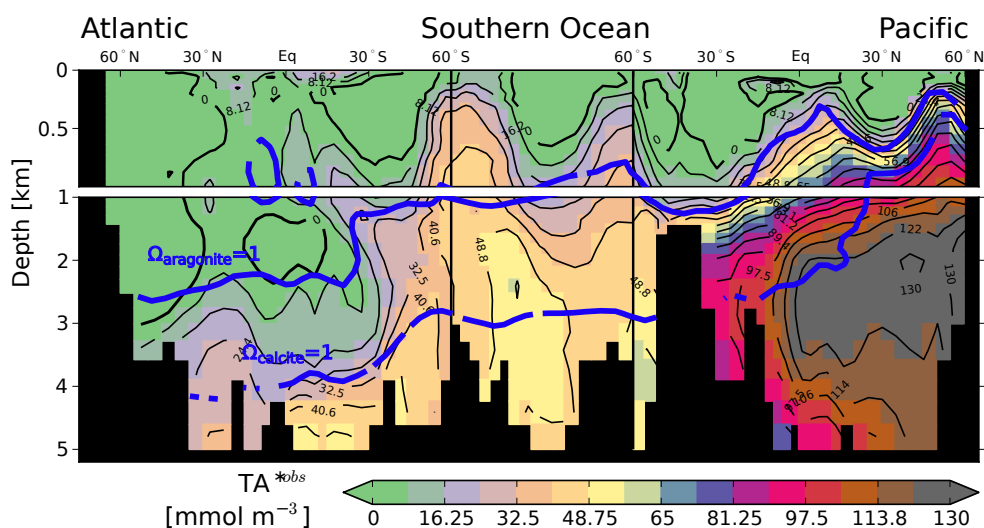


**Figure 1.** The TA\* tracer captures exclusively the influence of CaCO<sub>3</sub> dissolution on alkalinity. **Top:** an observationally-based estimate of the TA\* distribution [mmol m<sup>-3</sup>] (based on GLODAP Key et al. (2004) and WOA09 Locarnini et al., 2010; Antonov et al., 2010; Garcia et al., 2010a, b) yielding an inventory of ~37.5 Pmol C of which ~41% comes to lie above the calcite saturation horizon. **Bottom:** influence of ocean-sediment fluxes on TA\*. The calcite ( $\sigma_{\text{calcite}}=1$ ) mean offset in TA\* between simulations with and aragonite ( $\sigma_{\text{aragonite}}=1$ ) saturation horizon are without sediment module is shown by the blue lines ensemble members with the highest skill. Displayed are results for a cross-section through the Atlantic (25° W), across the Southern Ocean (58° S) into the Pacific, and through the Pacific (175° W).

**Table 4.** Constrained fluxes (median and 68 % confidence interval, c.i.) of biogenic CaCO<sub>3</sub> **PIE** [Gt-C yr<sup>-1</sup>].

	Atlantic		Pacific		Indian		Global	
	median	c.i.	median	c.i.	median	c.i.	median	c.i.
<b>Export at 75 m</b>								
70 – 30°N	0.021	[0.007-0.037]	0.081	[0.027-0.134]				
30°N – 35°S	0.061	[0.018-0.103]	0.307	[0.149-0.457]	0.143	[0.053-0.223]		
>35°S	0.041	[0.014-0.07]	0.174	[0.057-0.254]	0.088	[0.03-0.14]		
70°N – 90°S	0.121	[0.078-0.171]	0.549	[0.391-0.697]	0.23	[0.137-0.316]	0.897	[0.72-1.049]
<b>Dissolution in waters shallower than 1500 m</b>								
70 – 30°N	0.006	[0.002-0.011]	0.048	[0.015-0.086]				
30°N – 35°S	0.015	[0.004-0.03]	0.118	[0.049-0.2]	0.043	[0.016-0.08]		
>35°S	0.01	[0.003-0.021]	0.043	[0.013-0.082]	0.02	[0.006-0.042]		
70°N – 90°S	0.033	[0.018-0.054]	0.216	[0.125-0.32]	0.064	[0.032-0.11]	0.328	[0.202-0.444]
<b>Deposition on sediments shallower than 1500 m</b>								
70 – 30°N	0.003	[0.001-0.005]	0.008	[0.002-0.014]				
30°N – 35°S	0.003	[0.001-0.006]	0.008	[0.004-0.013]	0.015	[0.005-0.024]		
>35°S	0	[0.0-0.001]	0.007	[0.002-0.011]	0	[0.0-0.001]		
70°N – 90°S	0.007	[0.004-0.01]	0.023	[0.016-0.029]	0.016	[0.006-0.025]	0.045	[0.034-0.056]
<b>Dissolution in waters deeper or equal to 1500 m</b>								
70 – 30°N	0.008	[0.003-0.013]	0.014	[0.003-0.035]				
30°N – 35°S	0.03	[0.011-0.048]	0.133	[0.068-0.2]	0.053	[0.022-0.087]		
>35°S	0.023	[0.009-0.038]	0.085	[0.031-0.129]	0.043	[0.015-0.07]		
70°N – 90°S	0.06	[0.039-0.083]	0.233	[0.165-0.305]	0.097	[0.061-0.139]	0.395	[0.32-0.469]
<b>Deposition on sediments deeper or equal to 1500 m</b>								
70 – 30°N	0.003	[0.0-0.007]	0.002	[0.001-0.007]				
30°N – 35°S	0.009	[0.001-0.021]	0.031	[0.012-0.062]	0.019	[0.005-0.039]		
>35°S	0.005	[0.001-0.011]	0.02	[0.006-0.041]	0.016	[0.005-0.03]		
70°N – 90°S	0.018	[0.009-0.033]	0.056	[0.028-0.099]	0.035	[0.018-0.065]	0.116	[0.071-0.179]
<b>Deposition on all sediments</b>								
70 – 30°N	0.006	[0.001-0.012]	0.011	[0.003-0.021]				
30°N – 35°S	0.013	[0.002-0.027]	0.04	[0.017-0.073]	0.036	[0.011-0.061]		
>35°S	0.005	[0.001-0.012]	0.028	[0.008-0.051]	0.016	[0.005-0.03]		
70°N – 90°S	0.025	[0.014-0.043]	0.081	[0.049-0.126]	0.052	[0.026-0.087]	0.164	[0.113-0.227]

**Table 5.** Dissolution rates of biogenic  $\text{CaCO}_3$  [ $\text{Gt-C yr}^{-1}$ ] in the upper water column (200–1500 m depth levels) based on the TA\*-CFC age method as summarised in Berelson et al. (2007), and as constrained by TA\* data in our Latin-Hypercube ensemble (including the sediment correction, median and 68 % c.i.). The dissolution estimates by Berelson et al. (2007) were assigned an estimated uncertainty of  $\sim 50\%$ .

Location	Berelson et al. (2007)	This study	
		median	c.i.
Atlantic			
$>40^\circ >40\text{N}$	0.060	<u>0.006</u> <del>0.009</del>	[ <u>0.002-0.011</u> <del>0.024</del> ]
$40^\circ\text{N} - 40^\circ\text{N} - 40\text{S}$	0.010	<u>0.02</u> <del>0.023</del>	[ <u>0.008-0.036</u> <del>0.01-0.037</del> ]
$>40^\circ >40\text{S}$	0.040	<u>0.009</u> <del>0.012</del>	[ <u>0.003-0.017</u> <del>0.002-0.024</del> ]
Pacific			
$>40^\circ >40\text{N}$	0.070	<u>0.039</u> <del>0.038</del>	[ <u>0.013-0.067</u> <del>0.067</del> ]
$40^\circ\text{N} - 5^\circ\text{N} - 40\text{S}$	0.330	<u>0.063</u> <del>0.049</del>	[ <u>0.032-0.099</u> <del>0.024-0.087</del> ]
$5^\circ\text{N} - 5^\circ\text{N} - 5\text{S}$	0.020	<u>0.035</u> <del>0.025</del>	[ <u>0.015-0.058</u> <del>0.01-0.05</del> ]
$5^\circ\text{S} - 40^\circ\text{S} - 5 - 40\text{S}$	0.000	<u>0.039</u> <del>0.03</del>	[ <u>0.019-0.066</u> <del>0.015-0.058</del> ]
$>40^\circ >40\text{S}$	0.160	<u>0.034</u> <del>0.037</del>	[ <u>0.011-0.061</u> <del>0.014-0.062</del> ]
Indian			
$40^\circ\text{N} - 40^\circ\text{N} - 40\text{S}$	0.160	<u>0.062</u> <del>0.052</del>	[ <u>0.026-0.104</u> <del>0.023-0.095</del> ]
$>40^\circ >40\text{S}$	0.140	<u>0.021</u> <del>0.02</del>	[ <u>0.009-0.038</u> <del>0.005-0.039</del> ]
Total	1.0	<u>0.346</u> <del>0.33</del>	[ <u>0.225-0.461</u> <del>0.26-0.40</del> ]

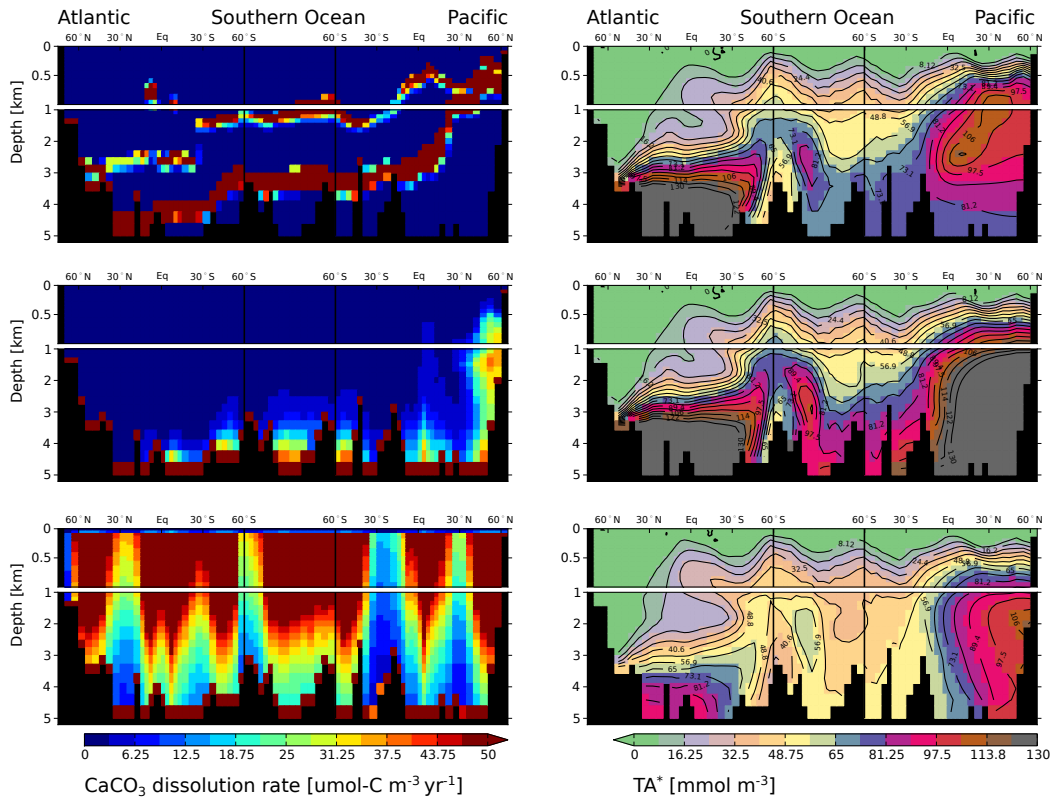


**Figure 2.** Results from sensitivity simulations applying three different illustrative dissolution schemes. Left column: alkalinity sources due to CaCO<sub>3</sub> dissolution rates. Right column: the resulting steady state TA\* for these three contrasting parameterisations of the CaCO<sub>3</sub> dissolution rate. The dissolution rate is set to increase fast (top row), slowly (middle row) with undersaturation of CaCO<sub>3</sub>, or is set constant throughout the water column (bottom row). The standard version of the Bern3D model without sediment module is applied and the fraction of CaCO<sub>3</sub> export in the form of aragonite is set to 10%. At least 4344% of the dissolution signal is simulated above the calcite saturation horizon irrespective of whether dissolution is allowed to occur above the saturation horizon (bottom row) or not (middle and top row). This points to the importance of physical transport in shaping the distribution of TA\*.

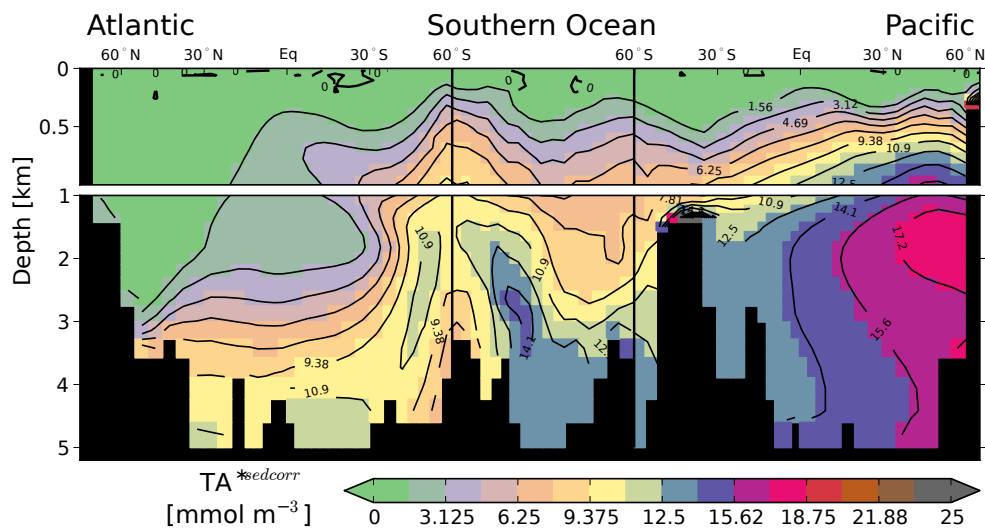


**Figure 3.** Influence of ocean-sediment fluxes on simulated  $\text{TA}^*$  column inventories. The mean offset in  $\text{TA}^*$  between simulations with export and without sediment module dissolution is shown for the 14 ensemble members with the highest skill enabled within one out of six ocean regions and set to zero elsewhere. Displayed are results for a rain ratio of 7 and a cross-section through the Atlantic constant dissolution coefficient ( $25^\circ \text{S } k_{\text{bg}} = 1/2900 \text{ W}$ ), across the Southern Ocean is applied. Similar patterns emerge for alternative dissolution parameterisations ( $58^\circ \text{S}$  not shown) into the Pacific, and through the Pacific ( $175^\circ \text{W}$ ). Note the colourbar. Thick horizontal black lines denote region boundaries.

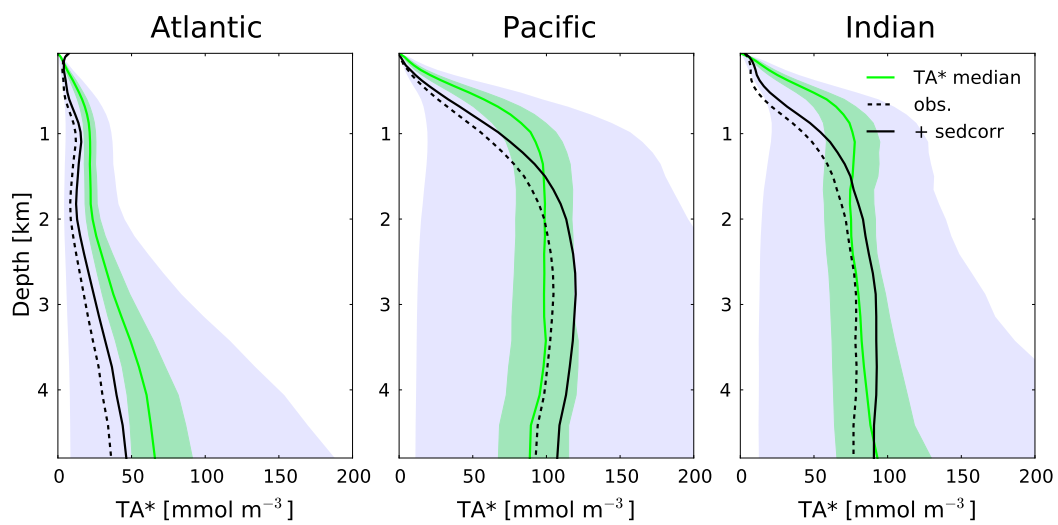


**Figure 4.** Model ensemble vs. observation-based basin-mean  $\text{TA}^*$  profiles. The grey shading shows the unconstrained prior and the green shading shows the constrained (68 % confidence interval) distribution of the model ensemble. Lines represent the median of the constrained ensemble (green), observation-based  $\text{TA}^*$  (black dashes), and observation-based  $\text{TA}^*$  corrected for a sediment burial flux of  $0.120.074 \text{ Gt-C yr}^{-1}$  (black solid). The corresponding Southern Ocean sector is included in the averaging.

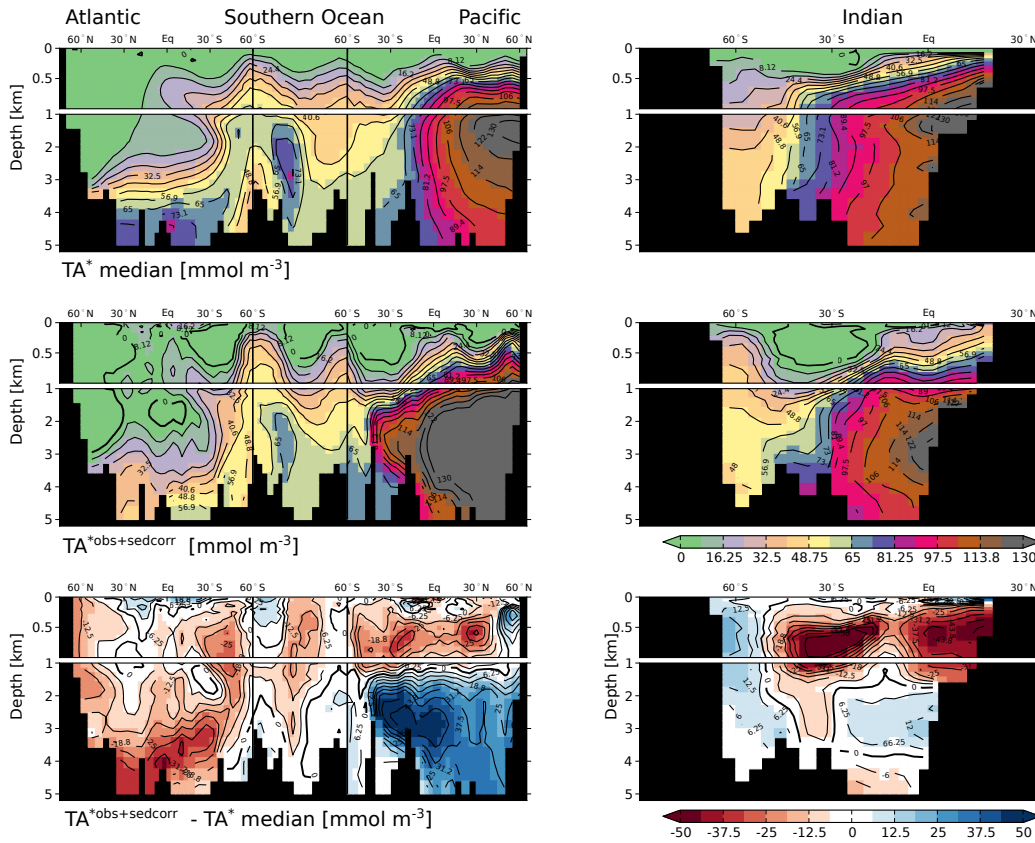


**Figure 5.** Observation-based vs. simulated  $TA^*$ . Left column: modelled (median)  $TA^*$ , observed  $TA^*$ , and their difference in a cross-section through the Atlantic ( $25^\circ$  W), Southern Ocean ( $58^\circ$  S), and Pacific ( $175^\circ$  W). Right column: the same for a cross-section along  $95^\circ$  E in the Indian Ocean. The correlation coefficient, relative standard deviation ( $\sigma_{rel}^{obs}$ ) and root mean square error (RMSE) between the simulated and observation-based fields are: 0.83, 1.09, and  $17.7 \text{ mmol m}^{-3}$  in the Atlantic; 0.88, 0.8, and  $23.8 \text{ mmol m}^{-3}$  in the Pacific; 0.87, 0.86, and  $19.8 \text{ mmol m}^{-3}$  in the Indian Ocean.

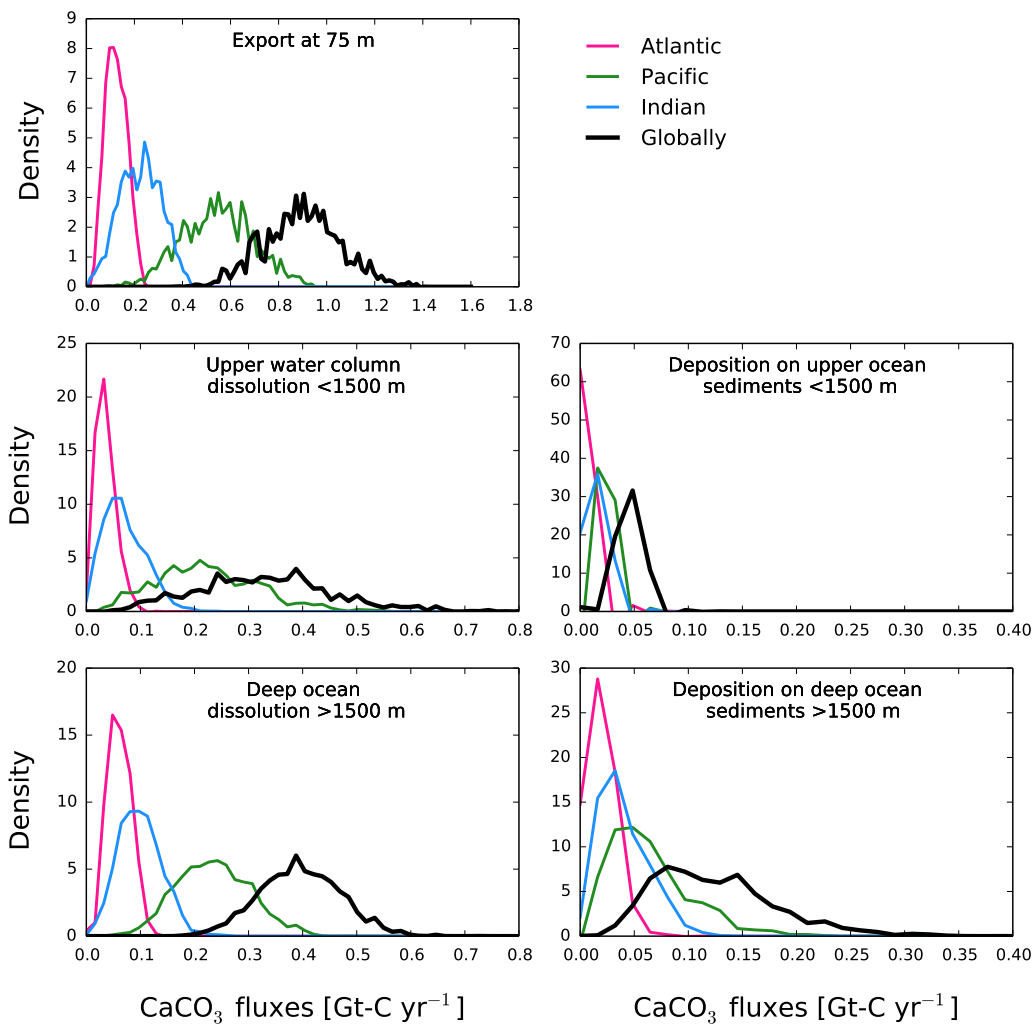


**Figure 6.** Probability density functions of basin-wide and global  $\text{CaCO}_3$  fluxes as constrained by the observation-based  $\text{TA}^*$  distribution (corrected for a sediment burial flux of  $0.12 \text{ Gt-C yr}^{-1}$ ). Note the different scaling of the  $x$  axes.

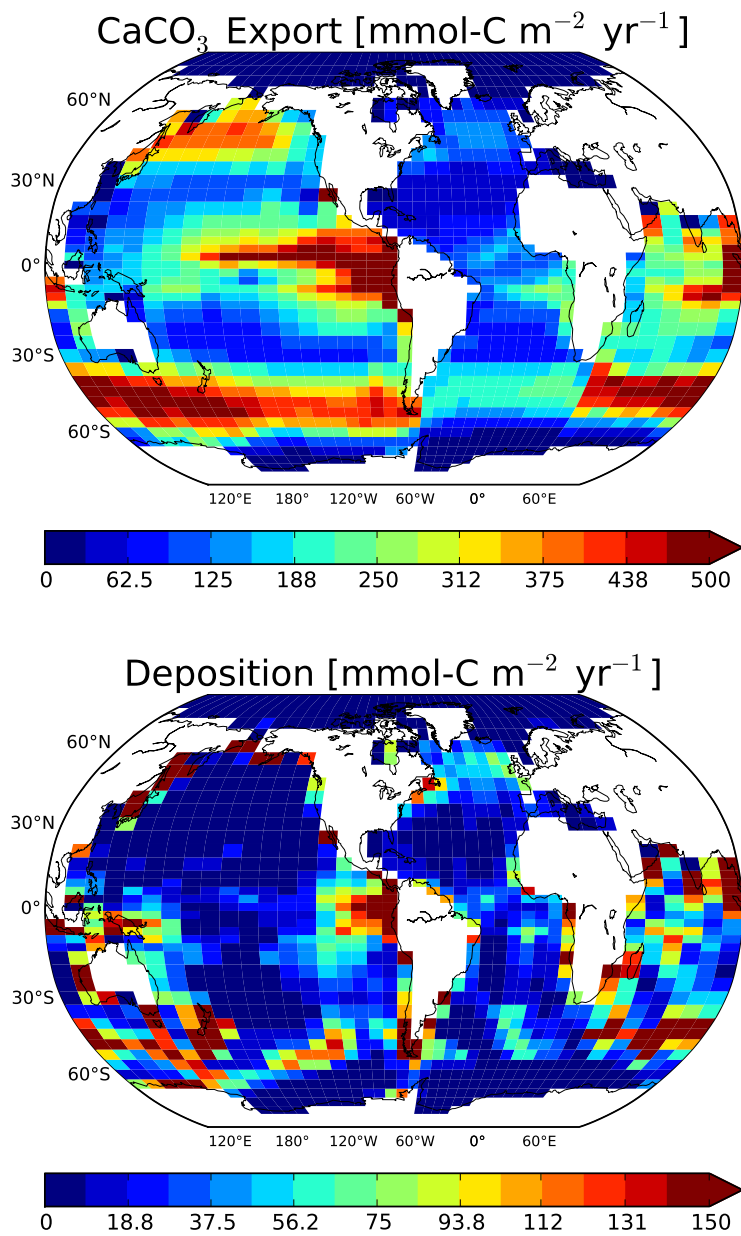


**Figure 7.** Top: median CaCO<sub>3</sub> export, globally 0.90 (0.72–1.05) Gt-C yr<sup>-1</sup>. Bottom: median CaCO<sub>3</sub> fluxes reaching the ocean floor, globally 0.164 (0.113–0.227) Gt-C yr<sup>-1</sup>. Note the different scaling of the colourbars.

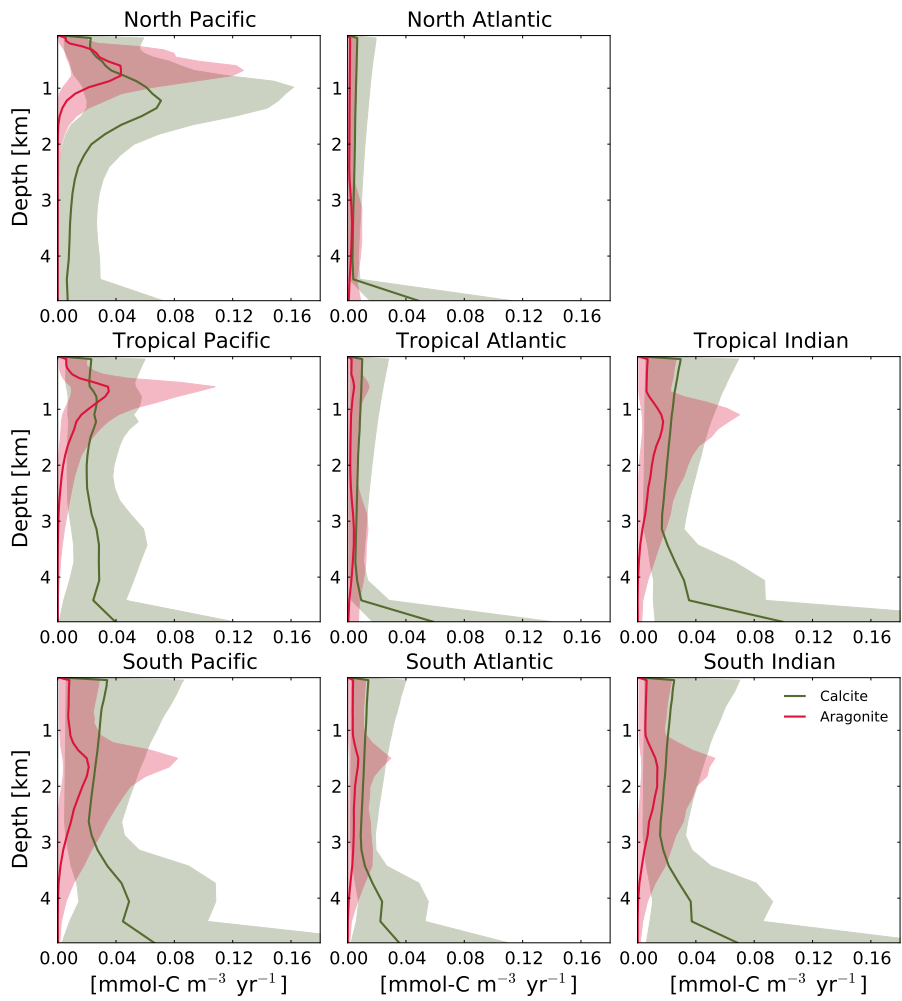


**Figure 8.** Constrained open-water dissolution rate profiles for aragonite (red) and calcite (olive). Ensemble medians (solid lines) and 68 % confidence intervals (shadings) are for spatial averages across individual regions and including only grid cells where the model water column extends to a depth of 5000 m.

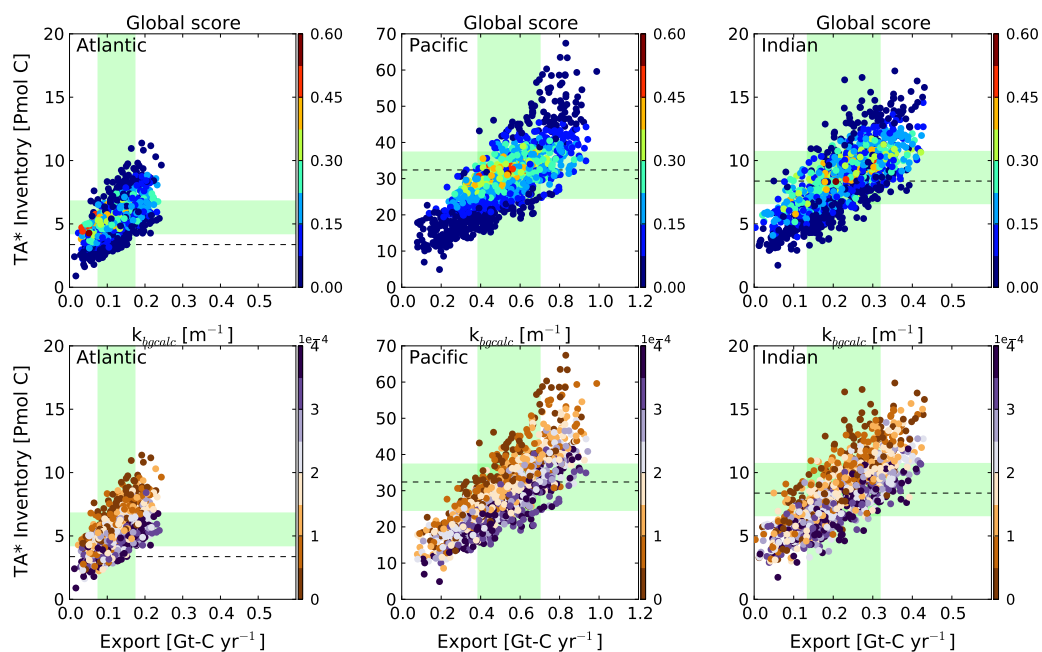


**Figure 9.** [The simulated  \$\text{TA}^\*\$  inventory vs. the simulated  \$\text{CaCO}\_3\$  export of each ensemble member, coloured according to model skill \(top\) and background dissolution rate \(bottom\) for the Atlantic, Pacific, and Indian Ocean \(columns\). Each circle represents results from an individual simulation and its colour indicates the regional skill score \(top\) or the value of the background dissolution coefficient for calcite \(bottom\). Green shadings show the 68% confidence range in basin-wide  \$\text{TA}^\*\$  inventories and  \$\text{CaCO}\_3\$  export of the constrained model ensemble and black-dashed lines indicate the estimated  \$\text{TA}^\*\$  inventories based on the observations \[including the sediment correction\]\(#\). Runs with low and high background dissolution can skillfully represent the  \$\text{TA}^\*\$  distribution. Runs with a higher  \$\text{CaCO}\_3\$  export tend to require a higher background dissolution to achieve a good skill.](#)

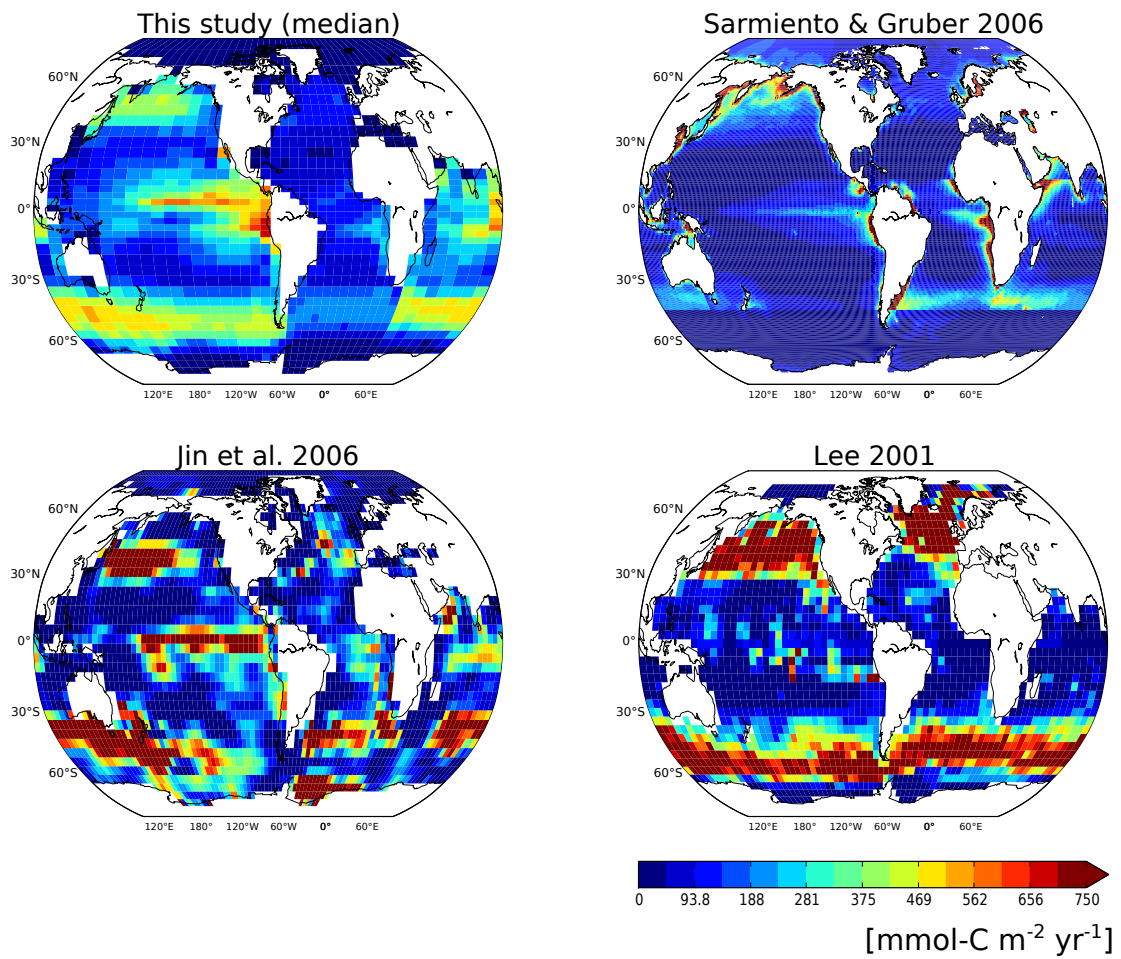


**Figure 10.** Observationally-constrained  $\text{CaCO}_3$  export fields as estimated by different studies. Global total export is estimated to 0.5 by Sarmiento and Gruber (2006), to 1.14 by Jin et al. (2006), to 1.1 by Lee (2001), and to 0.90  $\text{Gt-C yr}^{-1}$  by this study.

~~Observationally-constrained export fields as estimated by different studies. Global total export is estimated to 0.5 by , to 1.14 by , to 1.1 by , and to 0.82 by this study.~~

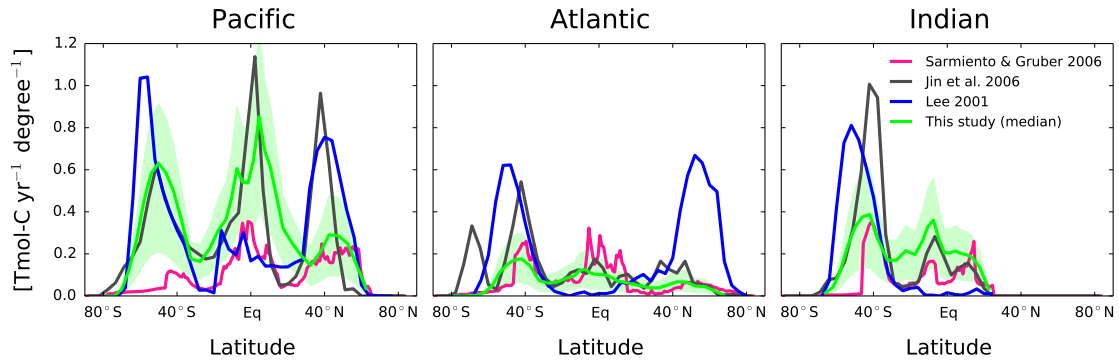


**Figure 11.** Zonally-integrated export fluxes of the constrained Bern3D-model ensemble (median and 68 % confidence interval) compared to estimates by Sarmiento and Gruber (2006), Jin et al. (2006) and Lee (2001).

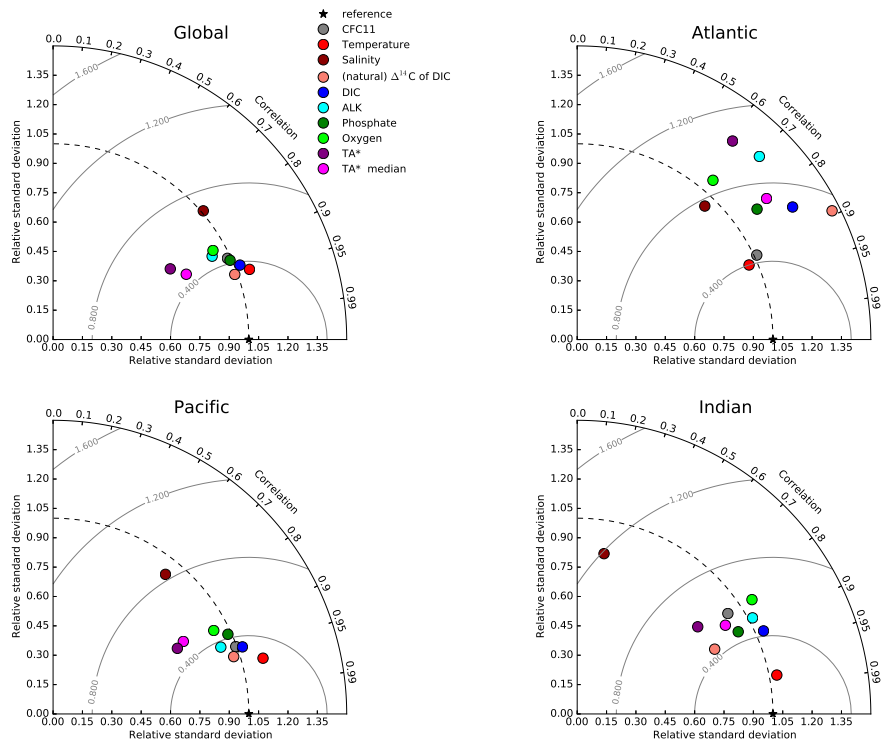


**Figure A1.** Taylor diagram (Taylor, 2001) for global and basin-wide volume-weighted oceanic tracer distributions as simulated by the Bern3D standard setup with  $k_{\text{dia}} = 0.2 \times 10^{-4} \text{ m}^2 \text{ s}^{-1}$ . Observation-derived fields are taken from GLODAP (Key et al., 2004) and the World Ocean Atlas 2009 (Locarnini et al., 2010; Antonov et al., 2010; Garcia et al., 2010a, b).

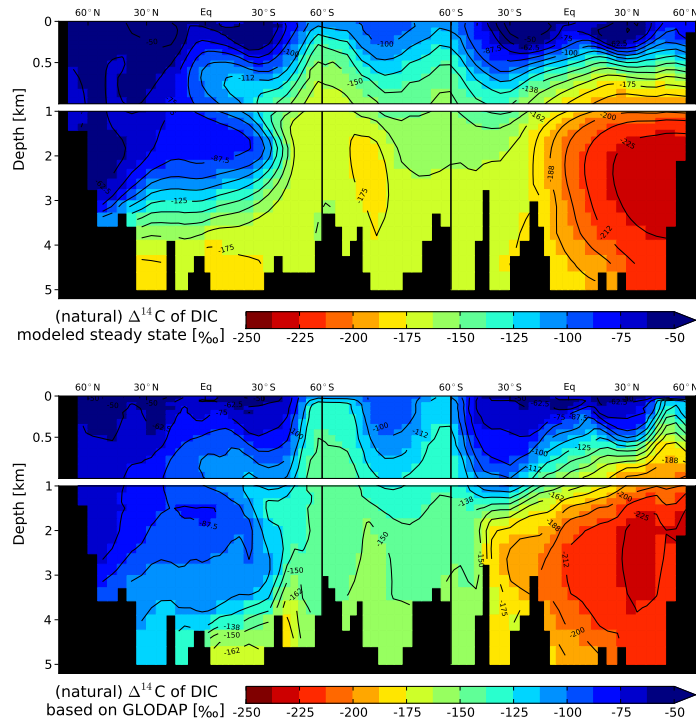


**Figure A2.** (Top) Distributions of (natural)  $\Delta^{14}\text{C}$  of DIC [‰] as simulated with a standard  $k_{\text{dia}}$  of  $0.2 \times 10^{-4} \text{ m}^2 \text{ s}^{-1}$  at steady state and (bottom) as estimated from  $\Delta^{14}\text{C}$  measurements (Key et al., 2004). The correlation coefficient,  $\sigma_{\text{rel}}^{\text{obs}}$ , and RMSEs are: 0.89, 1.461.43, 23.7722.65‰ in the Atlantic; 0.95, 0.97, 16.2816.08‰ in the Pacific; 0.9, 0.780.77, 21.120.63‰ in the Indian Ocean. The section displayed is through the Atlantic ( $25^\circ \text{ W}$ ), the Southern Ocean ( $58^\circ \text{ S}$ ), and the Pacific ( $175^\circ \text{ W}$ ).

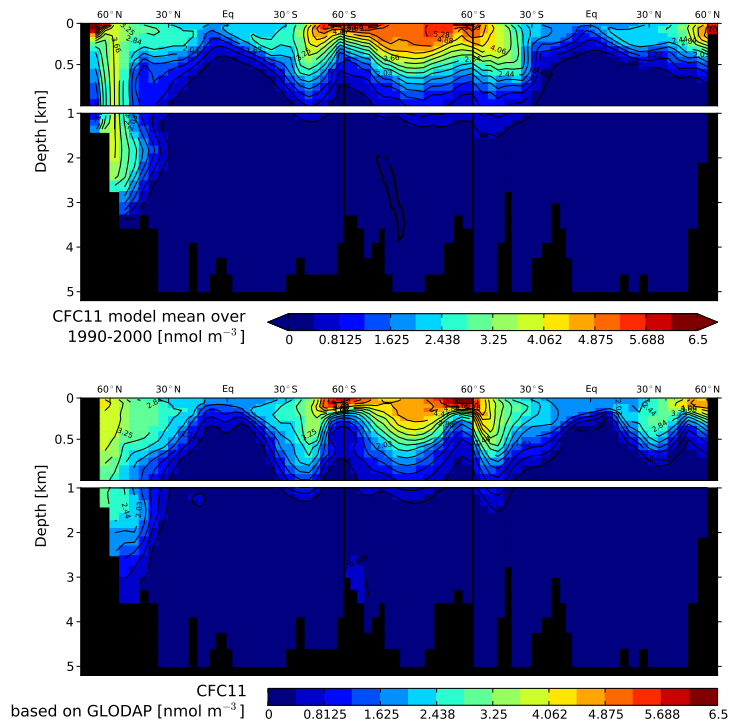


**Figure A3.** (Top) Distributions of CFC11 [nmol m<sup>-3</sup>] as simulated with a standard  $k_{\text{dia}}$  of  $0.2 \times 10^{-4} \text{ m}^2 \text{ s}^{-1}$  averaged over the at-model years 1990-2000 year 1994 and (bottom) as observed (Key et al., 2004). The correlation coefficient,  $\sigma_{\text{rel}}^{\text{obs}}$ , and RMSEs are: 0.9, 1.01, 0.45 nmol m<sup>-3</sup> in the Atlantic; 0.94, 1.09, 0.29 nmol m<sup>-3</sup> in the Pacific; 0.83, 0.92, 0.96, 0.54, 0.56 nmol m<sup>-3</sup> in the Indian Ocean. The section displayed is through the Atlantic (25° W), the Southern Ocean (58° S), and the Pacific (175° W).

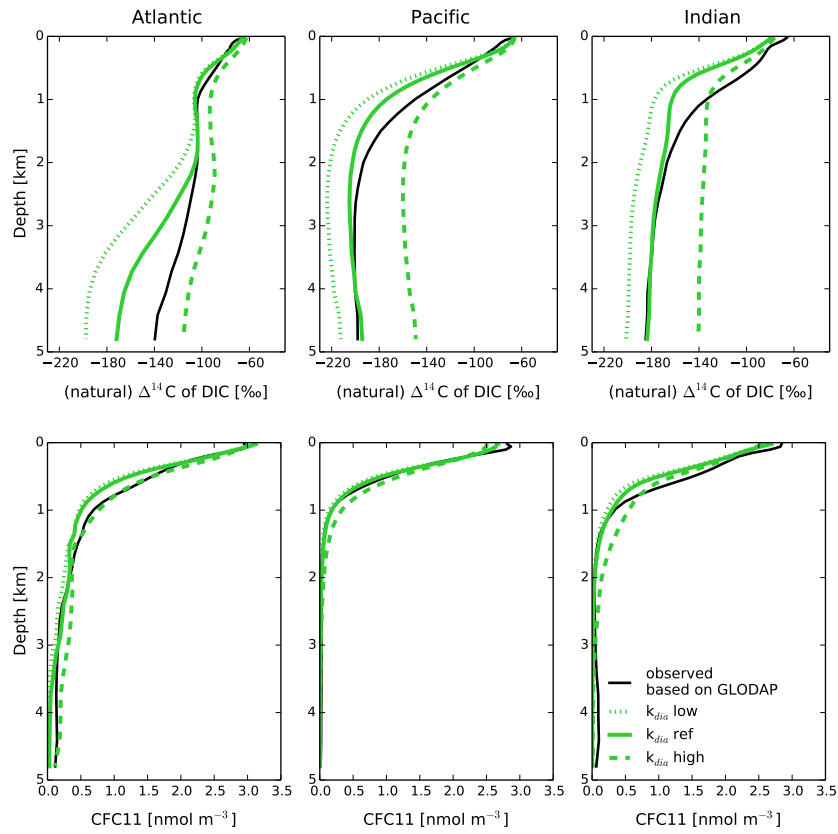


**Figure A4.** Basin-wide average profiles for (natural)  $\Delta^{14}\text{C}$  of DIC [‰] at steady state (top) and for CFC11 [nmol m<sup>-3</sup>] averaged over the at-model years 1990-2000 year 1994 (bottom). Results are for simulations with a low (green dotted), standard (green solid), and high (green dashes) value of the diapycnal mixing coefficient  $k_{\text{dia}}$  ( $0.1, 0.2$  and  $0.5 \times 10^{-4} \text{ m}^2 \text{ s}^{-1}$ ). Observation-based estimates are in black. The corresponding Southern Ocean sector is included in the averaging.

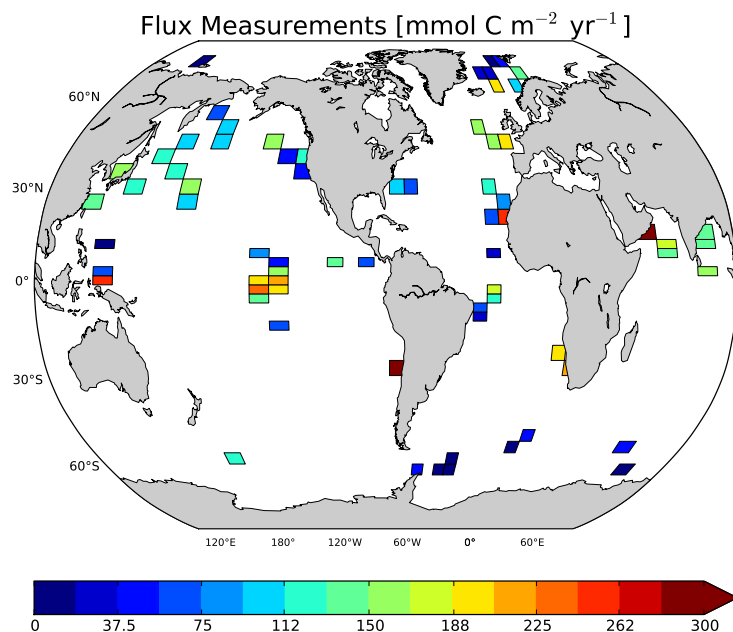


**Figure A5.** The global sediment trap data collection of Wilson et al. (2012, see their auxiliary material at doi:10.1029/2012GB004398) on the Bern3D grid. The measurements are located at different depths ( $> 1500 \text{ m}$ ). If more than one measurement was assigned to the same cell, the mean was chosen.

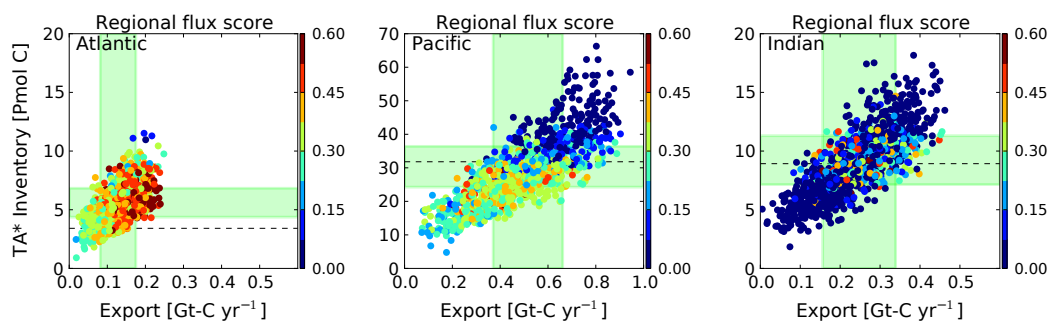


**Figure A6.** As Fig. 9 but coloured according to model skill with respect to the sediment trap database evaluated by basin. This target variable constrains export and dissolution to wider ranges (yellow to red colours) as compared to the  $\text{TA}^*$  target (light green shading). Generally, high skill scores with respect to regional, sediment-corrected  $\text{TA}^*$  are also associated with high skill scores with respect to regional fluxes. Only few models are in good agreement with the few flux measurements in the Indian Ocean.